Mathematical models of IL-10 regulation in macrophages stimulated with immunomodulatory molecules of parasitic nematodes

A systems biology approach

D I S S E R T A T I O N

zur Erlangung des akademischen Grades

Doctor Rerum Naturalium
im Fach Biophysik

eingereicht an der
Mathematisch-Naturwissenschaftlichen Fakultät I
Humboldt-Universität zu Berlin

von
M.Sc. Dipl. Ing. Ana Sofia Cabrita Figueiredo

Präsident der Humboldt-Universität zu Berlin:
Prof. Dr. Jan-Hendrik Olbertz

Dekan der Mathematisch-Naturwissenschaftlichen Fakultät I:
Prof. Dr. Andreas Herrmann

Gutachter:
1. Prof. Dr. Peter Hammerstein
2. Prof. Dr. Richard Lucius
3. Prof. Dr. Thomas Höfer

eingereicht am: 08.04.2011
Tag der mündlichen Prüfung: 05.07.2011

Para a Elenah e para o Jordi

Abstract

Many parasites and their hosts have developed a mode of coexistence during their evolution. The parasitic nematode *Acanthocheilonema viteae* can downregulate the immune response of their host by inducing immunoregulatory cytokines such as interleukin-10 (IL-10). In this thesis, I developed mathematical models of IL-10 regulation to investigate the mechanims of IL-10 regulation. These models were based on literature evidences and *in vitro* data on the production of IL-10 in macrophages in response to Av17, an immunomodulatory protein of *A. viteae*. IL-10 expression requires stimulation of the mitogen-activated protein kinases (MAPK) ERK and p38. I proposed that a negative feedback mechanism, acting at the signalling level, is responsible for transient IL-10 upregulation that can be followed by a sustained plateau. The model assumes that Av17 leads to phosphorylation of ERK and p38 and that IL-10 expression induced by Av17 in macrophages was tyrosine kinase sensitive and dependent on activation of both MAP kinases. These assumptions were validated with experimental data on ERK and p38 activation. To further elucidate how the activation of ERK and p38 regulates IL-10 expression, I combined theoretical and experimental approaches. I hypothesised several alternative ways of signalling regulation and developed a method of model selection that combines the theoretical predictions with experimental evidences and selected a model that was able not only to fit experimental data but also to correctly predict independent experimental data. Experimental testing of the *in silico* generated hypotheses identified dual specificity phosphatase (DUSP) 1 and 2 as integral feedback regulators in Av17 triggered macrophages *in vitro* and *in vivo*. In particular, dedicated experiments showed that DUSP1 was responsible for regulation of ERK and p38 phosphorylation and controlled the IL-10 expression in Av17 stimulated macrophages. Thus, this systems biology approach showed that Av17 handles activation and deactivation pathways of MAP kinases to induce a regulatory phenotype in macrophages. Furthermore, a sensitivity analysis suggested that p38 affects ERK via DUSP, but ERK does not affect p38, revealing an autocrine negative feedback between the signalling components. This model prediction was also validated experimentally. In general, host immune regulation mechanisms should be robust against variations, *e.g.*, by parasites like *A. viteae*. This prompted me to test the robustness of the selected model against extrinsic and intrinsic variations using a Monte Carlo approach. I compared the previously selected model, which implements an integral feedback, with a model with transient feedback. The results support the notion that the model with integral feedback is more robust against intrinsic and extrinsic variations than the model with transient feedback, in the specific case of IL-10 production and regulation in macrophages after their exposal to immunomodulatory molecules of the parasite *A. viteae*. Taken together, based on a systems biology approach that successfully combines theoretical knowledge and experimental expertise this thesis proposes a mechanism that describes how the parasite *A. viteae* interacts with the macrophages of its host in order to induce the expression of the immunoregulatory cytokine IL-10.

Zusammenfassung

Der parasitische Nematode Acanthocheilonema viteae kann die Immunantwort seines Wirtes abschwächen, indem er in diesem die Produktion immun-regulatorischer Cytokine Interleukin-10 (IL10) induziert. In dieser Arbeit entwickelte ich spezifische mathematische Modelle um die Mechanismen der IL10 Regulation zu erforschen. Die Annahmen des Modells waren:

1. Av17, ein immun-modulatorisches Protein von A. viteae, zur Phosphorylierung der MAP-Kinasen ERK und p38 führt;
2. Av17 induzierte IL10 ist ERK und p38 abhängig.

Beide Annahmen waren in Übereinstimmung mit experimentellen Ergebnissen zur Aktivierung von ERK and p38. Weiter habe ich mehrere Signalregulationsmodelle getestet und eine Methode entwickelt, die theoretische und experimentelle Ansätze kombiniert. Von hier aus konnte ich ein Modell auswählen, dass unabhängige experimentelle Daten korrekt vorhersagt. Modelle selection identifizierten die Duale-Spezifizität Kinasen (DUSP) als integrale Rückkopplungsregulatoren dieses Systems. Eine Sensitivitätsanalyse zeigte, dass p38 durch DUSP, ERK beeinflusst, das Gegenteil aber nicht. Dieser Befund legt eine autokrine Rückkopplung der Signalkomponenten nahe, die auch experimentell bestätigt werden konnte. Allgemein mssen die immunoregulatorischen Mechanismen im Wirt robust gegen Strungen, z.B. durch Parasiten wie A. viteae, sein. Dies veranlasste mich mit Hilfe eines Monte-Carlo Ansatzes die Robustheit der ausgewählten Modelle gegenüber Variationen zu testen. Ich verglich das zuvor ausgewählte Modell und ein Modell mit transienter Rückkopplung. Das Resultat ließ darauf schließen, dass in diesem Fall die integrale Rückkopplung robuster gegenüber Variationen ist als eine transiente Rückkopplung. Insgesamt verbindet der systembiologische Ansatz meiner Arbeit erfolgreich theoretisches Wissen mit experimenteller Expertise um einen Mechanismus vorzuschlagen, der beschreibt, wie der Parasit A. viteae mit Makrophagen seines Wirtes interagiert, um IL10 Exprimierung zu induzieren.

Contents

1. Thesis overview

Parasitic nematodes, in particular *A.viteae*, express an immunomodulatory protein, a cystatin known as Av17, which binds to the macrophages of their host and induce IL-10 expression, to dampen the immune response of the host. The first question of this thesis was to understand which pathways lead to IL-10 production in Av17 stimulated macrophages. To answer this question, I constructed mathematical models, based on literature evidences and experimental data on IL-10 kinetics. These models suggest that Av17 activates the MAPKs ERK and p38 to induce IL-10 expression. The available experimental data, showed that IL-10 has transient dynamics in Av17-stimulated macrophages. Therefore, I included a feedback regulation mechanism in the mathematical model (chapter 4.1). I fitted three different models to the available experimental data on IL-10 kinetics (chapter 4.2). These three different models included a model without regulation, one other where IL-10 dephosphorylates ERK via phosphatase activation and another where IL-10 dephosphorylates ERK via kinase inhibition. Model fitting showed that a model without regulation is not able to fit the experimental data as well as the other two models with regulation. Therefore, I rejected this model (chapter 4.3) and did two more general and theoretical studies: I compared phosphatase activation with kinase inhibition (chapter 5) and I did a sensitivity analysis by perturbing specific nodes and checking their influence on the overall network (chapter 6). To check the assumption of the model, that Av17 addresses both ERK and p38 to induce IL-10 expression in macrophages, these MAPKs were experimentally tested. The experimental evidences showed that both ERK and p38 are transiently activated after Av17 stimulation, and that both MAPK are essential to induce IL-10 production, confirming this hypothesis of the model (chapter 9). To quantitatively validate the model predictions, I compared the *in silico* predictions of both models for ERK and p38. Both models suggest that ERK is transient and p38 is sustained, but the experimental data show that both kinases are transient (chapter 9.1), therefore, a model refinement was necessary to better represent the biological data.

This propelled me to the next question of my thesis: what are the signalling events that regulate ERK and p38 and, consequently, IL-10 dynamics? (chapter 8). I assumed that ERK and p38 can be regulated through three different ways: 1) IL-10 itself deactivates the MAPKs expression. 2) Phosphatases such as DUSPs deactivate the MAPKs. 3) An independent molecule (*i.e.*, a molecule not activated by Av17) deactivates the MAPKs. I investigated systematically the possible biologically significant combinations of regulation at the signalling level. This yielded 35 models with alternative regulation mechanisms (chapter 10). I fitted the models several times, using different fitting algorithms and different parameters constraints and I

ranked them using Akaike Information Criteria (AIC). The best model incorporated a regulation mechanism through IL-10. Experimental validation of IL-10 kinetics when IL-10 blocking antibodies are added, suggested that IL-10 did not play a role in regulating the MAPKs. Consequently, I selected the best ranked model that did not contain a regulation mechanism through IL-10. The selected model suggested that DUSP deactivates ERK and p38 (chapter 11). To verify the predicted role of DUSPs, experimental testing revealed that several DUSPs were upregulated in macrophages after Av17 treatment *in vivo* and *in vitro*. The kinetics of the *in silico* DUSP matched the experimental ones. With this model at hand, I did a sensitivity analysis to understand how perturbations on ERK or p38 affect the expression levels of P38, ERK, IL-10 and DUSP. Effectively, this analysis revealed that DUSP mediates crosstalk between individual MAPKs and this was supported by experimental evidences (chapter 11.4). Moreover, it revealed a successfull systems biology approach, where experiments interlace with mathematical modelling.

Then, in the third part of my thesis, I did a theoretical analysis on the robustness of this selected model, when compared with a model where the MAPK regulation happens through IL-10. The type of feedback distinguishes both models: the model with regulation by DUSP has an integral feedback and the model with regulation by IL-10 has a transient feedback (chapter 13). I studied the robustness of each model with respect to internal and external random perturbations using a Monte Carlo analysis (chapter 14), and the results suggested that integral feedback is more robust to internal and external random perturbations than transient feedback. To understand if the type of feedback was determinant on the robustness of the model, I proned the arms that provide feedback on both models and I did the same analysis presented in chapter 14. Results suggest that the feedback mechanism clearly provides robustness to the selected model (chapter 15). I therefore conclude that this parasite-host interaction has been shaped to be robust throughout their evolutionary history. Figure 1.1 depicts the whole process described above.

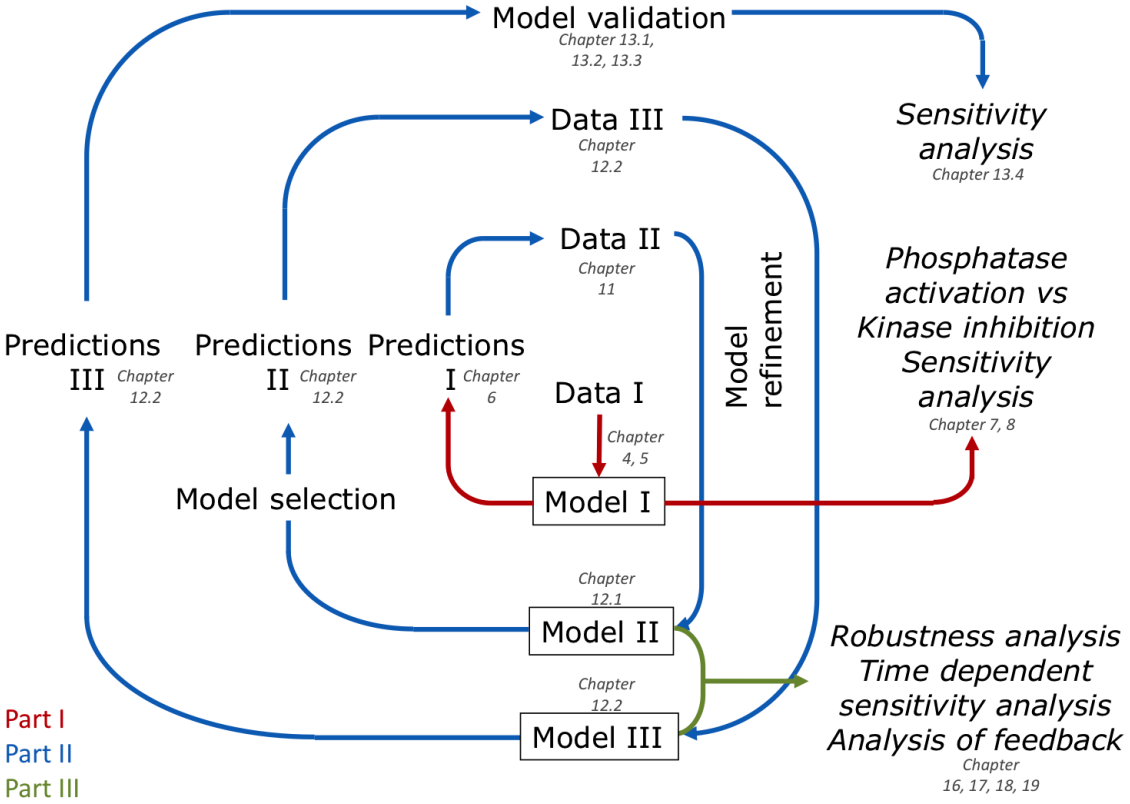

Figure 1.1.: Flow diagram describing the steps of this thesis.

2. General introduction

Biology is a complex science. It is amazing how nature generates life. From the interaction of two single cells and billions of years of evolution one complex organism emerges. When I ask myself "How does this happen?", I feel submersed in the sea of data and information available. Distilling knowledge from all this data and information can be a monstrous task. How can we learn from biology? The application of mathematics to understand that natural science can be a quaint and desirable approach for answering questions of this nature. Mathematics' etymology comes from the Greek, meaning *learning, study, science*. Applying mathematics in biology means using abstract mathematical tools to describe and eventually solve a concrete question in biology. The field of intersection between mathematics and biology is often termed systems biology. A definition-in-a-box for this emerging field in science is difficult to attain. According to Noble (2008),

> "Systems biology...is about putting together rather than taking apart, integration rather than reduction. It requires that we develop ways of thinking about integration that are as rigorous as our reductionist programmes, but different....It means changing our philosophy, in the full sense of the term"

2.1. General considerations on modelling

> "As far as the laws of mathematics refer to reality, they are not certain; and as far as they are certain, they do not refer to reality." - Albert Einstein.

Cells interact with each other, process signals and can change their phenotype according to their stimuli and, although surrounded by sometimes more noise than signal, build together a functional and interacting living organism.

Although mathematical modelling is one efficient and elegant way to test various hypotheses based on known evidences, according to Box and Draper (1987), "essentially, all models are wrong, but some are usefull". Mathematics provides a myriad of methods to formally represent a complex system, from its qualitative description to its quantification. Nevertheless, there is no unifying principle that can describe all processes in any system. The nature of the complex system and of the specific question the investigator wants to answer will dictate which method will best describe the problem at hand. Only so, mathematical modelling can improve the understanding of biological systems. In fact, mathematical models are approximations of reality. So,

there might be more than one model that describes the biological problem at hand. To select the best model, it is important to keep in mind some characteristics. First, how well can the model estimate the unknown parameters, given the experimental data? Second, overparametrization must be avoided. When generating a model, it is important to keep in mind the principle of parsimony: while keeping the number of parameters as low as possible, include all the components and reactions paramount to describe the system and where data are available. Model validation follows model selection: model predictions are compared with independent experimental data. Figure 2.1 depicts the steps of modelling generation, selection and validation.

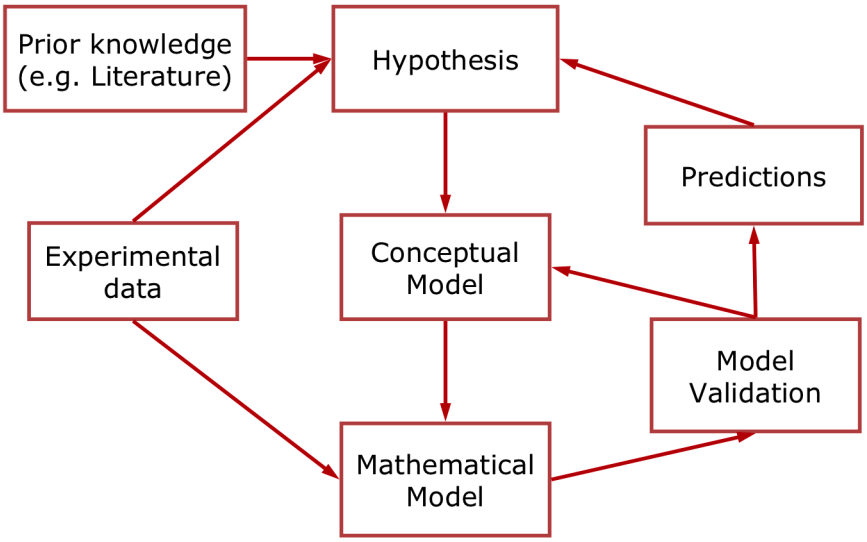

Figure 2.1.: Schematic representation of possible modelling steps. With prior knowledge based on observations/literature/experiments, the investigator proposes an hypothesis, that leads to the development of a conceptual model. From this conceptual model, a mathematical model that receives experimental data as input, can be developed. Model validation consists of comparing a model prediction with an independent experiment. If the model is not able to correctly predict the data, the model must be refined, leading to a redefinition of the conceptual model. The cycle composed by the triad "Conceptual Model - Mathematical Model - Model validation" is complete when the model can correctly predict the data and, now, the model predictions can be compared with the initial hypothesis.

Combining *dry lab* with *wet-lab* experiments has several advantages. First of all, the process of model conception brings together all the elements and their interactions, allowing a "bird's-eye" view of the problem at hand. Second, with a mathematical model it is possible to undergo simulations before doing *in vitro* experiments, which

saves time, money and, most importantly, the environment (Klipp et al., 2009). Finally, *in silico* experiments allow testing single element perturbations, which may not be possible or realistic to undergo *in vitro* or *in vivo*.

2.1.1. From the conceptual model to the mathematical model

Carefull thinking about the problem at hand is critical for delineating an approach to tackle the hypothesis being tested. Conceptual model development, containing prior knowledge is the first step. At this stage, theoreticians and experimentalists brain storm to distinguish between relevant and not so relevant information. This is dependent on the objective of the study. For instance, a model for studying the aerodynamics of a butterfly will not account for the colour patterns of its wings, which is a valid omission (Voit and Torres, 2002); this would be an important factor under the scope of biodiversity, for instance.

With the decision of the model framework comes the decision of the mathematical method to formalise the conceptual model. Models can be linear or nonlinear, deterministic or stochastic, static or dynamic. Methods like petri nets (Sackmann et al., 2009), boolean networks (Wittmann et al., 2009), ordinary differential equations (Figueiredo et al., 2009), game theory (Hammerstein, 1981) - which was specifically applied to understand host-parasite interactions (Renaud and de Meeüs, 1991) - linear programming (Figueiredo, 2005), difference equations (Koehncke et al., 2009) or statistical methods (Hilgenboecker et al., 2008) have been successfully applied to solve biological problems. Each method has its advantages and drawbacks, and the decision on the method is dependent on the question to answer and the available data. I used ordinary differential equations to develop the mathematical models present in this thesis.

Ordinary Differential Equations

Ordinary Differential Equations (ODE) are an effective way of mathematically describing the dynamics of a biochemical reaction network through its components and reactions. These equations allow the *in silico* representation of qualitative complex systems and the quantification of their parameters, providing insights into their emergent properties. According to Klipp et al. (2009), the dynamic behaviour of a deterministic system can be described, in vector notation, by the differential equations:

$$\frac{\mathrm{d}\,x}{\mathrm{d}\,t} = \dot{x} = f(\mathbf{x}, \mathbf{p}, t) \tag{2.1}$$

where $\mathbf{x} = (x_1, x_2, ..., x_n)^{\mathrm{T}}$, $f = (f_1, f_2, ..., f_n)^{\mathrm{T}}$ and $\mathbf{p} = (p_1, p_2, ..., p_m)^{\mathrm{T}}$. The vector $\mathbf{x}$ represents the elements of the network, $\mathbf{p}$ are the parameters and f are the functions that will normally represent the production and degradation reactions of element x_i.

Steady state

A system is considered in steady state when its amplitude variation over time is constant. The steady state is assumed for fast reactions (seconds or milliseconds), when compared to slow reactions, like cell growth. As the variations over time are constant, the differential equations of system 2.1 will be zero.

$$\frac{\mathrm{d}\,x}{\mathrm{d}\,t} = 0 \tag{2.2}$$

The law of mass action

The law of mass action is the simplest way of describing biochemical reaction kinetics. It states that the reaction rate is proportional to the concentration of the reactants, to the power of its molecularity (Klipp et al., 2009). Equation 2.3 represents the chemical equation of a reaction where one molecule of S_1 and one other of S_2 bind to form 2 molecules of P, where the number two is the molecularity of P.

$$S_1 + S_2 \rightleftharpoons 2P \tag{2.3}$$

In case the velocity of this reaction, i.e. its rate, obeys the law of mass action, the mathematical representation of the reaction rate is given by equation 2.3.

$$v = v_+ + v_- = k_+ \cdot S_1 \cdot S_2 - k_- \cdot P^2 \tag{2.4}$$

which can be described by the following ODE system:

$$\frac{\mathrm{d}}{dt}S_1 = \frac{\mathrm{d}}{dt}S_2 = -v \tag{2.5}$$

$$\frac{\mathrm{d}}{dt}P = 2v \tag{2.6}$$

To obtain the dynamic behaviour of the elements S_1, S_2 and P of the ODE system 2.6, this has to be integrated (Klipp et al., 2009).

Other types of biochemical kinetics

The reaction rate of a reaction might not only depend on the concentration of the substrates. In the case of reactions catalysed by enzymes, it has been observed that the reaction velocity saturates at a certain substrate concentration. The most famous rate law describing a saturation kinetics is the Michaelis-Menten kinetics, which describes an enzyme (E) catalised transformation of a substrate S into the product P, as described by the chemical equation 2.7.

$$E + S \rightarrow E + P \tag{2.7}$$

The Michaelis-Menten reaction rate is given by:

$$v = \frac{V_{max} S}{K_m + S} \tag{2.8}$$

where V_{max} is the maximum reaction rate and K_m is the half saturation constant that gives the concentration of substrate for which the reaction rate is half of its maximum. The Michaelis-Menten rate law can be mathematically derived from mass action kinetics using a quasi steady state assumption. For details, see Klipp et al. (2009); Goldbeter and Koshland (1981).

Another useful biochemical reaction rate law, is the Hill kinetic. It cannot be as easily derived from mass action principles as the Michaelis-Menten kinetics, but has been used widely to describe reactions that display phenomena of cooperativity. This means that molecules with higher affinity cooperatively act together, increasing the reaction rate in a non-proportional way. The biochemical reaction of Equation 2.7 can be mathematically described by Equation 2.9.

$$v = \frac{V_{max} S^h}{K_m^h + S^h} \tag{2.9}$$

where h is the Hill coefficient, that measures the cooperativity in a binding process, V_{max} is the maximum reaction rate and K_m is the half saturation constant that gives the concentration of substrate for which the reaction rate is half of its maximum.

2.1.2. Parameter estimation

A specific model can have different dynamic behaviours, depending on its parameter values. Therefore, a fundamental feature of parameter estimation is to minimise the error between the observed data (or experimental evidences) and the model predictions. There are several methods to estimate the parameters of a specific mathematical model. Please refer to Kühn (2010); Ljung (1999); Mueller (2002); Seber and Wild (2003) for a detailed description on parameter estimation methods. I used the software package COPASI (Hoops et al., 2006) to estimate the unknown parameters of my models. COPASI assumes that parameter estimation is an optimisation problem. The objective function of this problem is the squared distance between the measured experimental data and the model (SSR), represented in Equation 2.10.

$$SSR\left(\mathbf{p}\right) = \sum_{i=1}^{n} \omega_i \left(x_i - f_i\left(\mathbf{p}\right)\right)^2 \tag{2.10}$$

where ω_i are the weights of each element to be fitted, x_i are the experimental data points and p_i are the parameters to be estimated. The parameters are calculated to minimise the objective function $S\left(P\right)$. To solve this optimisation problem, COPASI uses global estimation algorithms. Global estimation algorithms have the advantage of avoiding local minima (Seber and Wild, 2003). In the particular parameter esti-

mation problem of the models studied in this thesis, I used two stochastic methods available in the referred software package, namely, simulated annealing and evolutionary programming. These are two typical global estimation algorithms used to estimate unknown parameters.

Simulated annealing is a popular global optimisation algorithm to calibrate unknown parameters inspired by statistical mechanics[1]. Evolutionary and genetic algorithms are optimisation methods inspired by biology and evolution. These algorithms generate a mutation (random perturbation) and construct a fitness function, which is used to filter out not useful mutations (Baldi and Brunak, 2001).

2.1.3. Model discrimination

Model discrimination follows two critical and essential steps in the investigation of a scientific problem: first, carefull thinking about the problem to solve is essential to have a well defined scientific question, second, well defined experimental design will provide good quality experimental data. At this stage, an investigator can define a model that expresses the information gathered by the data (Burnham and Anderson, 2002). With a core model at hand, alternative hypothesis can be considered.

According to Burnham and Anderson (2002), there are two main methods as a means of selecting a model: information criteria and hypothesis testing. Hypothesis testing has been used for longer than information criteria, but the former needs more computational power than the latter, specially when there are several high-dimensional candidate models. This renders information criteria a more attractive method to discriminate between models.

A very simple way to test how close the model reflects the experimental data is by simply calculating the distance between the experimental data point and the corresponding simulated point. This computationally light method, known as the sum of squared residuals and represented in Equation 2.10 has, however, heavy drawbacks: it does not take into account the complexity of the model neither if the overall dynamics of the experimental and the simulated values agree.

Therefore, to discriminate between candidate models, I used the Akaike Information Criterion.

Akaike Information Criterion

The Akaike Information Criterion (AIC) is a method of model discrimination that uses the Kullback-Leibler distance as a fundamental basis for model selection. The Kullback-Leibler distance denotes the information lost when model g is used to approximate model f. It assumes that the real model f is known, as well as its parameters (θ). In most of the situations, the data (y) are known, but the real model f is not and the parameters are estimated ($\hat{\theta}$). In these situations, the expected estimated Kullback-Leibler distance is used, instead of the minimal Kullback-Leibler distance

[1] Simulated annealing has its origin in mettalurgics, where certain metals must be cooled slowly, or annealed, and other must be cooled rapidly, or quenched.

over the set of candidate models. Aikaike found a relationship between Kullback-Leibler distance and the maximised log likelihood. This relationship is expressed in the formula 2.11 and has become known as the AIC.

$$AIC = -2\log\left(L\left(\hat{\theta}|y\right)\right) + 2k \tag{2.11}$$

The AIC is an effective way of selecting a "best approximating model" (Burnham and Anderson, 2002). It attributes a value to a model, calculated based on the weighted sum of squared residuals between estimated model curve and experimental data (SSR), number of parameters (k) and number of data points (n), rather than having a simple measure of the directed distance between two models. The AIC provides an estimate of the expected and relative distance between the fitted model and the (unknown) particular system that actually generated the observed data. Equation 2.11 can be simplified to equation 2.12, if all the candidate models assume normally distributed errors with constant variance (Burnham and Anderson, 2002).

$$AIC = 2k + n\left(\ln\frac{2\pi SSR}{n} + 1\right) \tag{2.12}$$

For a small sample size ($n > k - 1$), the AIC is corrected to the expression:

$$AIC_c = AIC + \frac{2k(k+1)}{n-k-1} \tag{2.13}$$

It is valuable to emphasise here the importance of carefull thinking when defining the candidates models, because AIC provides a *relative* measure of the goodness of one model, compared to the remaining models in the set. This best model might poorly describe the real system under study.

2.2. Noise in biology

Biological data are noisy. Cells can distinguish between noise and signal, filtering out the noise, even with a weak signal to noise ratio. This feature reveals robustness to variability in biological interactions.

2.2.1. Robustness of biological systems

Defining robustness is a challenge for today's biologists. A robust system keeps its performance under a wide range of conditions even if a part of the system fails. Living organisms sense changes in their environment and adapt to them, hence, sensitivity and robustness walk hand in hand. On the one hand, robustness is the insensitivity of a particular property of the system (Yi et al., 2000), on the other hand, the ability of a living system to survive depends on how quickly it is able to sense changes in the environment, or a failure in a module, and adapt to it by activating alternative modules as fast as possible. Robustness is an important property of

biological systems, because it assures the function of a biological system, in spite of parameter perturbations (Alon, 2007). Negative feedback mechanisms provide robustness to perturbations in the internal components of the system or to extrinsic noise (Sauro and Kholodenko, 2004; Klipp et al., 2009).

In Part III of this thesis, I studied the robustness of two mathematical models, by analysing the output response of the system when this was subject to perturbations in: 1. its internal components (intrinsic noise), 2. in the input (extrinsic noise).

I simulated intrinsic noise by applying the formula:

$$\tilde{p}_i = U\left[p_i \cdot 0.8, p_i \cdot 1.2\right] \tag{2.14}$$

where $\tilde{p}_i$ is the perturbed parameter value, which is sampled from an uniform distribution, $U[a, b]$. This distribution is limited between $a = p_i \cdot 0.8$ and $b = p_i \cdot 1.2$.

To simulate the extrinsic noise, I used the following formula:

$$s(t) = s_0[1 + \xi(t)] \tag{2.15}$$

where $\xi(t)$ is a Gaussian distribution with mean=0 and standard deviation=0.1 and s_0 the initial amplitude value.

Stochastic modelling permit to investigate the effect of intrinsic and extrinsic noise. A model with stochastic simulations allows the simulation of random phenomena (Wilkinson, 2006). It is described by a set of random variables, each with a certain probability of happening in a defined time interval. Each random variable describes different realisations of the mathematical model. These independent random variables (or white noise) are, commonly, independent and normally distributed variables (Ljung and Glad, 1994). Hence, a stochastic system has a set of solutions instead of having a single solution.

Monte Carlo analysis allows the simulation of these different realisations of a specific variable X of the model at hand (Wilkinson, 2006). These computational methods rely on defining an universe of possible inputs and randomly sampling from this set of inputs using a probability distribution. The output is then deterministically calculated for each element of the universe of inputs. This creates then a set of values that will constitute the final result of the Monte Carlo analysis.

2.2.2. General notions on feedback

Feedback is a mechanism where the output of a system feeds back into the input.The aim of a feedback loop is to control, or tune, the present and future output of a system using the output information of the past. The concept of feedback is present in our everyday life and in such discrepant fields as engineering, economics and finances, politics, education and life sciences.

Feedback motifs are present in biology and life sciences in the most different forms and scales. This concept is present in molecular motifs like signalling cascades, as well as in ecological networks and climate science, among many others.

Positive feedback *vs.* negative feedback

There are different forms of feedback. This section briefly distinguishes positive and negative feedback. Positive feedback loops provide an output with high gain and low stability and, eventually, bistability, whereas negative feedback loops provide an output with low gain and high stability. Both types of feedback can lead to oscillations.

One example of negative feedback in biology is homeostasis[2]. Positive feedback can be observed, for instance, in the process of lactation.

Integral feedback

Integral feedback is a mechanism, commonly used in control theory, that ensures that the system tracks the desired response, even in the presence of noise (Yi et al., 2000). A system with this type of feedback integrates over time the error between the desired and the effective output (Alon, 2007). This ensures the desired output level, regardless of the variations in the parameters. This is an effective way of providing robustness in a system, by adaptation or desensitisation. Figure 2.2 shows the block diagram of a general system with integral feedback.

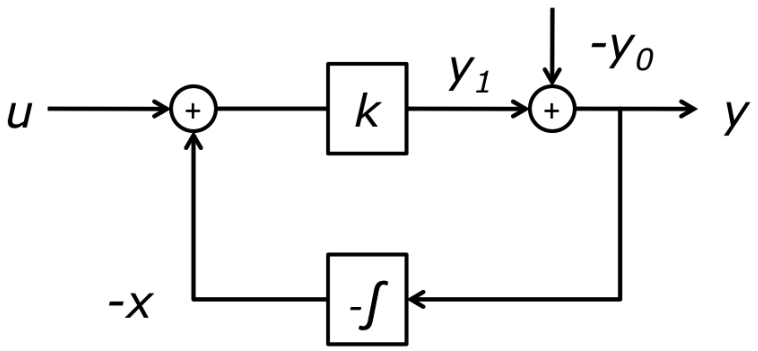

Figure 2.2.: Block diagram of a control system that implements integral feedback. u represents the input, y_1, the output before the feedback, y_0 is the desired output, y is the difference between both and x is this integrated difference.

[2]The term of homeostasis was coined by Cannon (1932), but its concept was studied before by Claude Bernard, as the *milieu intérieur*.

$$\dot{x} = y \tag{2.16}$$
$$y = k\,(u - x) - y_0 \tag{2.17}$$

This guarantees perfect adaptation. Theoretically, $y(t) \to 0$ when $t \to \infty$. There are two ways of achieving perfect adaptation: through integral feedback, as explained above, or through fine-tuning (Alon, 2007). In this method, the parameters are tuned for the system to yield the desired output, *i.e.*, $y(t) \to 0$ when $t \to \infty$. This method has two drawbacks: is harder to implement and the parameters are highly sensitive to allow this fine tuning. Indeed, one characteristic of integral feedback is to provide robustness. According to Alon (2007), '...biological circuits have robust designs such that their essential function is nearly independent of biochemical parameters that tend to vary from cell to cell." Regulation motifs may provide robustness against cellular noise.

2.2.3. Signalling networks as regulation motifs

Signal transduction is the process by which a cell transforms an initial signal or stimulus to one other, through the action of specific enzymes that catalyse specific reactions. Signal transduction pathways play a pivotal role fighting against invading pathogens. Mitogen activated protein kinases (MAPK) cascades transduce an extracellular signal and regulate specific intracellular activities, which are dependent on the extracellular stimulus. These highly conserved cascades respond to a myriad of stimuli and mainly control gene expression and regulation. Nevertheless, the complex interactions that control the different activities of the MAPK cascades are not yet fully understood. Mathematical models have been used to better comprehend the mechanisms behind the different behaviours of the same cascade. Heinrich et al. (2002) implemented mathematical models for different topologies of the receptor-stimulated kinase/phosphatase signalling cascades and analysed key parameters that characterise the signalling pathways (signal amplitude, signalling time and signal duration). Sasagawa et al. (2005) constructed a mathematical model of Extracellular signal-regulated kinases (ERK) signalling based on literature findings and predicted ERK dynamics in response to increases of the epidermal growth factor (EGF) and nerve growth factor (NGF). Both studies show that the same MAPK pathway can have a sustained or transient activation, as experimentally shown by Marshall (1995) and Santos et al. (2007).

Signalling cascades have "built-in" control functions at different levels that control the signal strength and duration. These cascades activate phosphatases that implement a negative feedback regulation and limit the cell response. Regulators like dual specificity phosphatases (DUSPs) limit the response of macrophages to extracellular stimuli (Chi et al., 2006). Specifically, DUSP-1 exerts a feedback control on the signalling cascades p38, ERK and JNK (Wang and Liu, 2007; Li et al., 2009). Activated ERK and P38 induces the production of DUSP-1 (Ananieva et al., 2008;

Hu et al., 2007), which in turn deactivates ERK and P38, respectively, accounting for the transient behaviour of this MAPK (Wang and Liu, 2007; Li et al., 2009).

This phosphatase is a major regulator of the immune response and controls the production of pro- and anti- inflammatory cytokines (Chi et al., 2006).

2.2.4. Sensitivity analysis

Mathematical modelling adds explanatory power to the experimental analysis, when studying the overall impact of perturbations on the biological network. *In silico* analysis of a biological network allows the investigator to perturb each element of the network and observe the impact of this perturbation in the other elements. This type of study would be a practically impossible task to undertake *in vivo* or *in vitro*: it is a question of time, money and resources.

The mathematical formula to calculate the sensitivity of an element to a specific perturbation, is the following:

$$S = \frac{\Delta O}{O} \cdot \frac{p}{\Delta p} \tag{2.18}$$

(O is the output and p is the perturbed parameter. $\Delta\{O, p\}$ is the difference between the perturbed and unperturbed values of $\{O, p\}$). If $|S| = 1$, means that the ratio of perturbation in p is equal to its effect in the output O. If $|S| >> 1$, then the system is sensitive to perturbations in the specific parameter p. The sign of S reflects the effect of the perturbation in the output. When S is positive, an inhibition of p will reflect an inhibition of O, else, if S is negative, an inhibition of p means that O will be amplified, whereas an amplification of p translates into an inhibition of O.

2.2.5. Time-dependent sensitivity analysis

Time-dependent sensitivity analysis (TDSA) was proposed by Ingalls and Sauro (2003) and describes the system's sensitivity along a temporal trajectory. This method is a derivation of the Metabolic Control Analysis (MCA) theory, which analyses the distribution of control between the elements of a network in steady state (Heinrich and Rapoport, 1974). Nevertheless, in transient or oscillatory systems, it might be important to study the sensitivity along non-steady trajectories (Ingalls and Sauro, 2003). Given an initial condition $s\,(0)$ and a set of parameter values p_0, which form a vector q_0, the time-varying concentration sensitivity is given by:

$$R^{s_i}_{q_j}(t) = \frac{\partial s_i(t,q)}{\partial q_j|_{q_j=q_{j_0}}} = \lim_{\Delta q \to 0} \frac{\partial i(t, q + \Delta q_j) - s_i(t,q)}{\Delta q_j} \tag{2.19}$$

These response coefficients can be scaled (Kühn, 2010):

$$\tilde{R}^s_q(t) = \frac{q_j}{s_i(t,q)} \frac{\partial s_i(t,q)}{\partial q_j}|_{q_j=q_{j_0}} \tag{2.20}$$

The coefficients are defined by the ordinary differential equation:

$$\frac{d}{dt}\frac{\partial s(t,q)}{\partial q} = N\left(\frac{\partial s(t)}{\partial q}\frac{\partial v(t)}{\partial s} + \frac{\partial v(t)}{\partial q}\right) \tag{2.21}$$

where N is the stoichiometric matrix and $\frac{\partial s(t)}{\partial q}$ and $\frac{\partial v(t)}{\partial s}$ are the concentration and parameter elasticities, respectively (Ingalls and Sauro, 2003; Kühn, 2010). MCA has proven to be a valid method on interpreting the control distribution of a system in steady state. A way of analysing the control distribution along a time trajectory, renders TDSA a valuable tool for the analysis of transient systems.

2.3. General considerations on the immune response to parasites

2.3.1. The immune system at a glance

Immunity has its etymology in the Latin word *Immunitas*, which meant exemption from civic duties and legal prosecution, offered to Roman Senators (Abbas et al., 2000). Today, according to Murphy et al. (2008), "immunology is the study of the body's defense against infection". This defence happens at the cellular and molecular level. The network of cells and molecules that provide immunity is the immune system, and their coordinated response to infection is the immune response. The early immune response to infection by potential pathogens is known as innate immunity. It takes place right after infection and has low specificity: reacts in the same way to different types of infection and is the gatekeeper of the adaptive immune response (Medzhitov and Janeway, 2000). This response is not specific to any pathogen nor provides lasting immunity. Nevertheless, it discriminates between self and nonself. Phagocytes involved in the adaptive immune response (macrophages, neutrophils and dendritic cells), recognise specific patterns of molecular structure and simple molecules, which are common to many pathogens but are not present on the body's own cells. These evolutionary conserved patterns are known as pathogen-associated molecular patterns (PAMPs), and the referred immune cells recognise them through receptors known as pattern recognition receptors (PRRs) (Murphy et al., 2008). Specifically, macrophages are in the first line of defence, after the pathogen breaks the physical and chemical barriers imposed by the skin, epithelia and gut. Through the PPRs, macrophages recognise the infecting agents with PAMPs and are activated in order to engulf these infective agents. Macrophages secrete specific cytokines and chemokines, which will signal to and attract other cells containing the specific receptors.

The innate immune system mounts an attack against the nonself and this triggers the adaptive immune response.

The adaptive immune response, present only in vertebrates, takes place between one or five days after infection. This response is more efficient on eliminating infec-

tion than the innate immune system, because is directed to the specific pathogen. Lymphocytes are the players of the adaptive immune response. These cells have on their surface highly specialised antigen receptors, which can recognise and respond to the specific antigen (Murphy et al., 2008).

The cells of the immune system arise from pluripotent hematopoietic stem cells, in the bone marrow. These cells can derive into lymphoid progenitors or myeloid progenitors. The cells that characterise the adaptive immune response and derive from lymphoid progenitors, are the T cells and the B cells [3]. T cells and B cells possess antigen receptors and are distinguished by their differentiation sites. T cells have their origin in the thymus and B cells, in the bone marrow. The B cells mediate the humoral arm of the adaptive immune response and are responsible for the production of antibodies (which are highly specific and have memory). The T cells differentiate into effector T-cells, with a variety of functions that fall in three classes: killing, activation and regulation (Murphy et al., 2008). I will focus on the Helper T cells, which stimulate B cells to differentiate and produce antibodies, or can also activate macrophages to become more efficient on the phagocytosis of pathogens. Helper T cells can polarise to different types of cells, *e.g.* Th1, Th2, Tregs or Th17. In the next section, I will focus on Th1 and Th2 cells.

The classical Th1/Th2 paradigm

The innate and/or adaptive immunity takes the decision to polarise T cells to, *e.g.*, Th1, Th2, Tregs or Th17 cells, depending on the specific cytokine environment (Spellberg and Edwards, 2001), controlling the effector immune response (O'Garra and Vieira, 2007).

The Th1 cells stimulate type I immunity, profiled by the production of IL-2, IFN-γ, lymphotoxin-α and phagocyte activity. Production of IL-4, IL-5, IL-9, IL-13 and IL-10 characterises the Th2 response, which stimulates the type II immunity, with high levels of antibody production (Spellberg and Edwards, 2001). The definiton of Th1 or Th2 cells depends on the expression of IL-4 and IFN-γ. Th1 cells express IFN-γ but not IL-4 and Th2 cells express IL-4 but not IFN-γ (Spellberg and Edwards, 2001).

Nevertheless, these responses are not exclusive, meaning that in specific situations, Th1 cells can mount a type II immunity response (Spellberg and Edwards, 2001). For instance, Th1 cells can produce IL-10 to regulate themselves (O'Garra and Vieira, 2007).

Interleukin-10

Interleukin-10 (IL-10) is a cytokine with immunoregulatory properties. It is at the interface between the adaptive and the innate immune response and executes its function on wide range of immune cells (Moore et al., 2001; Asadullah et al., 2003).

[3] Natural Killer cells (NK cells) also derive from lymphocytes, but are part of the innate immune system. These cells lack antigen specificity.

IL-10 was first described as cytokine synthesis inhibitory factor (CSIF) from mitogen stimulated T helper 2 cells inhibiting pro-inflammatory cytokine production such as interferon-gamma in T helper 1 cells (Fiorentino et al., 1989; Zdanov et al., 1995). Later studies revealed that many other cell types from the innate and adaptive arm of the immune response can produce IL-10 under certain conditions. These cells include monocytes, macrophages, B cells, eosinophils and mast cells (Asadullah et al., 2003) and more recently also various IL-10 producing T cell subsets have been described, including different regulatory T cell populations, CD8+ T cells and Th1 cells (Vieira and O'Garra, 2007). Macrophages, in particular, are a source and target of this cytokine. One important function of IL-10 is to control and ultimately annihilate excessive immune responses during infections and autoimmunity (Moore et al., 2001; Asadullah et al., 2003). It inhibits the production of pro-inflammatory cytokines in macrophages and other cell types (Vieira and O'Garra, 2007). This moderates for instance overshooting T-cell responses during inflammation which otherwise may lead to immunopathological damage (Moore et al., 2001; Couper et al., 2008). IL-10 deficient mice develop spontaneous colitis under normal conditions (Kühn et al., 1993) and are more prone to immunopathology in general, being able to clear infection by intracellular pathogens more effectively than wild type mice (Schnoeller et al., 2008; Vieira and O'Garra, 2007). These observations highlight the importance of IL-10 as a cytokine with immunoregulatory properties.

2.3.2. Parasitic nematodes and their interference with the immune system

Parasites are organisms that live in or on a different organism, obtaining sustenance from it and thus damaging it (Lucius and Loos-Frank, 2008). Parasitic nematodes, in particular, are highly specialised multicellular organisms that dwell in specific niches within their hosts. In all of these sites, the host steadily attacks the parasites with various immune responses. However, many parasitic nematode species reach life spans of years. This fact is due to elaborated immune evasion mechanisms set up by the parasitic nematodes. *Onchocerca volvulus*, for example, is a parasitic nematode that causes the tropical disease River Blindness and is transmitted to its human host by the arthropode *Simulium yahensecan*. This parasite remains in its host for more than 10 years (Plaisier et al., 1991) and affects around 20 million people wordwide. The rodent nematode *Acanthocheilonema viteae* is a model organism, used to study basic questions of host-parasite interaction, such as host immune responses and parasite immune evasion mechanisms (Figueiredo et al., 2009). Infections by parasitic nematodes induce a type 2 T helper cell (Th2) response, which can efficiently kill parasitic nematodes by triggering immune effector mechanisms. Nevertheless, these organisms seem to modify this immune response and vigorous effector mechanisms do not develop. One way to dampen the immune effector mechanism is to stimulate the production of anti-inflammatory cytokines such as IL-10. This cytokine minimises inflammatory reactions and, as a consequence, compromises the ability of the host to kill the parasites. This balance allows survival of parasites and hosts. Blunted

Th2 responses may represent a benefit for the host. The ensuing downregulation of effector mechanisms decreases diseases that result from an imbalance of the immune system, like autoimmune responses and allergies. Indeed, often a correlation between allergies or auto immune diseases, and the lack of exposure to infective agents, such as parasites has been observed (Araujo and de Carvalho, 2006; Carvalho et al., 2006). Moreover, long-lasting worm infections can change the regulation of the immune system, with a tendency to reduce allergies (Lucius and Loos-Frank, 2008). These facts can be a breakthrough in developing pharmaceuticals to fight immune disorders. Accordingly, it is of major importance to identify the molecules and pathways that modulate host immune responses.

A. viteae cystatin (Av17) is a cysteine protease inhibitor that is constantly secreted by the nematode. It has important functions in immune processes such as antigen processing and presentation (Hartmann and Lucius, 2003; Gregory and Maizels, 2008). Furthermore, recombinant *A. viteae* cystatin (rAv17) has recently been shown to specifically inhibit allergic and inflammatory responses in mice (Schnoeller et al., 2008). In this scenario, rAv17 induced IL-10 production in macrophages as a key element of immunomodulation. To understand the mechanisms leading to IL-10 production in Av17 stimulated macrophages, and the consequent modulation of the host immune response, I developed several mathematical models.

Part I.

IL-10 production and regulation in macrophages stimulated with an immunomodulator of parasitic nematodes

3. Synopsis

This part is an extended version of Figueiredo et al. (2009). The experiments here referred, in vitro IL-10 protein and il-10 mRNA kinetics, were conducted in the Department of Parasitology, Humboldt-Universität, Berlin. The experimental details are described in Figueiredo et al. (2009).

Parasitic nematodes modulate the immune response of their hosts by inducing immunoregulatory cytokines such as IL-10. To determine the mechanisms of IL-10 production in Av17 stimulated macrophages, I developed mathematical models of IL-10 production and regulation. I proposed that IL-10 expression requires stimulation of the MAP kinases ERK and p38 and that a negative feedback mechanism, acting at the signalling level, is responsible for transient IL-10 production. Specifically, I implemented two valid models with negative feedback that account for the experimental data of *in vitro* IL-10 kinetics. I assumed that this feedback can be achieved by kinase inhibition or phosphatase activation. I refer to kinase inhibition if the feedback regulation is achieved by inhibiting the reaction that phosphorylates ERK. I refer to phosphatase activation if the feedback regulation is achieved by promoting the reaction that dephosphorylates ERK. I did a comparative study on these two types of feedback by varying the amplitude signal (Av17) and comparing the kinetics of the different elements of the network. I also studied the concepts of maximal amplitude, width at half amplitude, steady state, integral and overshoot when the models were faced with input variations. Moreover, to understand the influence of one element of the network on one other, I performed a sensitivity analysis (eq. 2.18) by varying each parameter and checking its influence on the steady state of phospho -ERK phospho -p38 and IL-10.

4. Modelling IL-10 production and regulation in macrophages exposed to Av17

4.1. Construction of the mathematical models

The promoter region of the *il-10* gene in macrophages contains binding sites for several transcription factors, of which SP1 and STAT3 are examples (Lucas et al., 2005). These transcription factors regulate the gene expression and are controlled by ERK (Yang et al., 2007) and p38 (Gee et al., 2007). In a sequential mechanism, the ERK signalling cascade remodels the chromatin of the *il-10* promoter region by phosphorylating its Histone 3 (H3) sites and the p38 signalling pathway activates the transcription factors SP1 and STAT3 (Lucas et al., 2005). These transcription factors bind to the phosphorylated H3 sites and thereby initiate *il-10* gene expression (Zhang et al., 2006). Moreover, CREB induces IL-10 expression in macrophages (Cao et al., 2006) and monocytes (Gee et al., 2007). Macrophages express the IL-10 receptor complex on their surface, suggesting a feedback regulation by IL-10. A negative autoregulatory role for IL-10 is suggested for LPS or lipoprotein stimulated IL-10 production in monocytes and monocyte-derived macrophages (de Waal Malefyt et al., 1991; Giambartolomei et al., 2002; Staples et al., 2007; Ward et al., 2005). Based on these evidences, I assumed that Av17 activates the signalling pathways ERK and p38 in macrophages, leading to IL-10 production, and I hypothesised that IL-10 regulates itself via a negative feedback mechanism. In this mechanism, secreted IL-10 binds to the macrophages and deactivates the ERK signalling pathway. This is represented in Figure 4.1.

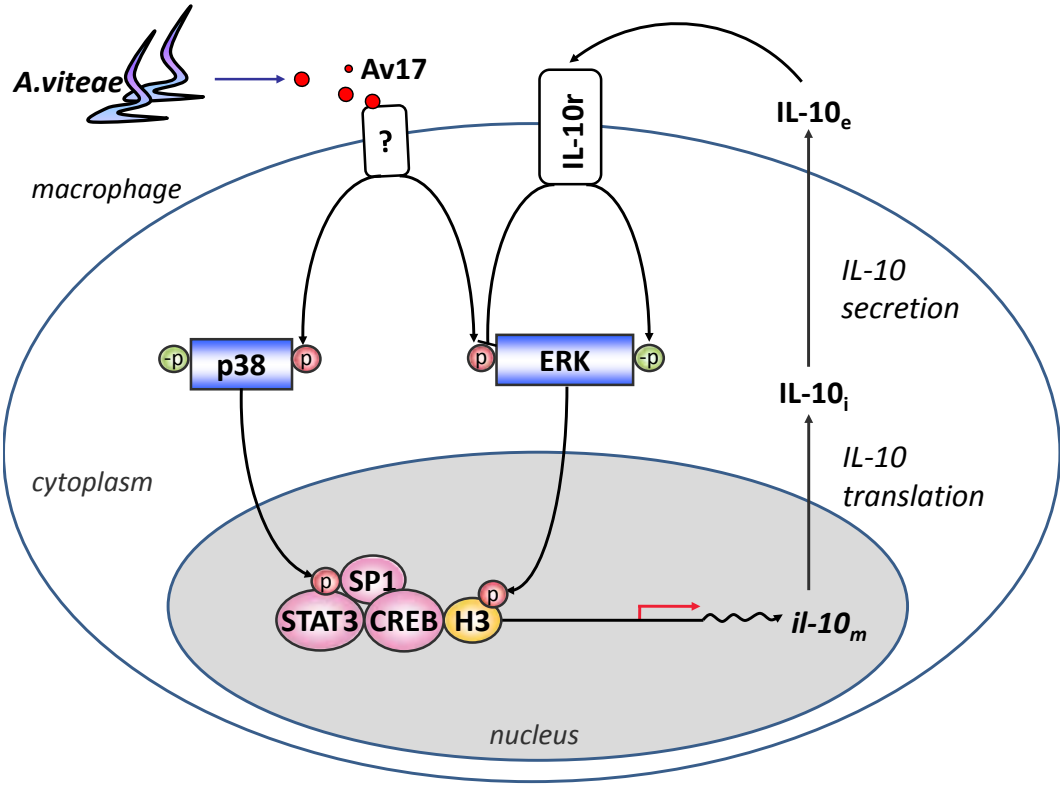

Figure 4.1.: Schematic representation of IL-10 induction and regulation. Av17 binds to the macrophage and activates the p38 signalling pathway (that will activate the transcription factors SP1 and STAT3) and the ERK signalling pathway (that will phosphorylate the H3 site of the *il-10* promoter region). These transcription factors bind to this promoter site, inducing *il-10* mRNA expression. IL-10 protein is subsequently produced and secreted. I assumed that extracellular IL-10 binds to the IL-10 receptor of macrophages (IL-10r) and deactivates phospho-ERK, either by kinase inhibition or by phosphatase activation, hence regulating its own production in a negative feedback loop.

With these evidences, I developed mathematical models on IL-10 regulation in Av17 stimulated macrophages. These models reflect two different hypothesis about regulation mechanisms, namely, that regulation can be achieved by kinase inhibition or phosphatase activation. Model development was based on the principle of parsimony. In order to keep the number of parameters as small as possible, I included only those components and processes that I considered paramount to describe the systems dynamics and where data were available (see Table 4.1 and Figure 4.2 for all components and reactions included in the models).

Process	Equation
ERK phosphorylation on Av17 stimulation and constitutive dephosphorylation	Model 1: $v_1 = k_1 \cdot [ERK_t - ERK_p(t)] \cdot j \cdot s(t) \,/\, \left[1 + k_f \cdot IL10e(t)^h\right]$ $v_2 = k_2 \cdot ERK_p(t)$ Model 2: $v_1 = k_1 \cdot [ERK_t - ERK_p(t)] \cdot j \cdot s(t)$ $v_2 = k_2 \cdot ERK_p(t) \cdot IL10e(t)^h$
P38 phosphorylation on Av17 stimulation and constitutive dephosphorylation	$v_3 = k_3 \cdot j \cdot s(t) \cdot [p38_t - p38_p(t)]$ $v_4 = k_4 \cdot p38_p(t)$
Transcription factor activation and constitutive deactivation	$v_5 = k_5 \cdot A_t \cdot p38_p(t)$ $v_6 = k_6 \cdot A_p(t)$
Histone phosphorylation and dephosphorylation	$v_7 = k_7 \cdot ERK_p(t) \cdot H3(t)$ $v_8 = k_8 \cdot H3_p(t)$
Complex formation, constituted by the transcription factor bound to the phosphorylated H3 site and constitutive disaggregation	$v_9 = k_9 \cdot H3_p(t) \cdot A_p(t)$ $v_{10} = k_{10} \cdot H3A_p(t)$
Induction of *il-10* mRNA expression	$v_{11} = k_{11} \cdot H3A_p(t)$
Degradation of *il-10* mRNA	$v_{12} = k_{12} \cdot IL10_m(t)$
Transcription and translation to IL-10 intracellular protein	$v_{13} = k_{13} \cdot IL10_m(t)$
Degradation of IL-10 extracellular protein	$v_{14} = k_{14} \cdot IL10_e(t)$

Table 4.1.: Description of reactions and its equations for both models of IL-10 production and regulation. $s(t)$ is the stimulus (input) and corresponds to Av17. j corresponds the the different concentrations that Av17 may have.

Assumption	$ERK_t = ERK(t) + ERK_p(t)$ $p38_t = p38(t) + p38_p(t)$

Table 4.2.: Assumptions for the equations' system of table 4.1.

$$\frac{dERK_p}{dt} = v_1 - v_2 \tag{4.1}$$
$$\frac{dp38_p}{dt} = v_3 - v_4 \tag{4.2}$$
$$\frac{dA_p}{dt} = v_5 - v_6 + v_9 - v_{10} \tag{4.3}$$
$$\frac{dA}{dt} = v_6 - v_5 \tag{4.4}$$
$$\frac{dX0}{dt} = v_8 - v_7 \tag{4.5}$$
$$\frac{dX1}{dt} = v_7 - v_8 + v_9 - v_{10} \tag{4.6}$$
$$\frac{dX2}{dt} = v_{10} - v_9 \tag{4.7}$$
$$\frac{dIL10_m}{dt} = v_{11} - v_{12} \tag{4.8}$$
$$\frac{dIL10_e}{dt} = v_{13} - v_{14} \tag{4.9}$$

I propose two distinct feedback mechanisms via IL-10 (model 1 and model 2) and compare it to a model with no feedback (model 0). Model 1 assumes promotion of ERK dephosphorylation via IL-10 (kinase deactivation). Model 2 assumes inhibition of ERK phosphorylation via IL-10 (phosphatase activation). The components and reactions of these models are described in Table 4.1. I have implemented these models using ODEs (equations' system 4.9 and reactions' description at Table 4.1) and fitted them to experimental data on *il-10* mRNA and IL-10 protein time series, and *il-10* mRNA half life.

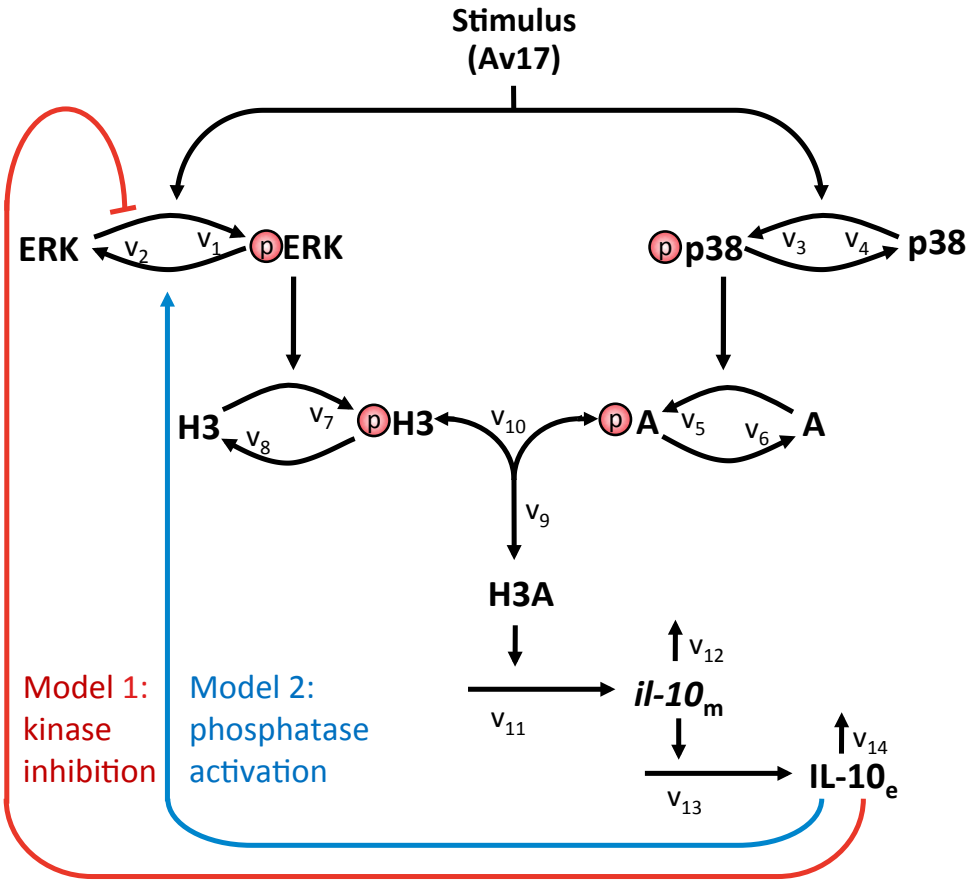

Figure 4.2.: Mathematical model of IL-10 production and regulation. The model receives the input stimulation (Av17) as a step function (from 0 to 1), which activates ERK and p38. Phospho-ERK phosphorylates the H3 sites of the *il-10* promoter region. Phospho-p38 activates the set of transcription factors (A) necessary to induce *il-10* gene expression (il-10m). Transcription and translation take place. IL-10 is secreted by the macrophage (IL-10e) and promotes the feedback regulation. I hypothesised that extracellular IL-10 (IL-10e) binds to the macrophage and deactivates phospho-ERK, either by kinase deactivation (model 1) or by phosphatase activation (model 2). These two models have in common the regulation by negative feedback.

4.2. Model fitting to the data

The different models were fitted to experimental data on IL-10 protein and *il-10* mRNA time series and *il-10* mRNA half-life (please refer to (Figueiredo et al., 2009) for the experimental details). Figure 4.3(a) shows IL-10 protein and *il-10* mRNA time series. The maximum relative *il-10* mRNA expression was measured at 2 h after stimulation. After 4 h, the mRNA levels reached background levels again. IL-10 protein in the cell supernatant was detectable after 2-3 h, showed a steady increase over time until 8 h, and declined after 14-24 h.

I fitted the models to the data using a global optimisation procedure, described in section 2.1.2 and using the software COPASI (Hoops et al., 2006). The details of the particular fits can be found in Appendix A.2. The different regulation models fit the experimental data for *il-10* mRNA and IL-10 secreted protein. The Hill coefficient of model 2, expressed as h in equation v_2 of the respective model, yielded a value close to 1. Therefore, in order to minimise the number of parameters, I did not consider the parameter h. Figures 4.3(b) 4.3(c) and 4.3(d) show the model fittings to the experimental data of Figure 4.3(a).

These data show that model 0 is not able to fit the decrease of IL-10 production observed experimentally, keeping it at a sustained level, whereas the models with feedback regulation (model 1 and model 2) can fit the increase and decrease in IL-10 levels. For a complete listing of the best fitting parameters, constraints and initial conditions for each model, see Appendix A.3

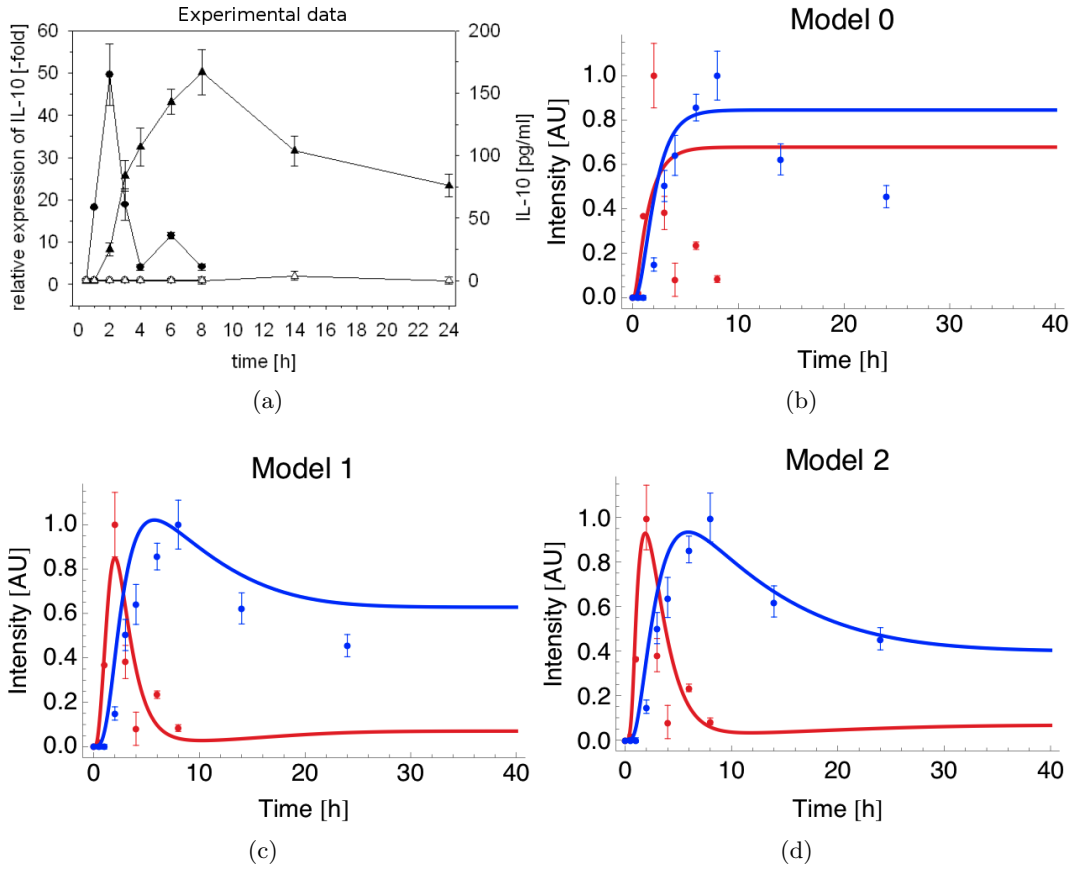

Figure 4.3.: (a) IL-10 protein (white dots) and *il-10* mRNA (black dots) kinetics after stimulation of macrophages with the immune modulator Av17. The experimental details can be found in Figueiredo et al. (2009). (b-d) Fitted (lines) and experimental values (dots) for IL-10 secreted protein (maximum value at 8 h) and *il-10* mRNA (maximum value at 2 h). (a) Model 0: no feedback. (b) Model 1: inhibition of ERK phosphorylation via IL-10. (c) Model 2: activation of ERK dephosphorylation via IL-10. The models fit the data for both regulation hypotheses. Model 0 follows the production of IL-10, but cannot follow the decrease, because there is no regulation, leading to cumulative production of IL-10, which reaches a steady state.

4.3. Model selection

The fitting results allowed to select models. The experimental data (Figure 4.3(a)) show that IL-10 production in macrophages after Av17 stimulation is transient. This decrease in IL-10 production is an evidence for a regulation mechanism by negative feedback. Therefore, I discarded model 0, which includes no regulation and presents sustained IL-10 production. Moreover, the disagreement between fitted and experimental values is very high (Figure 4.3). I calculated the Akaike Information Criterion (AIC)[1] and the residual sum of squares (RSS) between the estimated values and the experimental data for the three models, and model 0 yielded the highest value (compare Table 4.3). I discarded model 0 and focused on the models of regulation via IL-10 (model 1 and model 2). I compared the two different regulation mechanism that each models implements, kinase inhibition (model 1) with phosphatase activation (model 2).

Model	AIC	RSS
0	-13.16	0.37
1	-31.44	0.15
2	-41.74	0.13

Table 4.3.: AIC and RSS for the three models. Model 0 yields the highest value and model 2 the lowest value.

[1]For details about this criterion, please refer to Section 2.1.3

5. A comparative study of kinase inhibition and phosphatase activation

Here I investigated the feedback properties that distinguish negative regulation by kinase inhibition (model 1) and negative regulation by phosphatase activation (model 2).

According to Kholodenko (2006), phosphatases are homogeneously distributed in the cytoplasm, whereas kinases are in the supra-molecular structures or in the cell membrane. I assume that the regulation mechanism of the biological system can switch from a kinase inhibition to a phosphatase activation mechanism, depending on its position in the cell and the availability of kinases or phosphatases.

I changed the input level of Av17 and calculated the amplitude, integral, duration, steady state and overshoot of the simulated IL-10 time course to understand how kinase inhibition and phosphatase activation can be distinguished.

5.1. Level of the input stimulus controls the output signal dynamics

The parasite load can vary within the host. Consequently, the concentration of secreted Av17 may also vary. To check wether this disturbs the system performance, I changed the concentration of Av17 (increasing and decreasing it) and examined how this affects the behaviour of key components of each model. I implemented one-step changes (from 0.1 to 70) and studied their effect on the dynamics of phospho-ERK (Figure 5.5) and IL-10 (Figure 5.7) for kinase inhibition (model 1) and phosphatase activation (model 2).

Phosphatase activation vs. kinase inhibition

Phosphatase activation has a linear activation and inhibition, whereas kinase inhibition is non-linear, as Equations 5.1 and 5.2 describe and Figure 5.1 complements.

$$v_k = \frac{k \cdot m_1 p}{1 + k_{f2} \cdot X^n} \tag{5.1}$$

$$v_p = k_{f1} \cdot m_1 p \cdot X^n \tag{5.2}$$

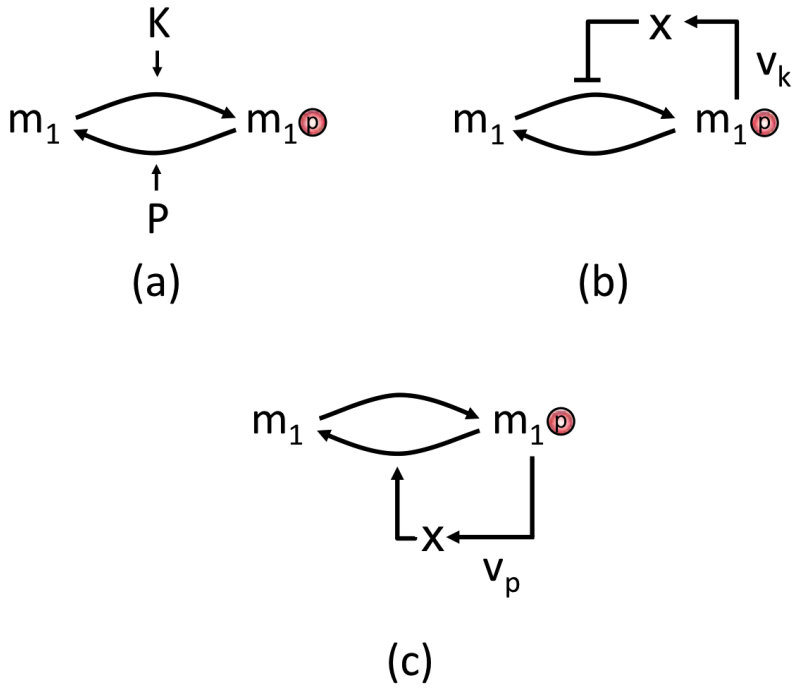

Figure 5.1.: A phosphorylation/dephosphorylation cycle. (a) without feedback; (b) with feedback inhibiting the kinase activity; (c) with feedback activating the phosphatase activity.

The feedback factor of the mechanism of phosphatase activation is X^n, whereas the feedback factor of kinase inhibition is nonlinear and is $1/(1 + k_{f1} \cdot X^n)$. Figure 5.2 shows the feedback function for both cases. The kinase inhibition starts with the value of one, when there is yet no IL-10. As IL-10 is being produced, the feedback factor decays. When IL-10 reaches its maximum the feedback factor reaches its minimum. The reverse happens with phosphatase activation. It has a positive and linear relation to IL-10. This linearity is due to the fact that the exponent n, a free parameter constrained between 1 and 10, was fitted to the value $n = 1.1$ (for details about the value of each parameter, please consult Appendix A.3).

Figure 5.3 pictures how does ERK activation and deactivation relates to IL-10 production . Both models start with a null concentration of phospho-ERK and IL-10. Model 1 has an immediate activation of phospho-ERK, which instantaneously reaches its maximum. Phospho-ERK stays in a short plateau and decays with the shape of a negative exponential, while IL-10 reaches its maximum (Figure 5.3 (a)). Model 2 has a linear activation and deactivation of ERK phosphorylation. Activation of ERK phosphorylation is quite quick, but not instantaneous. When ERK phoshorylation reaches its maximum, deactivation gets stronger than the activation and ERK goes

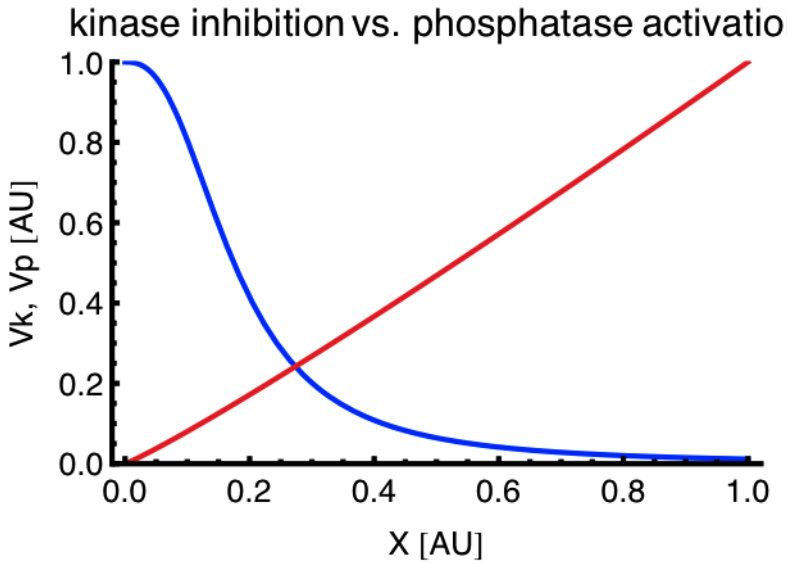

Figure 5.2.: Graphic visualisation of the mathematical term responsible for the negative feedback regulation. Blue line represents the feedback factor of kinase inhibition and red line represents the feedback factor of phosphatase activation. X of equations 5.1 and 5.2 is IL-10. The parameters k, k_{f1} and k_{f2} took the respective values assigned in model 1 and model 2.

immediately down. IL-10 keeps growing until its maximum and goes down to its steady state. At this stage, phospho-ERK is already in steady state (Figure 5.3 (b)).

To better visualise the differences between regulation by phosphatase activation and regulation by kinase inhibition, I plotted the feedback coefficient of each model, *i.e.*, I plotted the rates of phosphorylation and dephosphorylation of ERK (Figure 5.4).

Phospho-ERK

Changing the stimulus concentration, changes the amplitude of phospho-ERK. Phospho-ERK of model 1 reaches maximal activation instantaneously and stays in a constant amplitude value. This plateau is necessary to guarantee IL-10 production. When the feedback kicks in, there is an instantaneous deactivation of phospho-ERK (Figure 5.5(a)) and, consequently, of IL-10 (Figure 5.7(a)). The response to these input variations in model 2 is different: first, phosphorylation levels go up linearly until reaching maximal activation. At this point, the deactivation immediately happens and is linear, *i.e.*, the phosphorylation levels of ERK decrease as the input increases; and second, the time point of maximal amplitude is reached sooner as the input stimulus increases (Figure 5.5(b)). This slow, linear deactivation of phospho-ERK has consequences at the level of IL-10 production.

The mechanism of kinase inhibition (model 1) assumes a cooperative behaviour

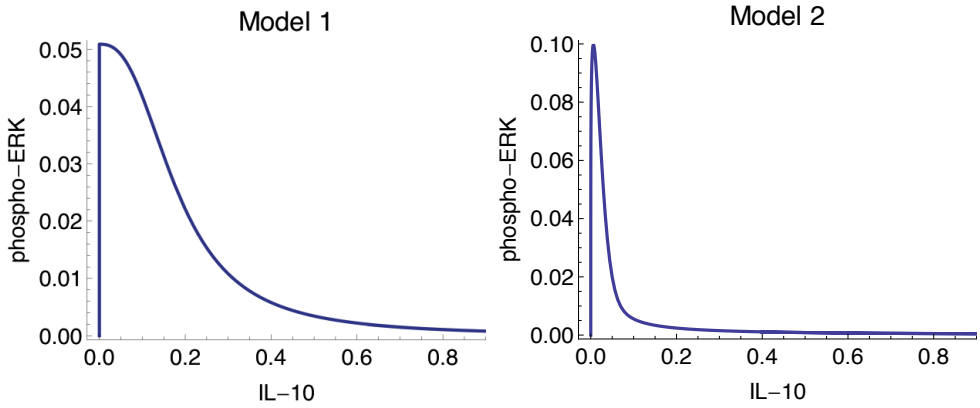

(a) (b)

Figure 5.3.: Difference between phosphatase activation and kinase inhibition. Parametric plots of phospho-ERK versus IL-10 for (a) model 1 and (b) model 2. Please note the different ERK phosphorylation levels (y-axis) between the models. ERK phosphorylation has its maximum at 0.05 for model 1 and at 0.1 for model 2.

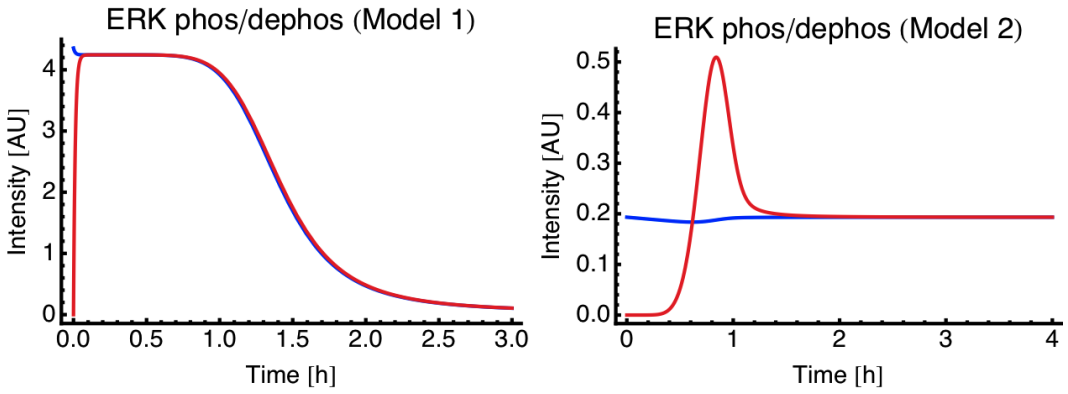

(a) (b)

Figure 5.4.: Dynamics of ERK phosphorylation/dephosphorylation for (a) model 1 and (b) model 2. Blue curve: phosphorylation. Red curve: dephosphorylation

(Hill coefficient of 2.5). Therefore, the inhibition has a switch-like behaviour and becomes effective only with a certain delay, during which the phospho-ERK is maximally active. When the feedback kicks in, there is a rapid deactivation of phospho-ERK following the plateau of maximal activity (Figure 5.5(a)). In model 2, the negative regulation by the increase in phosphatase activity is assumed to be a linear function of IL-10. Therefore, the inhibition constantly increases, causing direct deactivation after reaching the maximum (Figure 5.5(b)).

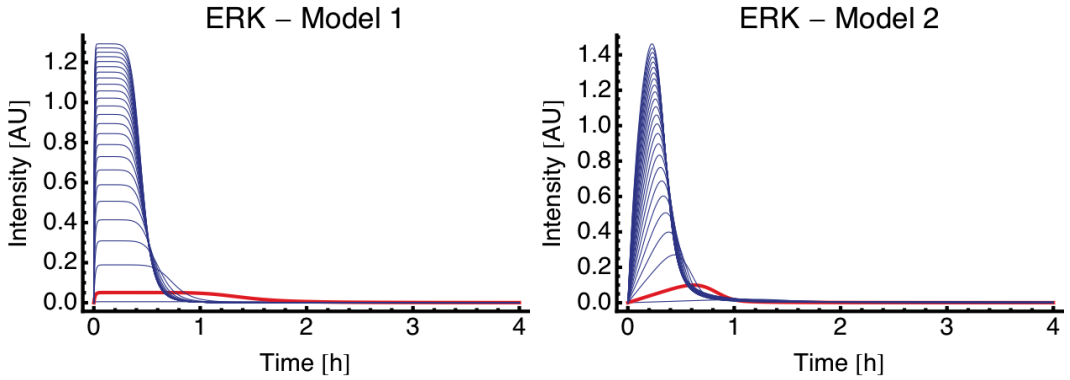

(a) (b)

Figure 5.5.: Phospho-ERK kinetics for different input amplitudes (0.1 to 70). (a) Model 1. (b) Model 2. Red line: input amplitude = 1

Phospho-p38

P38 activation is sustained for both models after increasing Av17 concentration. The amplitude of phospho-p38 of both models increases until attaining saturation (2 arbitrary units (AU)), but as phospho-p38 activation is faster for model 1 than for model 2, the former reaches saturation faster than the latter (Figure 5.6).

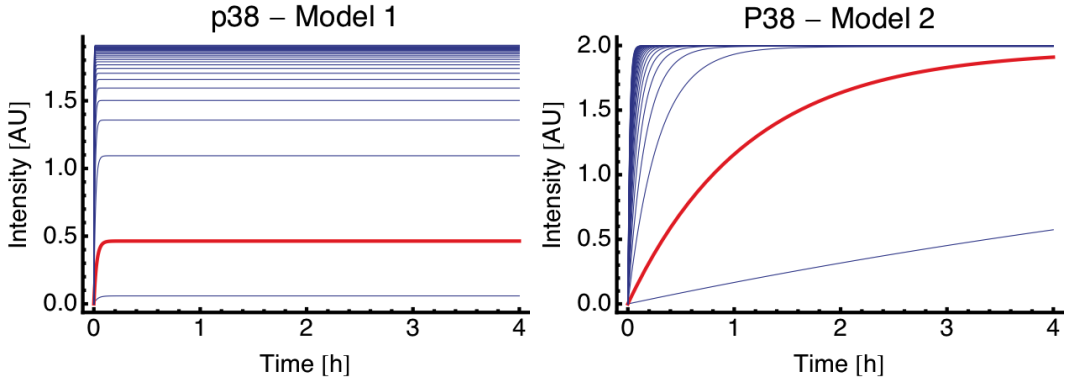

(a) (b)

Figure 5.6.: Phospho-p38 kinetics for different input amplitudes (0.1 to 70). (a) Model 1. (b) Model 2. Red line: input amplitude = 1

Extracellular IL-10 (IL-10)

Figure 5.7 shows how the different Av17 concentrations affect IL-10 dynamics. The comparison of Figures 5.7(a) and 5.7(b) shows a shift in IL-10 behaviour. In terms of signal amplitude, model 1 produces higher concentration of IL-10 than model 2.

For both models, a decrease in Av17 concentration yields a concentration of IL-10 close to zero. This suggests that the macrophage starts producing IL-10 only after a certain threshold of Av17 concentration is reached. When this threshold holds, IL-10 production overshoots and goes down to a steady-state level. As the input concentration increases, so does the maximum value of IL-10.

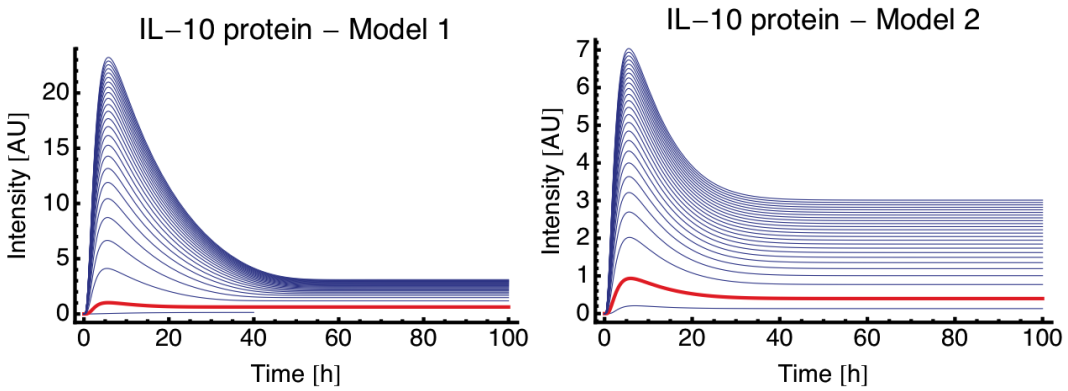

(a) (b)

Figure 5.7.: IL-10 kinetics for different input amplitudes (0.1 to 70). (a) Model 1. (b) Model 2. Red line: input amplitude = 1.

There is no significant difference between model 1 and model 2 for IL-10 rise time (time to reach maximum production), but IL-10 downregulation is faster for the former.

Negative regulation by kinase inhibition and negative regulation by phosphatase activation have different outcomes for IL-10 dynamics. In terms of IL-10 production and regulation, kinase inhibition is more effective than phosphatase activation. This is because kinase inhibition produces produces more IL-10 than the model with phosphatase activation, although the former phosphorylates less ERK than the latter (Figure 5.5). Moreover, the regulation mechanism of kinase inhibition is more effective than the one of phosphatase activation, because kinase inhibition can reach a steady state closer to the original steady state value (IL-10 steady state for Av17=1, red line of Figure 5.7) than phosphatase activation.

Complex formation and transcription factor activation

According to Zhang et al. (2006), activated ERK phosphorylates the histone sites of the *il-10* promotor and activated p38 phosphorylates the transcription factors that can bind to the open chromatin of *il-10* promoter. In the present mathematical models, I defined this process as a complex formation with three states:

- closed: Histone 3 (H3) site of IL-10 promotor is unphosphorylated and deactivated (element X0);

- open: H3 is phosphorylated (element X1);
- active: the activated transcription factor binds to the active H3 site and forms a complex that leads to *il-10* gene expression (element X2).

Figures 5.8, 5.9 and 5.10 illustrates the dynamics of the complex formation for both models.

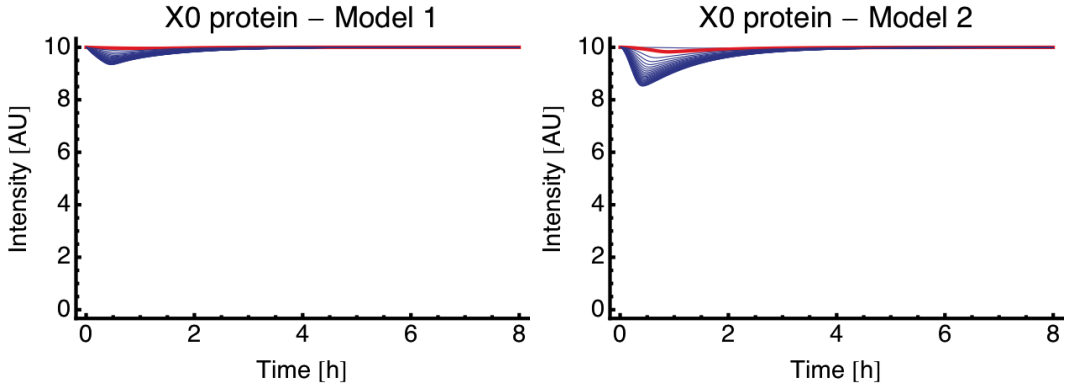

(a) (b)

Figure 5.8.: X0 kinetics for different input amplitudes (0.1 to 70). (a) Model 1. (b) Model 2. Red line: input amplitude = 1

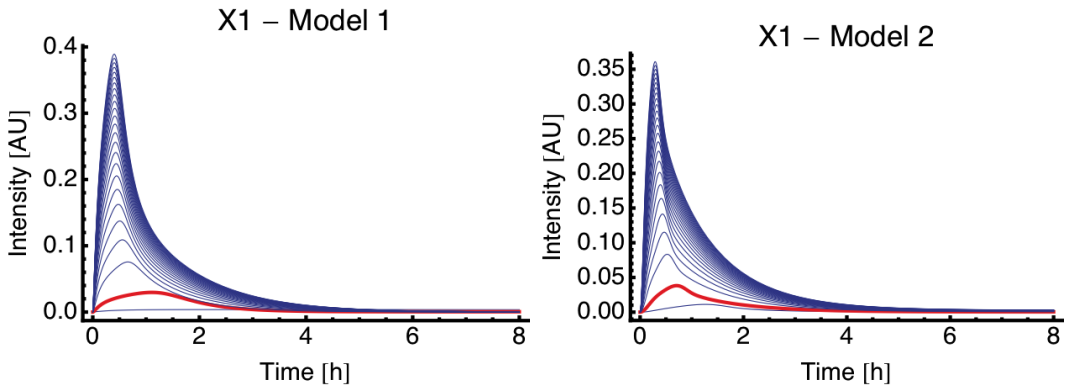

(a) (b)

Figure 5.9.: X1 kinetics for different input amplitudes (0.1 to 70). (a) Model 1. (b) Model 2. Red line: input amplitude = 1

The three states of the complex formation are very similar for both models. However, it is important to notice that the amplitude of X2 is higher in model 2 than in model 1 and that model 1 needs more time to reach maximal amplitude than model 2 in states X1 and X2.

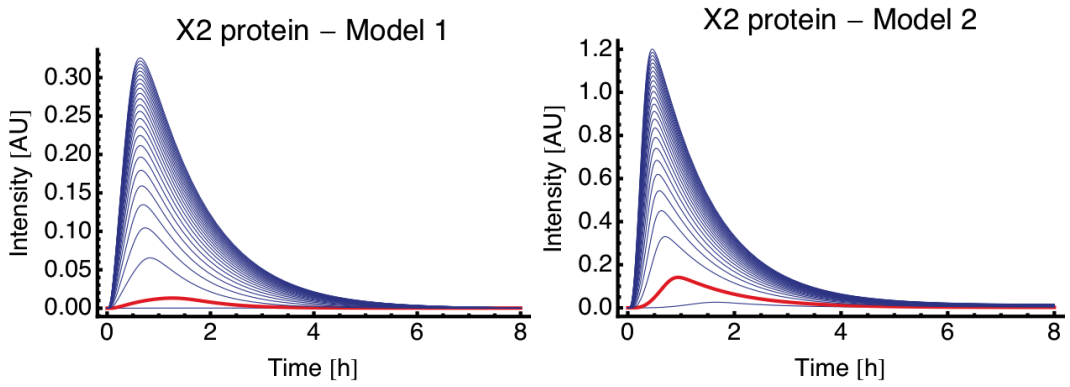

(a) (b)

Figure 5.10.: X2 kinetics for different input amplitudes (0.1 to 70). (a) Model 1. (b) Model 2. Red line: input amplitude = 1

I also compared the phosphorylation profiles of the transcription factors set, represented by A and A_p in the equation system 4.9. This is represented in Figure 5.11.

Interestingly, the phosphorylation of the transcription factors is very low in model 1. In model 2, A is totally transformed in A_p, *i.e.*, the total amount of transcription factors is phosphorylated.

5.2. The effects of phosphatase activation and kinase inhibition on phospho-ERK and IL-10

To further characterise the differences between phosphatase activation and kinase inhibition, I studied the characteristics of phospho-ERK and IL-10 using the following concepts:

- Maximal amplitude (a): maximal concentration of the biological element under study;
- Steady state (ss): point at which the dynamics of the element do not change over time;
- Overshoot (o): the difference between maximal amplitude and steady state; it yields the decay level of each element;
- Integral (i): total concentration of the biological element under study;
- Duration (w): the signal width at half of its maximal amplitude.

These concepts are represented in Figure 5.12.

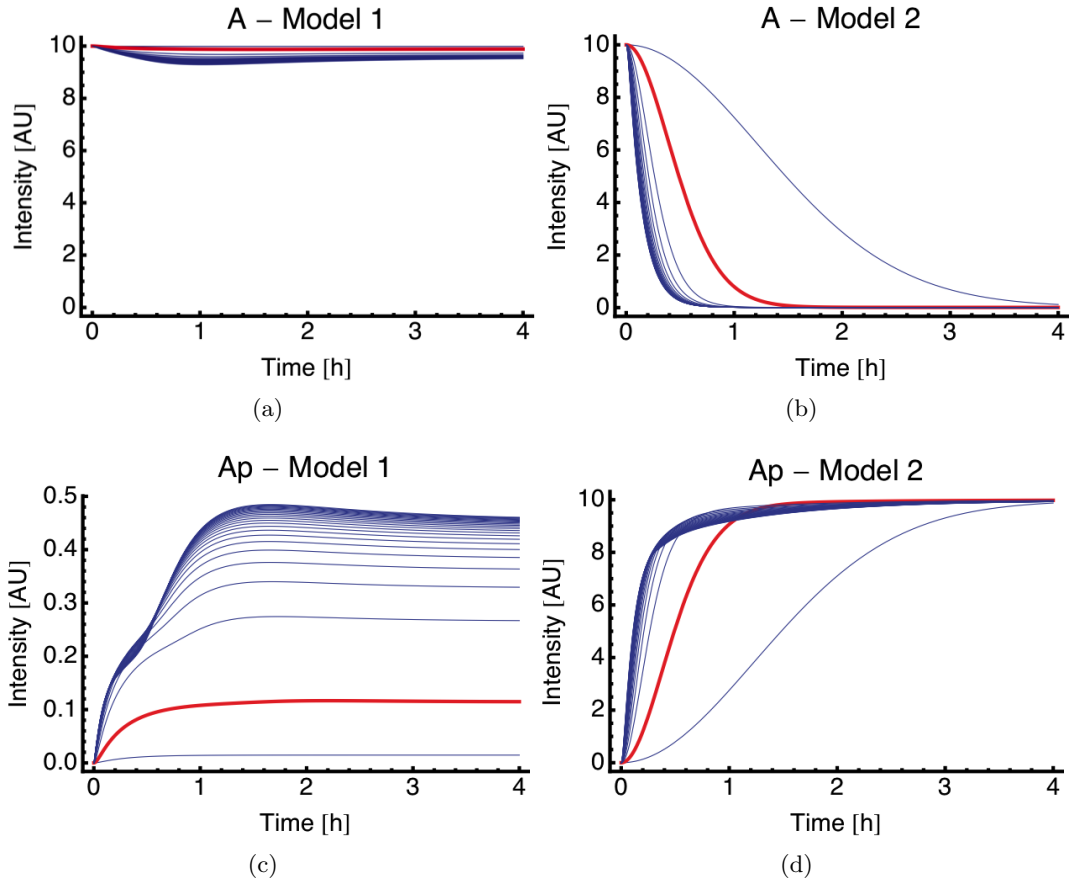

Figure 5.11.: Kinetics of A and Ap for different input amplitudes (0.1 to 70). A represents the unphosphorylated transcription factors, whereas A_p represents the phosphorylated transcription factors. (a, b) Model 1. (c, d) Model 2. Red line: input amplitude = 1

Kinase inhibition is a more efficient amplifier than phosphatase activation

To infer the ERK phosphorylation levels and IL-10 concentration produced by this biological system, I analysed the maximal amplitude and integral (Figures 5.13 and 5.14) for both models.

Figure 5.13 shows that kinase inhibition produces much higher levels of IL-10 than phosphatase activation, in terms of its maximal concentration and total amount produced. This is in striking contrast with ERK phosphorylation levels. The system with kinase inhibition cannot phosphorylate as much ERK as the system with phosphatase activation (Figure 5.14), but the former seems more efficient as an amplifier than the latter. Indeed, a lower phosphorylation level of ERK relays a higher IL-10 concentration for a regulation by kinase inhibition than regulation by phosphatase activation, in terms of maximal and total concentration level (comparing Figures 5.13 and 5.14).

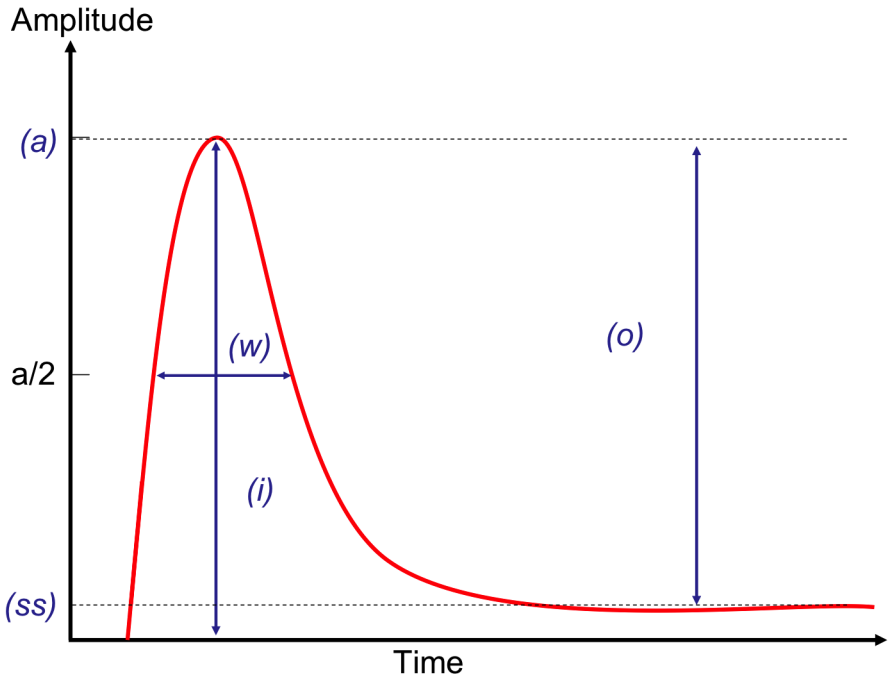

Figure 5.12.: Generic representation of the concepts of maximal amplitude (a), steady state (ss), overshoot (o), integral (i) and duration, (w).

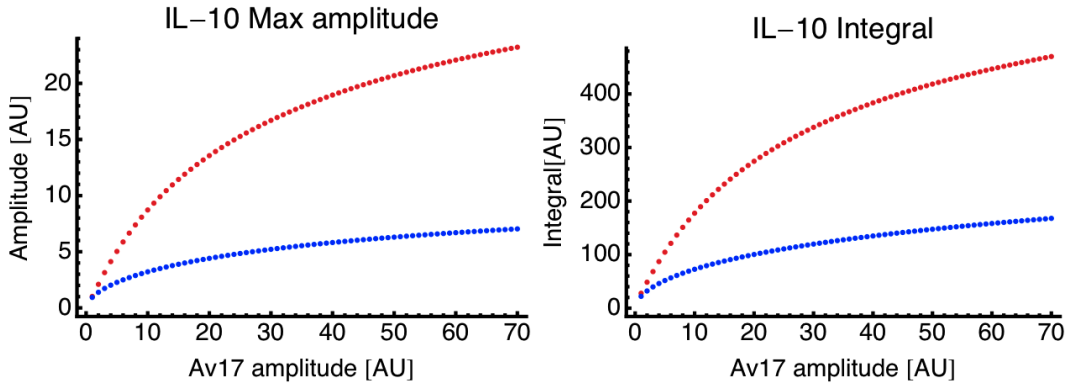

(a) (b)

Figure 5.13.: Comparison of model 1 (red) and model 2 (blue), in terms of IL-10 (a) maximal amplitude and (b) integral

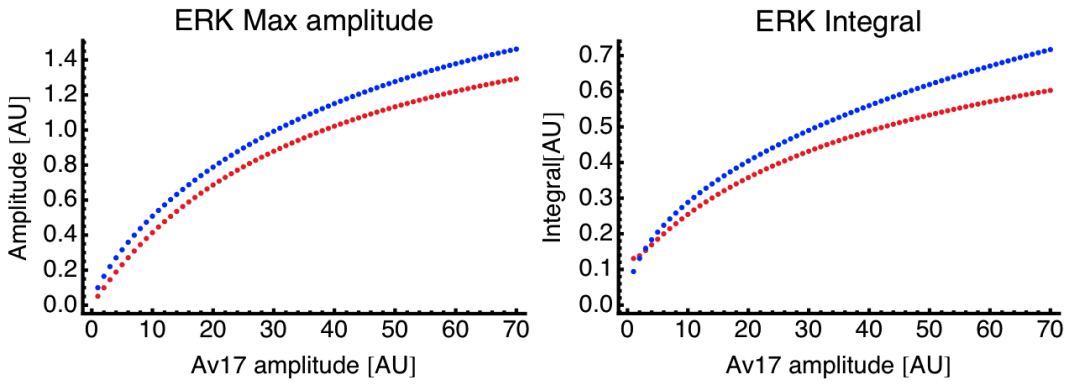

(a) (b)

Figure 5.14.: Comparison of model 1 (red) and model 2 (blue), in terms of phospho-ERK (a) maximal amplitude, (b) integral. The amplitude and total amount of ERK phosphorylation have the same trend in both models, but model 2 phosphorylates more ERK than model 1.

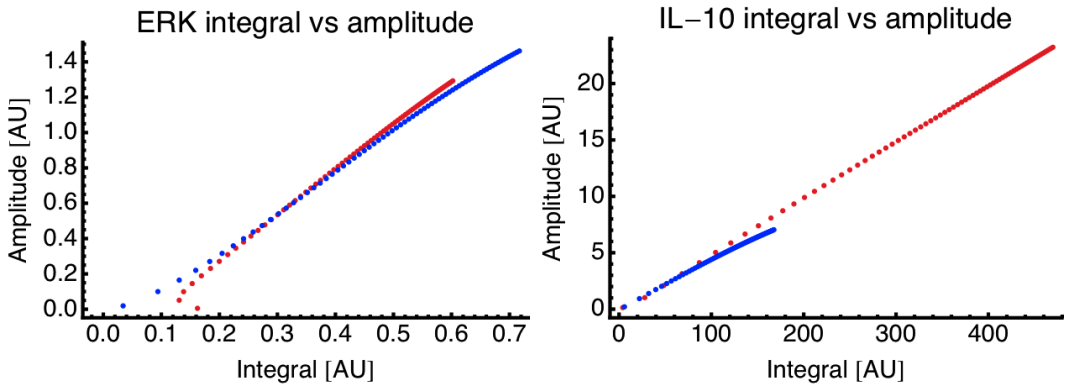

(a) (b)

Figure 5.15.: Comparison of model 1 (red) and model 2 (blue), in terms of (a) phospho-ERK and (b) IL-10 amplitude vs. integral.

These results are supported by Figure 5.15, where one can see that ERK phosphorylation levels are lower for kinase inhibition than for phosphatase activation, but IL-10 production is much higher in terms of integral and maximal amplitude for kinase inhibition than for phosphatase activation.

This renders the mechanism of regulation by kinase inhibition more efficient as an amplifier than the regulation mechanism of phosphatase activation.

IL-10 adaptation is stronger for kinase inhibition than for phosphatase activation

Kinase inhibition can adapt faster than phosphatase activation, which is explained by a stronger non-linear Hill coefficient in the feedback mechanism of kinase inhibition.

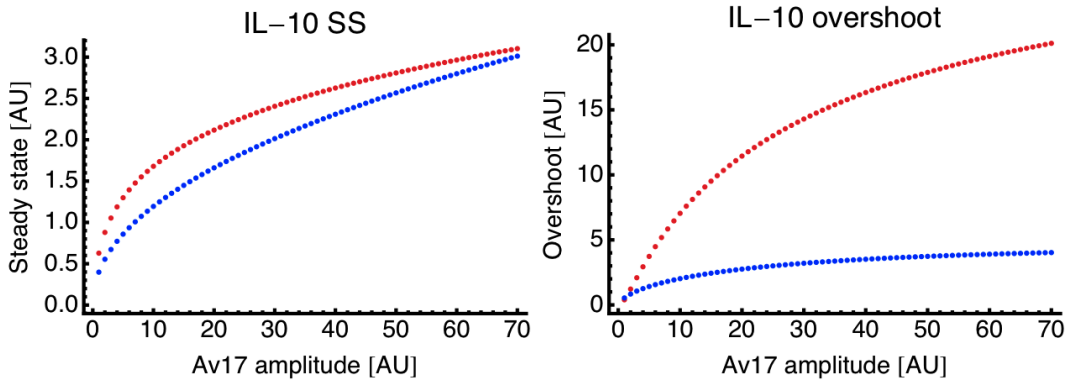

(a) (b)

Figure 5.16.: Comparison of model 1 (red) and model 2 (blue), in terms of IL-10 (a) steady state, (b) overshoot. IL-10 steady state was measured at t=80 h.

In terms of IL-10, Figure 5.16 (a) shows that both models converge to a similar steady state value. But the difference between the maximal amplitude and the steady state (overshoot) is much higher for model 1 than for model 2 (Figure 5.16 (b)). The fact that the maximal amplitude of IL-10 is higher in model 1 than in model 2 and that model 1 reaches a lower and constant steady state in spite of input variations (Figure 5.13 (a)), explains the higher overshoot levels of model 1 and suggests that regulation by kinase inhibition adapts better to a low steady state level than regulation by phosphatase activation. On the contrary, Figure 5.17(a) shows that phospho-ERK steady state for model 2 keeps increasing with input increases (although in a very low level) whereas for model 1, there are no significant changes in the steady state level, in spite of the input changes. This, together with the fact that model 2 phosphorylates more ERK than model 1, is then reflected in a similar overshoot trend for model 1 and model 2.

These results indicate that kinase inhibition is a more effective way of producing high levels of IL-10 for the same input value than phosphatase activation, because the former regulation mechanism produces more IL-10 with less ERK phosphorylation and has a better adaptation mechanism than the latter. This may render kinases a more attractive regulation mechanism, in terms of total signal and adaptation to a steady state level.

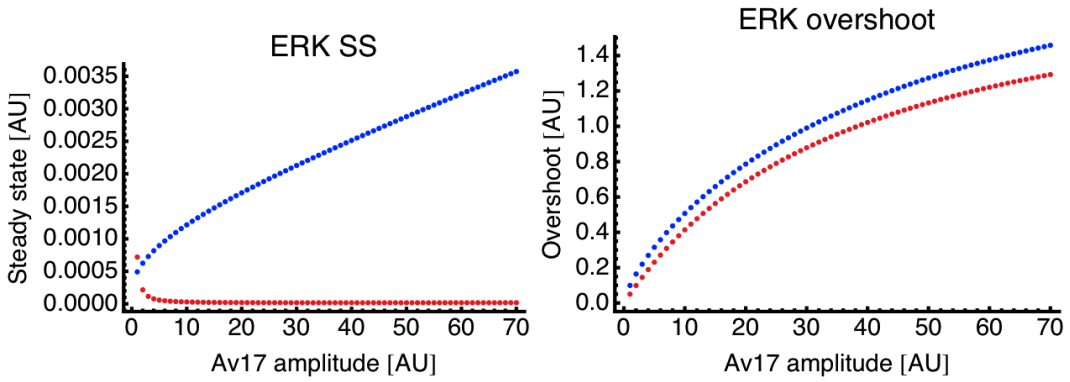

(a) (b)

Figure 5.17.: Comparison of model 1 (red) and model 2 (blue), in terms of phospho-ERK (a) steady state, (b) overshoot. phospho-ERK steady state was measured at t=4 h.

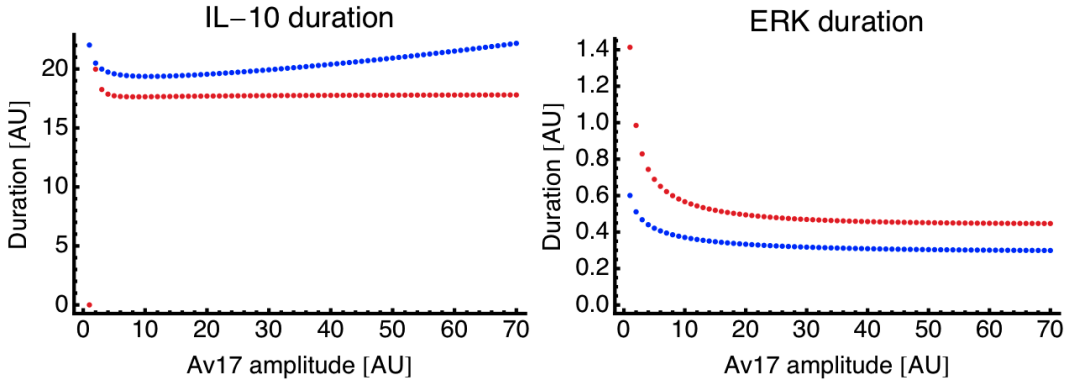

(a) (b)

Figure 5.18.: Comparison of model 1 (red) and model 2 (blue) in terms of signal duration for (a) IL-10 and (b) phospho-ERK

Phosphatase activation is more efficient limiting IL-10 duration than kinase inhibition

Measuring the signal width at half amplitude is a way of effectively quantifying the signal duration. Figure 5.18 compares both models in terms of phospho-ERK and IL-10 duration at half amplitude.

Interestingly, in terms of IL-10 production, the model with a phosphatase activation mechanism lasts longer than the model with kinase inhibition, although the latter produces much higher levels of IL-10 than the former.

In terms of ERK phosphorylation, model 1 has a longer duration than model 2. Nevertheless, the behaviour of both models is quite similar in terms of input dynamics: as the input concentration changes, the signal duration decreases, reaching

both a steady state around the same input concentration.

When the feedback with kinase inhibition kicks in, the concentration of IL-10 goes down steeply, due to the non-linearity of this feedback. In the case of phosphatase activation, the decrease of IL-10 concentration happens slower and in a linear fashion, explaining why the duration of IL-10 is higher in this case than in the case of kinase inhibition.

As expected, phospho-ERK can adapt better in the model of kinase inhibition than in the model of phosphatase activation. Phospho-ERK steady state grows with the input amplification for phosphatase activation feedback, whereas in kinase inhibition the steady state value of phospho-ERK does not change in spite of changes in the input. Nevertheless, the relationship between ERK amplitude and duration is similar for both models (Figure 5.19(a) and (b)). In contrast, IL-10 duration keeps constant when the amplitude increased in the case of regulation by kinase inhibition. In the case of regulation by phosphatase activation, as the amplitude increases, the signal duration goes down and up again (Figure 5.20(a) and (b)).

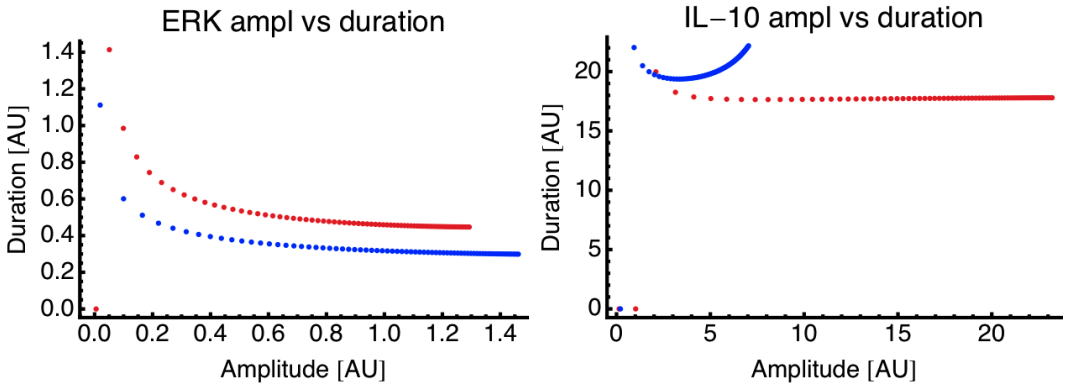

(a) (b)

Figure 5.19.: Comparison of duration with amplitude and integral for model 1 (red) and model 2 (blue), in terms of phospho-ERK (a) and (c) and IL-10 (b) and (d).

In biological terms, negative regulation by kinase inhibition can be more effective in terms of ensuring a high overshoot activation with low final steady state and a high amount of IL-10. Negative regulation by phosphatase activation, in turn, can be more effective to limit signal duration.

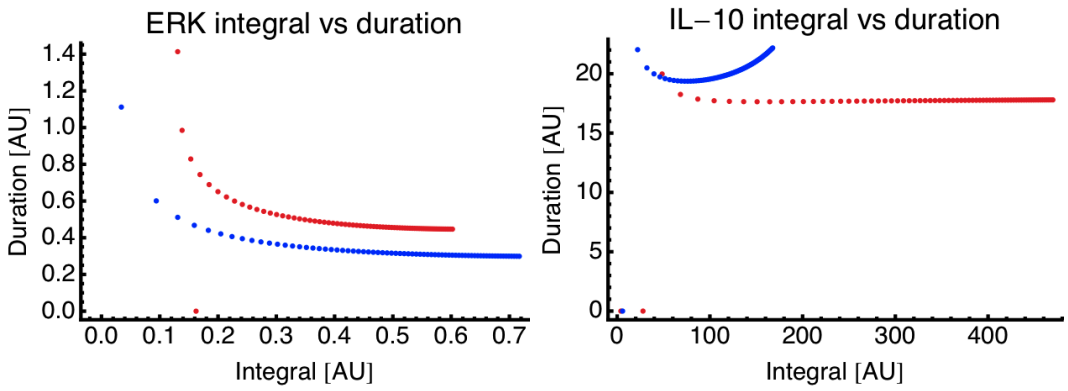

(a) (b)

Figure 5.20.: Comparison of duration with amplitude and integral for model 1 (red) and model 2 (blue), in terms of phospho-ERK (a) and (c) and IL-10 (b) and (d).

6. Sensitivity analysis suggests an autocrine crosstalk between ERK, P38 and IL-10

I performed a sensitivity analysis in order to understand how perturbations in the system affect the output (IL-10 production). Therefore, I perturbed each parameter of each model in a systematic manner and checked their influence on phospho-ERK, phospho-p38 and IL-10 protein, in terms of steady state. The sensitivities were calculated using the formula 2.18.

I imposed perturbations of 0.1 and 10 on each of these parameters. A perturbation factor of 0.1 translates into the chemical inhibition of phosphorylation of one of the MAPKs and a perturbation factor of 10 translates into the increase of the phosphorylation levels of one of the MAPKs.

Tables 6.1 and 6.2 show the calculated sensitivities for model 1 and model 2, respectively. These are the sensitivities of each parameter when perturbations at the steady state level of ERK, p38 and IL-10 protein are imposed.

Model 1 and model 2 have different behaviours. Nevertheless, h is the most sensitive parameter of both models. This parameter determines the feedback strength of the models.

6.1. Model 1: phospho-ERK affects IL-10 production

Figure 6.1 shows the variations of parameter k_1 of model 1. The perturbations imposed to phospho-ERK affect its duration and amplitude (Figure 6.1(a)). As the perturbation increases, the amplitude of phospho-ERK increases and the duration decreases. These same perturbations also affect the amplitude and the duration of *il-10* mRNA (Figure 6.1(b)) and IL-10 protein (Figure 6.1(c)). The steady state of IL-10 protein is also affected, but not the steady state of *il-10* mRNA. These perturbations have no direct effect on p38, phospho-p38 maintaining its curve over the whole perturbation range (Figure 6.1(d)).

6.2. Model 1: phospho-p38 affects phospho-ERK and IL-10 production

I perturbed the phosphorylation rate constant of p38, k_3 (Figure 6.2) and observed that p38 activity, although not directly affected by the negative feedback, has an

Model 1

k	ERK		P38		IL-10	
	0.1	10	0.1	10	0.1	10
k_1	0.56	0.1	0	∼0	0.56	0.1
k_2	-0.99	-0.05	∼0	∼0	-1.04	-0.05
k_3	-3.55	-0.06	0.97	0.24	0.51	0.04
k_4	0.62	0.35	-2.48	-0.09	-0.43	-0.05
k_5	-4.35	-0.08	∼0	∼0	0.55	0.1
k_6	0.87	0.43	∼0	∼0	-0.96	-0.05
k_7	-4.38	-0.08	∼0	∼0	0.56	0.1
k_8	1.04	0.43	∼0	∼0	-2.2	-0.05
k_9	0.96	0.43	∼0	∼0	-1.39	-0.05
k_{10}	-4.38	-0.09	∼0	∼0	0.56	0.11
k_{11}	-4.39	-0.09	∼0	∼0	0.56	0.1
k_{12}	1.08	0.43	∼0	∼0	-3.51	-0.05
k_{13}	-4.39	-0.09	∼0	∼0	0.56	0.1
k_{14}	0.89	0.43	∼0	∼0	-1	-0.05
k_f	-0.99	-0.05	∼0	∼0	-0.99	-0.05
h	**-89410.2**	0.05	**-1699.66**	∼0	1.11	0.06

Table 6.1.: Sensitivities of ERK, p38 and IL-10 protein to perturbations of a factor of 0.1 or a factor of 10, on each parameter of model 1. k is the perturbed parameter. The Hill coefficient, h, is the most sensitive parameter.

indirect impact on the feedback mechanism by influencing the production of IL-10 and, consequently, ERK activity. This reveals autocrine feedback between the MAPKs.

In this model, secreted IL-10 binds to the macrophage and promotes the dephosphorylation of phospho-ERK, establishing in this way a negative feedback mechanism. Hence, the production of IL-10 interferes with the ERK signalling pathway, higher IL-10 production reflecting higher feedback strength and lower duration of phospho-ERK (Figures 6.2(c), 6.2(d)). By comparing both perturbations on parameters k_1 for phospho-ERK and k_3 for phospho-p38, I can observe that phospho-ERK has a stronger influence on *il-10* mRNA and IL-10 protein amplitude and that phospho-p38 exerts control over the feedback mechanism strength.

6.3. Model 2: phospho-ERK affects IL-10 production

I perturbed ERK activation by factors of 0.1 and 10 (Figure 6.3) and, as in the previous case, I see that perturbations of ERK do not affect p38 activation (Figure 6.3(d)). They affect IL-10 production at the protein and mRNA levels in terms of amplitude and duration, but only IL-10 protein in terms of steady state, similarly to model 1

Model 2

k	ERK		P38		IL-10	
	0.1	10	0.1	10	0.1	10
k_1	0.73	0.22	∼0	∼0	0.74	0.22
k_2	-2.24	-0.07	∼0	∼0	-2.19	-0.07
k_3	-0.01	∼0	0.16	∼0	0.01	∼0
k_4	∼0	∼0	-0.01	-0.01	∼0	∼0
k_5	-0.01	∼0	∼0	∼0	0.01	∼0
k_6	∼0	∼0	∼0	∼0	∼0	∼0
k_7	-2.61	-0.07	∼0	∼0	0.74	0.22
k_8	0.94	0.26	∼0	∼0	-5.11	-0.07
k_9	0.93	0.26	∼0	∼0	-4.79	-0.07
k_{10}	-2.62	-0.08	∼0	∼0	0.74	0.38
k_{11}	-2.61	-0.07	∼0	∼0	0.74	0.22
k_{12}	0.95	0.26	∼0	∼0	-5.65	-0.07
k_{13}	-2.61	-0.07	∼0	∼0	0.74	0.22
k_{14}	0.77	0.26	∼0	∼0	-2.18	-0.07
h	**-7866.78**	**-32.18**	**-38.43**	0.85	1.11	**145.61**

Table 6.2.: Sensitivities of ERK, p38 and IL-10 protein to perturbations of a factor of 0.1 or a factor of 10, on each parameter of model 1. k is the perturbed parameter. The power factor, h, is the most sensitive parameter.

(Figures 6.3(b) and 6.3(c)). ERK activation is also affected by its perturbations, in terms of amplitude and duration, but not its steady state (Figure 6.3(a)).

6.4. Model 2: phospho-p38 affects phospho-ERK but has no influence on IL-10 production

p38 perturbations affect ERK activation (as in model 1) due to the feedback mechanism. A high perturbation reflects high feedback strength, as observed by a lower amplitude and duration of phospho-ERK (Figure 6.4(a)). IL-10 protein and mRNA are not affected in terms of steady state and duration. The curves for no perturbation and a perturbation factor of 10 are identical. This might be due to a possible saturation effect. For a perturbation factor of 0.1, the amplitude is lower (Figure 6.4(b), 6.4(c)). Finally, Figure 6.4(d) shows that p38 activation is faster with increasing perturbation factor.

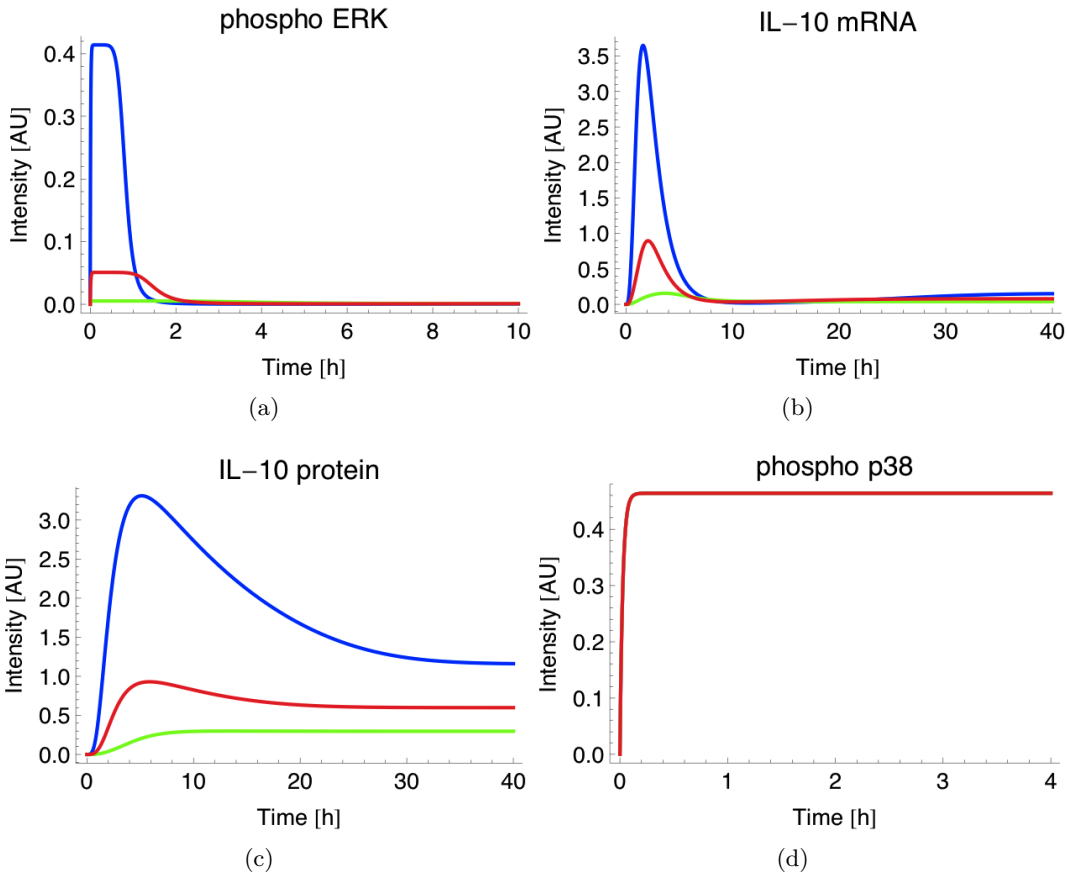

Figure 6.1.: Perturbations of phospho-ERK (model 1). Range of perturbation: factor 10 and factor 0.1. Red line: no perturbation. Green line: perturbation factor is 0.1. Blue line: perturbation factor is 10. (a) Phospho-ERK: phospho-ERK affects its duration and amplitude, but not steady state. (b) *il-10* mRNA: perturbations affect its amplitude and the duration but not the steady state. (c) IL-10 protein: perturbations affect its amplitude, duration and steady state. (d) Phospho-p38 is not affected at all by phospho-ERK perturbations.

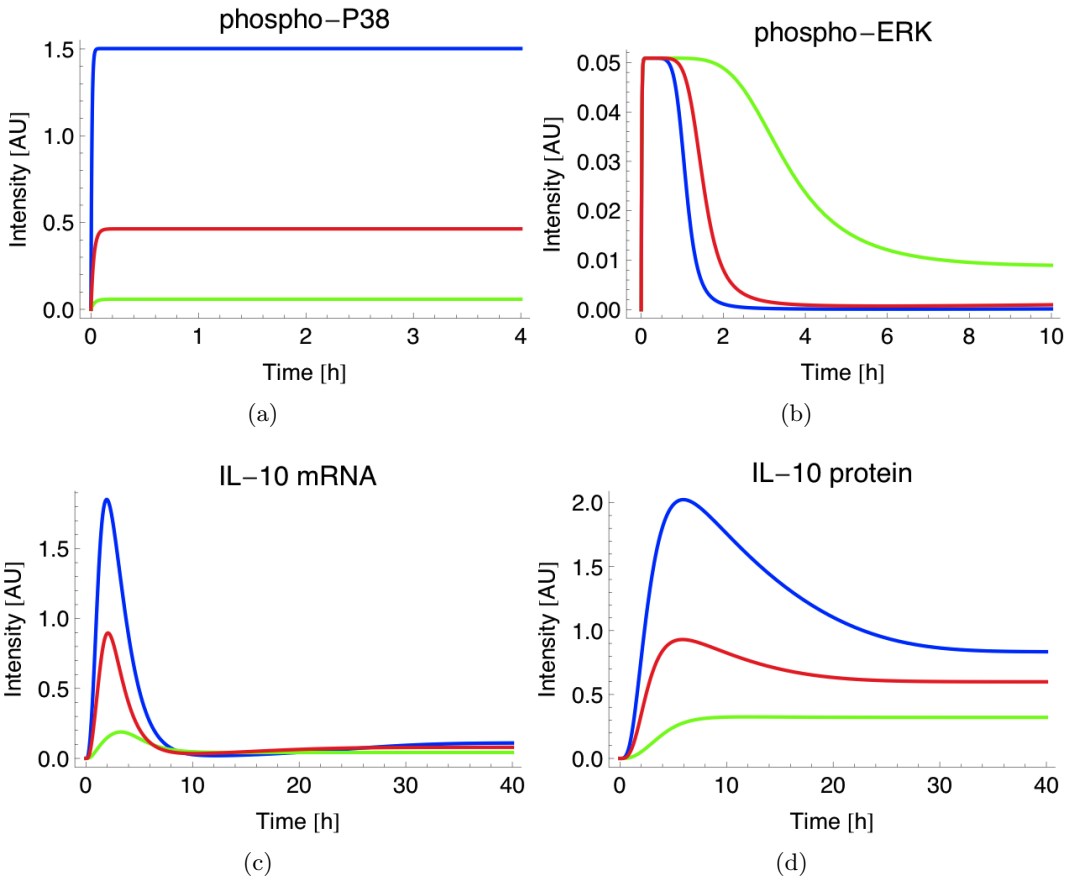

Figure 6.2.: Perturbations of phospho-p38 (model 1). Range of perturbation: factor 10 and factor 0.1. Red line: no perturbation. Green line: factor of perturbation is 0.1. Blue line: factor of perturbation is 10. (a) Phospho-p38: perturbing phospho-p38 affects its amplitude. (b) Phospho-ERK: phospho-ERK is sensitive to phospho-p38 perturbations, owing to the feedback mechanism. Its amplitude maintains a constant level, its duration increases as the perturbation decreases, and for a perturbation factor of 0.1, its steady state increases. (c) *il-10* mRNA: amplitude and duration are sensitive to perturbations of phospho-p38, but not the steady state. (d) IL-10 protein: amplitude, duration and steady state are sensitive to perturbations of phospho-p38.

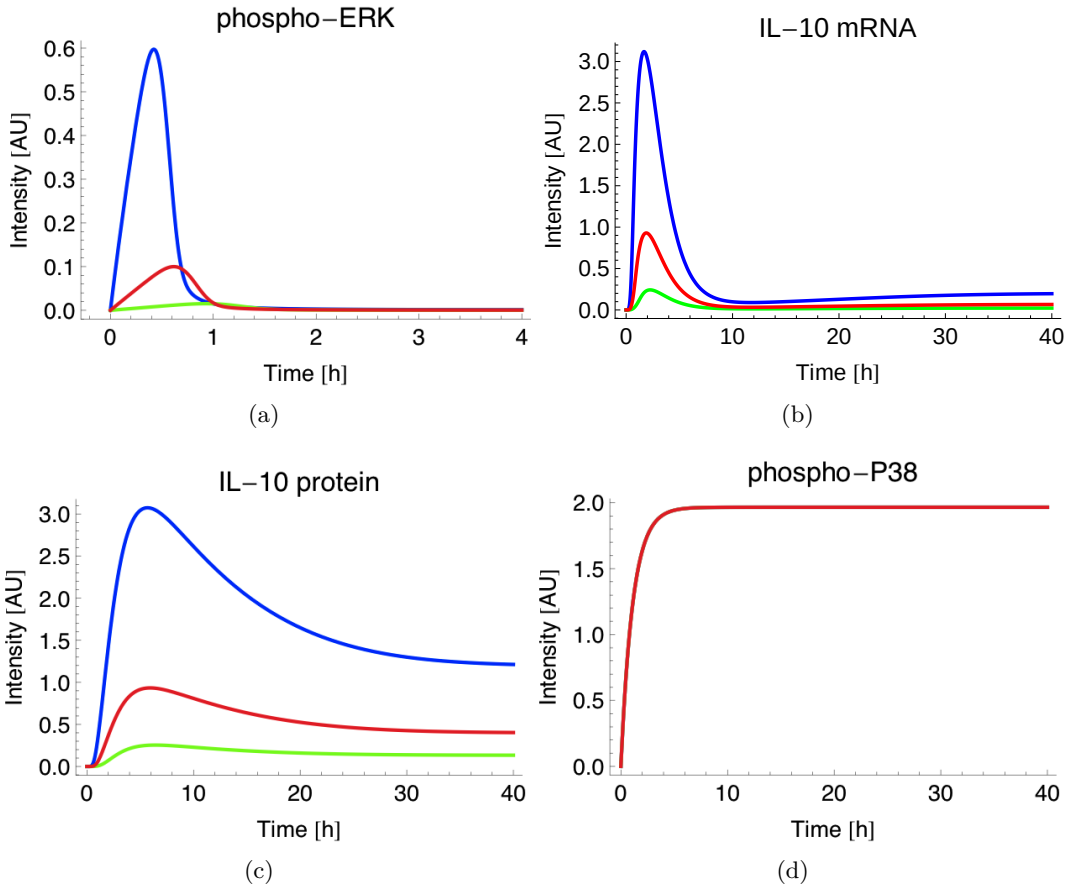

Figure 6.3.: Perturbations of phospho-ERK (model 2). Range of perturbation: factor 10 and factor 0.1. Red line: no perturbation. Green line: factor of perturbation is 0.1. Blue line: factor of perturbation is 10. (a) Phospho-ERK: perturbing phospho-ERK affects its amplitude, but not duration or steady state. (b) *il-10* mRNA: perturbations affect its amplitude and duration, but not steady state. (c) IL-10 protein: perturbations affect its amplitude, duration, and steady state. (d) Phospho-p38 is not affected at all by phospho-ERK perturbations.

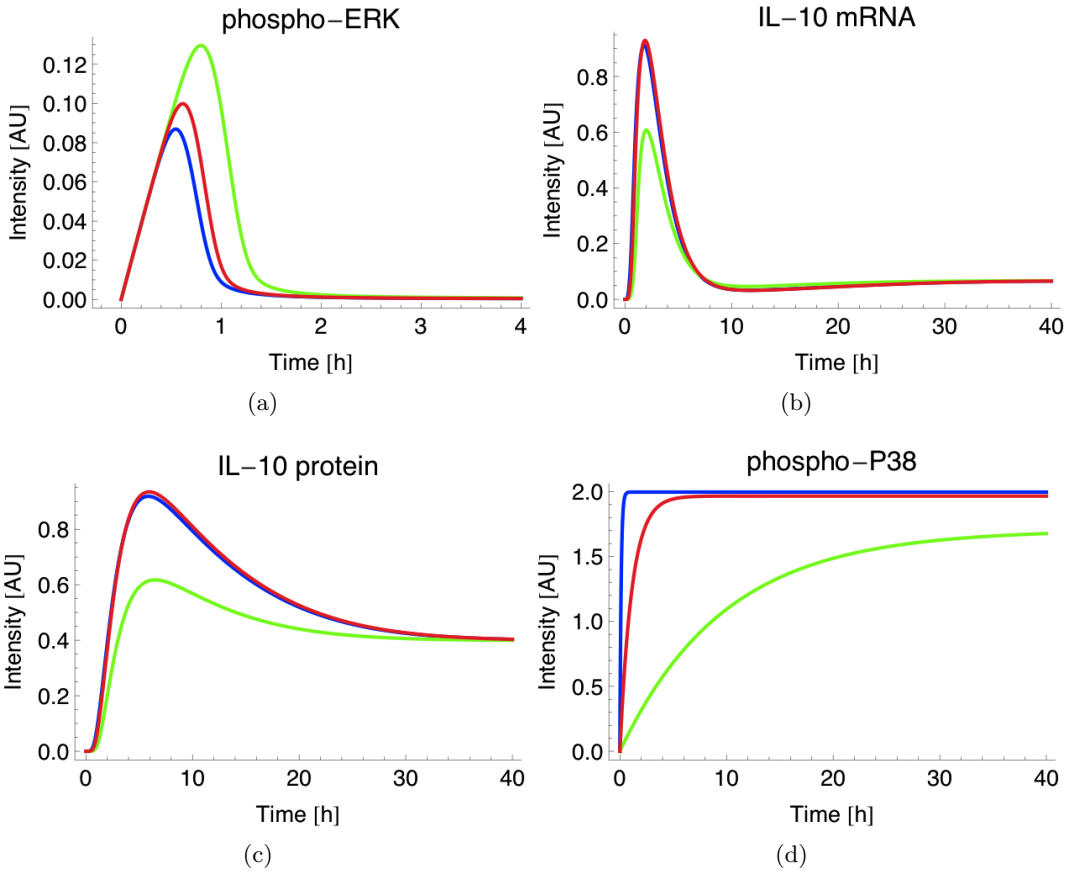

Figure 6.4.: Perturbations of phospho-p38 (model 2). Range of perturbation: factor 10 and factor 0.1. Red line: no perturbation. Green line: factor of perturbation is 0.1. Blue line: factor of perturbation is 10. (a) Phospho-ERK: perturbing phospho-p38 affects phospho-ERK amplitude and duration but not steady state. (b) il-10m is insensitive except for a perturbation factor of 0.1, which shows a decrease in amplitude. (c) IL-10 protein: shows the same behaviour as *il-10* mRNA. (d) Phospho-p38: phospho-p38 is sensitive to its perturbations in terms of activation (its activation is faster as the interference increases) and in terms of amplitude in a linear manner.

7. Discussion of Part I

Parasitic nematodes modulate the immune response of their hosts by inducing IL-10 expression. In this part of my thesis, I modelled IL-10 production and regulation in Av17 stimulated macrophages. I assumed that the production and regulation of IL-10 happens via the MAPKs ERK and p38. Experimental data on IL-10 kinetics, show that there is a regulatory mechanism dampening IL-10 concentration until a low, constant basal level is reached. This motivated the design of models with two different negative feedback mechanisms and one without feedback. I fitted them to the observed time course for *il-10* mRNA and IL-10 protein quantities.

The models assume that IL-10 protein, secreted from the macrophage, binds to the same cell through the IL-10 receptor and deactivates ERK either by kinase inhibition (model 1) or by phosphatase activation (model 2). Literature suggests that kinases are localised in supra-molecular structures or in the cell membrane, whereas phosphatases are homogeneously distributed in the cytoplasm (Kholodenko, 2006). This prompted me to study the difference between choosing a phosphatase or a kinase to start the feedback mechanism.

Model 1 and model 2 suggest a transient activation of ERK and a sustained activation of p38.

First, I analysed the dynamics of ERK and p38. Both models suggest transient ERK and sustained p38 activation. According to Yang et al. (2007), bone marrow macrophages exposed to immune complexes and *Leishmania mexicana* present transient ERK and sustained p38 activation. Other authors suggest that the transient kinetics of ERK could be due to internalisation and degradation of the growth factor receptor (Sasagawa et al., 2005), a scenario not considered in this work. Following the biological fact that the parasitic nematode *A. viteae* secretes Av17 in a constant fashion (Hartmann et al., 1997), these models assume constant stimulation of macrophages with Av17. In a more systemic view, the feedback effect could have implications for the macrophage fate (activation/deactivation and differentiation). Av17 binds to the macrophages and induces IL-10 production (Hartmann and Lucius, 2003), and IL-10 deactivates macrophage function (O'Garra et al., 2008). I hypothesised that this deactivation is achieved by the regulation of ERK via IL-10. Other studies have shown that sustained activation of ERK on macrophage-colony-stimulating-factor (M-CSF) mediated macrophages leads to differentiation (Suzu et al., 2007). In mammalian PC12 cells, different ERK dynamics have different infuences in the cell fate (Marshall, 1995; Santos et al., 2007; Sasagawa et al., 2005). This raises the question of whether different ERK dynamics have a different impact in the fate of Av17-exposed macrophages.

Second, I modified the input concentration (Av17) and checked key features of

ERK, p38 and IL-10 to understand the differences between phosphatase activation and kinase inhibition. I checked the signal amplitude, duration, integral, steady state and overshoot. The results indicate that activation of phosphatases (model 2) is a more efficient negative feedback mechanism for controlling signal duration than inhibition of kinases (model 1). This can be explained by the fact more phosphatase accelerates dephosphorylation, whereas the dephosphorylation rate of the kinase inhibition mechanism is constant. Interestingly, the inhibition of kinases is a more efficient amplifier, in terms of signal maximal amplitude and integral, than the activation of phosphatases. The ratio between IL-10 maximal amplitude and ERK phosphorylation levels is much higher in model 1 than in model 2, indicating that the model with kinase inhibition can produce more IL-10 with less phospho-ERK than the model with phosphatase activation. Moreover, IL-10 overshoot indicates that regulation through the inhibition of kinases presents better adaptation than regulation through phosphatase activation. Model 1 can regulate IL-10 steady state to a value much closer to IL-10 steady state without perturbations than model 2. IL-10 steady state of model 2 is always approximately half of its maximal amplitude, independently of different Av17 levels. Increasing input stimulation changes the duration and the amplitude of ERK dynamics in both models. The dynamics of p38, after increasing Av17 level, are sustained for both models and model 1 presents faster activation than model 2. Hornberg et al. (2005a) have shown that phosphatases tend to control signal duration and amplitude, which is in accordance with these results.

Av17 increases change IL-10 dynamics. IL-10 needs a certain minimum level of Av17 to be produced and, as the concentration of Av17 in the present models increased, the IL-10 concentration rose. However, the downregulation of IL-10 production became less, and sustained production of IL-10 was achieved. The effect of high levels of IL-10 production on the macrophage population in particular and on the immune system in general is a question that remains unanswered.

Third, I performed a sensitivity analysis to study the effect that specific perturbations in components of the system have on IL-10 production. Specifically, I perturbed the parameter associated with ERK activation (k_1) and checked the effect of this perturbation on p38 phosphorylation levels and IL-10 (mRNA and protein) levels. Then, I perturbed the parameter associated with p38 activation (k_3) and checked the effect of this perturbation on ERK phosphorylation levels and IL-10 (mRNA and protein) levels. Perturbing ERK activation has no effect on p38 activation but, interestingly, perturbing p38 activation affects ERK activation. This revealed that ERK and p38 crosstalk through an autocrine feedback and that p38 has a prominent role on the feedback mechanism that dampens IL-10 signal. Moreover, this analysis suggested that k_1) influences the amplitude, duration and steady state of IL-10 in model 1 and model 2, whereas k_3 has the same influence only in model 1. These perturbations in model 2 revealed no change in IL-10 behaviour except for the perturbation factor of 0.1, affecting IL-10 amplitude.

Understanding the process behind IL-10 regulation and macrophage deactivation could open the door to understanding the the role of ERK in macrophage fate. Av17

and IL-10 deactivate macrophages and this could be a consequence of the transient time course of ERK. According to Staples et al. (2007), IL-10 activates the JAK.STAT signalling pathway when bound to macrophages, inducing IL-10 (protein and mRNA) production on activated macrophages, but can also suppress *il-10* mRNA production in the same cells. Sánchez-Tilló et al. (2007) point out that IL-10 activates JNK1, which in turn activates DUSP1 expression. As the lack of DUSP1 causes prolonged ERK activation this would suggest that DUSP1 is a feedback mediator of IL-10 production.

Taken together, this part of my thesis proposes a mathematical model that suggests how is IL-10 produced and regulated in macrophages exposed to immunomodulatory molecules of parasitic nematodes. It suggests that:

- IL-10 is regulated in an autocrine fashion;
- Av17 activates ERK and P38;
- IL-10 production is dependent on ERK and P38 activation;
- the feedback mechanism of kinase inhibition is a better amplifier than phosphatase activation in terms of IL-10 maximal and total production;
- Phosphatase activation is more effective on limiting signal duration than kinase inhibition;
- phospho-p38 affects ERK via secreted IL-10, indicating an autocrine crosstalk between the two MAPKs.

A mathematical model goes hand in hand with experimental data. In order to validate and refine the model, I propose the following experiments:

- measure the activity of MAPK phosphorylation;
- test the dose response of IL-10 protein and phospho-ERK to Av17 increases;
- inhibit the autocrine IL-10 signalling pathway with anti IL-10R antibodies and measure IL-10 levels at different time points, as well as phospho-ERK and phospho-p38 time series.
- test if the transcription factors CREB, SP1 and STAT3 are involved in IL-10 expression and, furthermore, if they are MAPK dependent.

Part II.

Signalling events regulate IL-10 production in macrophages stimulated with an immunomodulator of parasitic nematodes

8. Synopsis

This work is partially published in Klotz et al. (2011), where the experimental procedures can be found. The experiments here referred, were conducted by Christian Klotz and Thomas Ziegler, from the Department of Parasitology, Humboldt-Universität zu Berlin.

Here I combine a theoretical approach with experimental data to understand the signalling events triggered by Av17 in macrophages. I applied mathematical modelling to characterise signalling elements involved in the manipulation of the macrophage. As suggested in the previous part, IL-10 expression in Av17 stimulated macrophages was tyrosine kinase sensitive and dependent on activation of both ERK and p38 MAP kinases. The fact that both kinases have transient dynamics, suggests that there is a regulation mechanism acting at the signalling level to regulate IL-10 production. To understand how this regulation happens, I hypothesised several alternative ways of signalling regulation. I developed a method of model selection that combines the theoretical predictions with experimental evidences to select a valid model that can correctly predict the experimental data. This systems biology approach allowed to grasp regulatory characteristics of the biological network, that would have not been feasible solely by using an experimental approach.

9. MAPK ERK and p38 are essential for IL-10 production in Av17 stimulated macrophages

Macrophages respond to external cues by activating specific signalling pathways. In the previous part of this thesis, I suggested that Av17 activates the MAPK signalling cascades ERK and p38 to induce IL-10 expression. In this part of my thesis, I combined mathematical modelling with experimental data to understand which signalling events induced by Av17, lead to IL-10 expression and regulation in macrophages.

9.1. Validation of model 1 and model 2

The involvement of ERK and p38 was experimentally tested and confirmed the hypothesis raised by the model: Av17 activates ERK and p38 in macrophages and IL-10 production depends on the parallel activation of both signalling cascades.

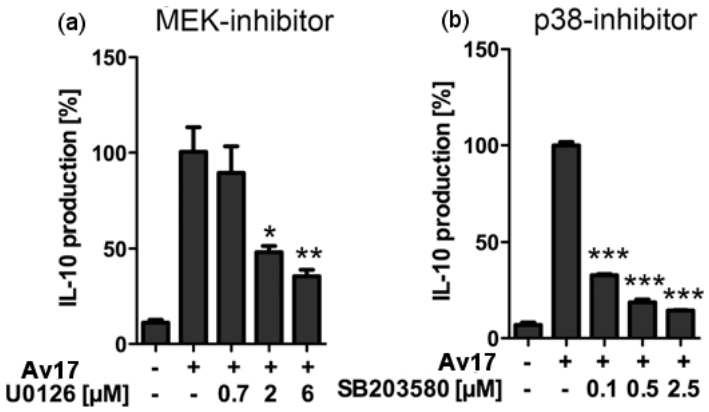

Figure 9.1.: IL-10 expression in Av17-stimulated macrophages in the presence of MAPK inhibitors (a) MEK inhibitor, which inhibits the ERK signalling cascade (b) p38 inhibitor. Both MAPKs are essential for IL-10 production in Av17-stimulated macrophages. The experimental details of this work can be found in Klotz et al. (2011).

Experimental testing of IL-10 expression was done using the specific inhibitors of both MAPK kinases. Results show that ERK and p38 are both essential for IL-10

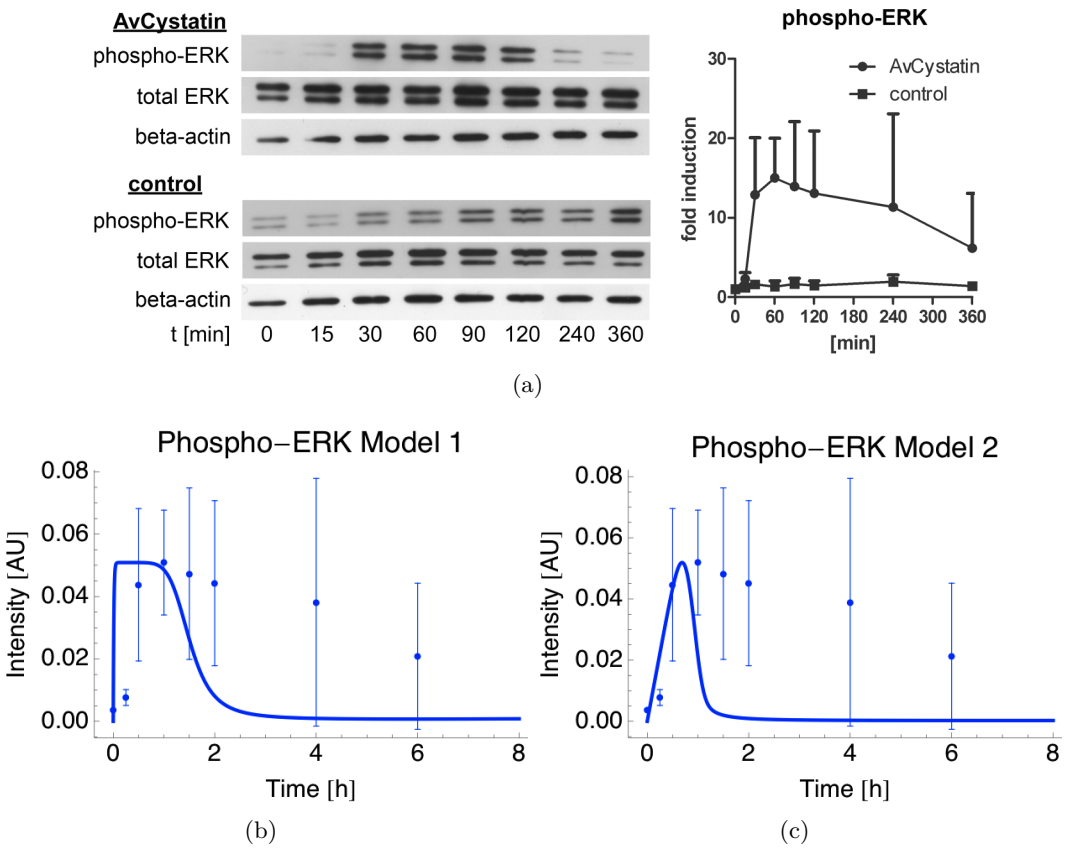

(a)

(b)

(c)

Figure 9.2.: ERK phosphorylation in Av17-stimulated macrophages. (a) Western blot of ERK phosphorylation measured in Av17-stimulated macrophages. (b), (c) Prediction and validation of ERK dynamics. Solid line: predicted phospho-ERK dynamics; dots: experimental values for phospho-ERK. The experimental details of this work can be found in Klotz et al. (2011).

production, according to the model hypothesis. Figure 9.1 shows the experiment confirming this hypothesis.

Furthermore, the activation of both kinases is transient, as Figures 9.2(a) and 9.3(a) illustrate. I validated model 1 and model 2 of Part I by comparing the experimental results with the model predictions. Both models correctly predict the behaviour of phospho-ERK, as represented in Figures 9.2(b) and 9.2(c).

Both models predict a sustained P38 activation, which is not observed experimentally, as Figure 9.3 shows.

This motivated the design of a feedback mechanism acting both on ERK and p38. In fact, these kinases activate specific phosphatases - by induction of gene expression or by protein phosphorylation - which have the ability to dephosphorylate the same kinases that activate them, revealing a negative feedback circuit (Blüthgen et al., 2009; Patterson et al., 2009).

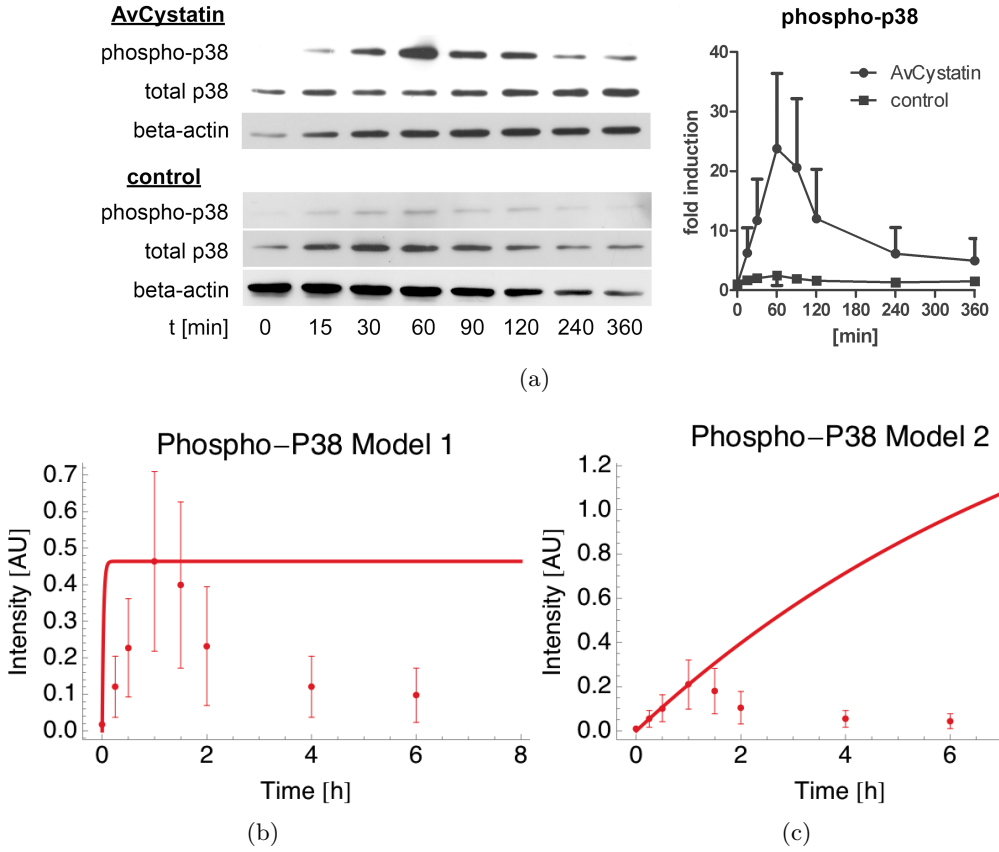

Figure 9.3.: Prediction of P38 dynamics. Solid line: predicted phospho-p38 behaviour; dots: experimental values for phospho-p38. (a) Model 1. (b) Model 2.

Other signalling molecules can also have an active role on the regulation of IL-10 production. The activation of AKT was also tested and, despite the fact that its specific inhibitor indicated a role for PI3K pathway in Av17 induced IL-10 production, no specific phosphorylation of AKT was detectable after Av17 stimulation (Klotz et al., 2011). This suggests that endogenous, physiological levels of phospho-AKT suffice for optimal cytokine production in macrophages after Av17 stimulation.

Bringing these facts together with the hypothesis suggested in Part I, that IL-10 regulates its own production, I propose three alternative regulation principles, explained in the next chapter.

10. Definition of alternative mechanisms of IL-10 regulation

To understand how the MAPKs interact and regulate IL-10 expression and to accommodate the new data, I adapted the mathematical model published in Figueiredo et al. (2009) to incorporate a negative feedback mechanism acting at the MAPK level, specifically on ERK and p38. Based on this, I constructed and tested various mathematical models and investigated their ability to predict the experimental findings. I hypothesized three underlying regulating mechanisms:

1. IL-10 itself deactivates the MAPKs (Autocrine feedback);

2. Phosphatases such as DUSPs deactivate the MAPKs;

3. An independent molecule (IM) (*i.e.*, a molecule not activated by Av17) deactivates the MAPKs.

I conducted a systematic analysis of the biologically feasible combinations of these mechanisms. A master model illustrates the scope of this analysis (Figure 10.1).

10.1. Construction of the mathematical models

This master mathematical model containing regulation reactions of interest was implemented using ordinary differential equations (ODE) in the Systems Biology Markup Language (SBML) format (Hucka et al., 2003).

Within the frame of this master model (Figure 10.1), 35 more specific models (each representing a specific hypothesis about the underlying feedback mechanisms) were generated and tested using the software tool for model generation and discrimination ModelMaGe (Flöttmann et al., 2008) [1].

In order to reduce the number of possible combinations, I assumed that:

- DUSP acts only as one single phosphatase;

- IL-10 acts either as phosphatase or kinase, but never both at the same time;

- IM acts either as phosphatase or kinase, but never both at the same time.

[1] `http://www.modelmage.org`

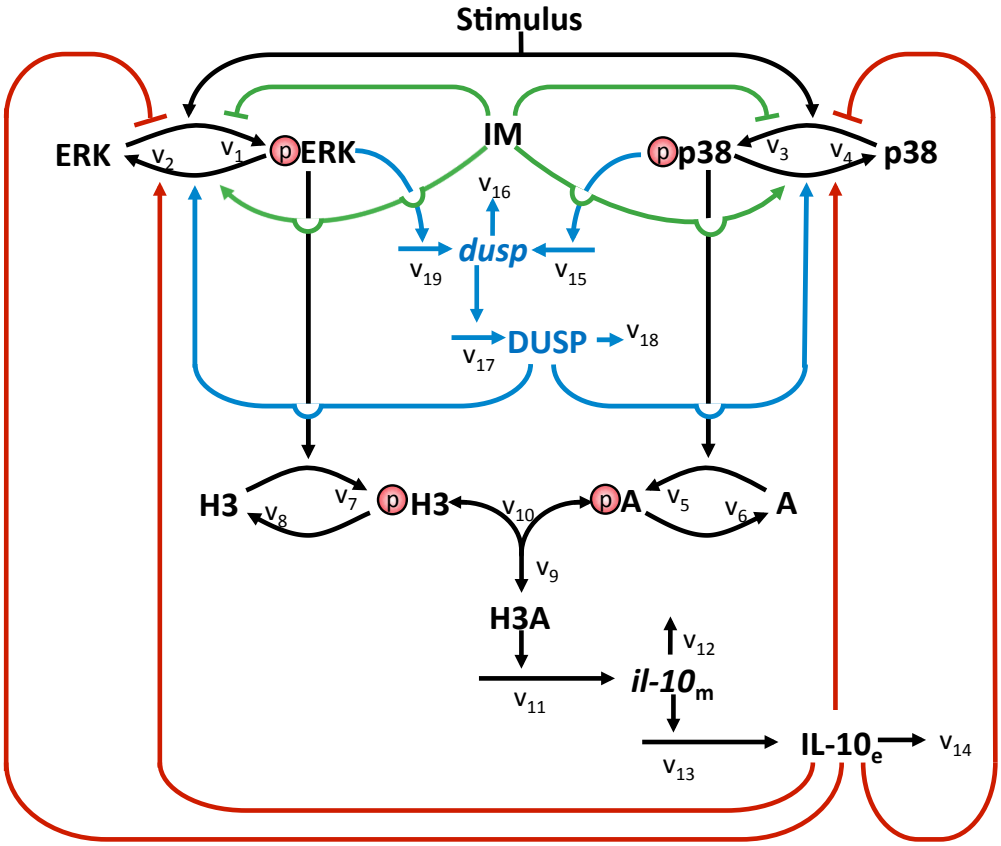

Figure 10.1.: **Wiring scheme of the master model of IL-10 production and regulation in macrophages after Av17 stimulation**. This graphical model represents possible IL-10 regulation mechanisms (regulation of IL-10 through DUSP, IL-10 or an independent molecule (IM)) and comprises the possible mechanism of achieving this regulation. Green lines represent the regulation reactions dependent on IM, blue lines represent the regulation reactions dependent on DUSP and red lines represent the regulation reactions dependent on IL-10. Black lines represent the reactions of the core model, which does not change independent of the regulation mechanism.

Table 10.1 lists the 35 alternative models.

Model	Model design
1	ERK → DUSP ⊣ ERK and IL-10 ⊣ P38 KI
2	ERK → DUSP ⊣ ERK and IL-10 ⊣ P38 PA
3	ERK → DUSP ⊣ P38 and IL-10 ⊣ ERK KI
4	ERK → DUSP ⊣ P38 and IL-10 ⊣ ERK PA
5	ERK → DUSP ⊣ (P38 and ERK)
6	P38 → DUSP ⊣ P38 and IL-10 ⊣ ERK KI
7	P38 → DUSP ⊣ P38 and IL-10 ⊣ ERK PA
8	P38 → DUSP ⊣ ERK and IL-10 ⊣ P38 KI
9	P38 → DUSP ⊣ ERK and IL-10 ⊣ P38 PA
10	P38 → DUSP ⊣ (P38 and ERK)
11	(ERK and P38) → DUSP ⊣ ERK and IL-10 ⊣ P38 KI
12	(ERK and P38) → DUSP ⊣ ERK and IL-10 ⊣ P38 PA
13	(ERK and P38) → DUSP ⊣ P38 and IL-10 ⊣ ERK KI
14	(ERK and P38) → DUSP ⊣ P38 and IL-10 ⊣ ERK PA
15	(ERK and P38) → DUSP ⊣ (P38 and ERK)
16	IL-10 ⊣ (ERK and P38) KI
17	IL-10 ⊣ (ERK and P38) PA
18	IM ⊣ ERK KI and IL-10 ⊣ P38 KI
19	IM ⊣ ERK PA and IL-10 ⊣ P38 KI
20	IM ⊣ ERK KI and IL-10 ⊣ P38 PA
21	IM ⊣ ERK PA and IL-10 ⊣ P38 PA
22	IM ⊣ ERK KI and P38 → DUSP ⊣ P38
23	IM ⊣ ERK PA and P38 → DUSP ⊣ P38
24	IM ⊣ ERK KI and ERK → DUSP ⊣ P38
25	IM ⊣ ERK PA and ERK → DUSP ⊣ P38
26	IM⊣ P38 KI and IL-10 ⊣ ERK KI
27	IM ⊣ P38 PA and IL-10 ⊣ ERK KI
28	IM ⊣ P38 KI and IL-10 ⊣ERK PA
29	IM⊣ P38 PA and IL-10 ⊣ ERK PA
30	IM ⊣ P38 KI and ERK → DUSP ⊣ ERK
31	IM⊣ P38 PA and ERK → DUSP ⊣ ERK
32	IM ⊣ P38 KI and P38 → DUSP ⊣ ERK
33	IM⊣ P38 PA and P38 → DUSP ⊣ ERK
34	IM ⊣ (P38 and ERK) KI
35	IM ⊣ (P38 and ERK) PA

Table 10.1.: Mathematical models derived from the master model shown in Figure 10.1. IM: independent molecule, KI: kinase inhibition, PA: phosphatase activation, →: activation, ⊣ : inhibition.

10.2. Model selection procedure

The workflow of Figure 10.2 illustrates the process of model selection described in the following sections.

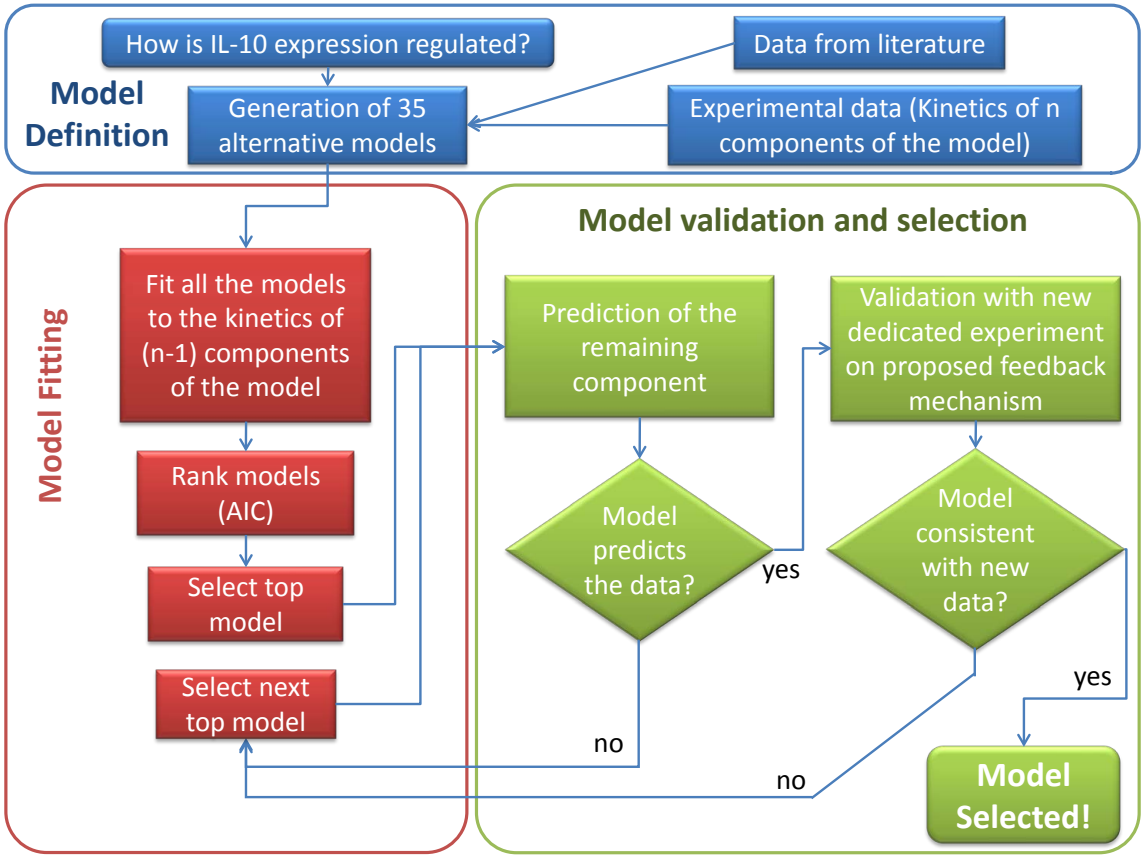

Figure 10.2.: Work flow describing the process of model selection. 35 alternative models are generated based on literature and experimental data, fitted to the available experimental data (ERK, p38, and IL-10) and ranked based on the AIC. The best model is selected and checked if it predicts the experimental data. If not, the next best model is selected until having one that fits the data. If yes, a dedicated experiment is done in order to test the specific method of regulation mechanism of the selected model. If the model is consistent with this new experiment, then the model will be selected. (Adapted from Klotz et al. (2011)).

10.2.1. Model fitting

To span over a wide range of possible parameter sets, I fitted each model several times, combining different data sets with different algorithms and parameter constraints. I fitted each model to two different data sets. Data set 1 comprised the kinetic data of IL-10 (mRNA and protein, Figure 4.3(a)) and half-life of *il-10* mRNA (for the half-life values, see Appendix A.2), together with p38 kinetics. Data set 2 comprised the same kinetic data of IL-10 (mRNA and protein) and half-life of *il-10* mRNA, but together with ERK kinetics. Each model was fitted eight times to each data set, using different algorithms and parameter ranges. I used global estimation methods to fit the different models to the data. Details about global estimation methods can be found in section 2.1.2. These were algorithms for Evolutionary Programming and Simulated Annealing. I constrained the free parameters between 0.0001 and 10 or 0.0001 and 100. To fit the models to the data, I used the software COPASI (Hoops et al., 2006).)

10.2.2. Model discrimination and selection strategy

Model discrimination was done with ModelMaGe (Flöttmann et al., 2008), using the AIC. AIC yields a relative value that scores the model, where the lowest value is the best score. (please refer to Burnham and Anderson (2002) and section 2.1.3). I calculated the AIC for each model and each fitting method, obtaining 16 different AIC values for each model. I then ranked the models (according to the lowest AIC) for each fitting method. To select between models, I then computed how often each model occurred among the“ top 10” lists. These lists can be consulted in appendix A, section B. I selected the most frequently occurring model and checked its consistency with the experimental data by comparing its predictions of ERK or p38 kinetics with the respective experimental values.

Validation and falsification of the first model This model, 17 of table 10.1, included an IL-10 dependent mechanism of the transient MAPK activation and IL-10 regulation seen in macrophages after Av17 treatment. To simplify the mathematical model I assumed that IL-10 could directly act on ERK and/or p38, whereas in reality a feedback would involve surface-located IL-10 receptors. In order to verify assumption 1, that IL-10 itself regulates the MAPKs expression (autocrine feedback), the IL-10 receptor was experimentally blocked applying anti-IL-10 receptor antibodies (anti-IL-10R ab) and the level of IL-10 expression in macrophages after Av17 treatment was compared [2] (Figure 10.3). No effect was seen on IL-10 regulation (18h and 24h) in the absence of IL-10 receptor signalling, thus excluding a feedback mechanism by IL-10 itself.

Selection of the next best model In response to this result, I searched, in the top 10 frequency list, for the models that did not include a feedback mechanism through IL-

[2] Experiment performed in the Department of Parasitology, Humboldt-Universität zu Berlin

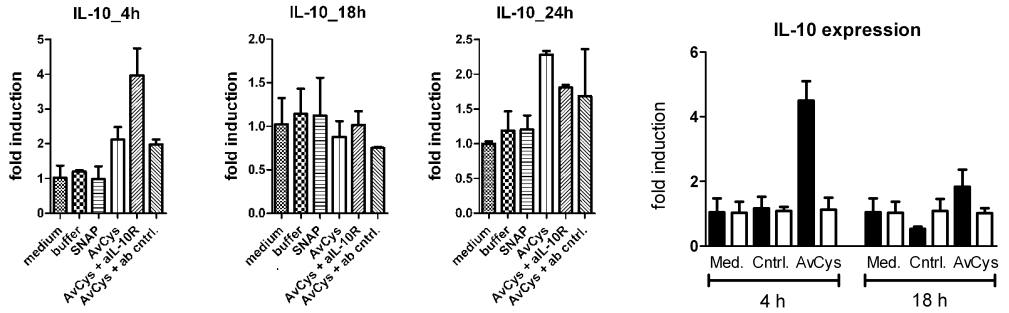

(a) (b)

Figure 10.3.: (a) IL-10 expression in macrophages stimulated with Av17 and anti-IL-10R ab at several time points. (b) IL-10 expression in Av17 stimulated macrophages from *il-10*$^{-/-}$ mice. Black bars correspond to wild type (wt) mice and white bars correspond to *il-10*$^{-/-}$ mice. At the level of IL-10 regulation, there is no significance difference between IL-10 expression in Av17 stimulated macrophages and the same cells with Av17 and anti-IL-10R ab or in *il-10*$^{-/-}$ mice. These results indicate that IL-10 does not play a role on the regulation of itself. AvCys corresponds to Av17. The materials and methods of this experiment can be found in Appendix A.4.

10. These were model 15 and model 25. To distinguish both, I calculated the average of the AIC and I created again an ordered list with the best 10 models. Model 15 was the top ranked model which did not include an IL-10 feedback mechanism. To check for the robustness of this selection method, I computed the median of the AIC and created a list with the top 10 ranked models. Again, model 15 was the best ranked model without an IL-10 feedback mechanism. Figure 10.4 shows the Venn diagram of the three "top 10" sets.

The model The selected model (model 15 of Table 10.1) assumed activation of p38 and ERK leading to DUSP expression that in turn negatively regulates both ERK and p38 (Figure 10.5). The model assumes only one variable for the activated DUSPs as a first approximation to the biological system.

Figures 10.6 illustrate how the model fits to the experimental data, showing that this model mimics the experimental findings.

I further compared the model predictions and experimental data for phospho-ERK and found a similar trend for ERK dynamics 10.7. The selected model predicts a peak of ERK dynamics at time point t=0.8 h and this is supported by the experimental data. The model curve for phospho-ERK has a faster decay than experimental phospho-ERK.

To understand the differences between *in silico* and *in vitro* phospho-ERK dynamics, I searched for another parameter set that could predict ERK phosphorylation with similar dynamics to the experimental data. I also reduced the model by supressing *il-10* and *dusp* mRNA transcription steps. In both cases, I found a parameter

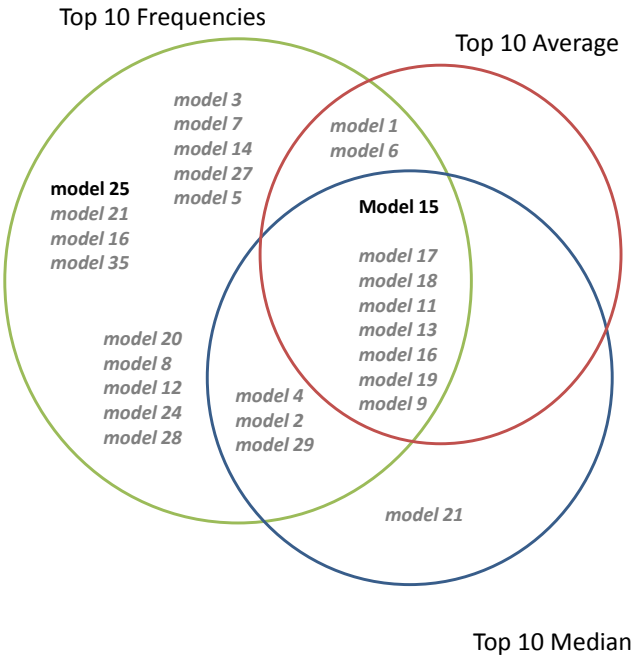

Figure 10.4.: Venn diagram of the three different top 10 sets. The green set corresponds to the "top 10" rated frequencies; the red set corresponds to the "Top 10" average and the blue set is the "top 10" median. Model 15 is the only model that intersects the three sets and does not include a regulation mechanism through IL-10. Models written in gray/italics were excluded after the dedicated experiment testing if IL-10 was responsible for the regulation mechanism.

set that predicted the ERK dynamics with a lower error than the phospho-ERK prediction of Figure 10.7. Then, to select the best model out of these three versions, I did a robustness analysis by randomly perturbing the input and analysing the effect of these perturbations on the IL-10 steady state level (please refer to section 14 for details about the method). The analysis shows that the first parameter set of model 15 is more robust than the remainder model versions Therefore, I selected model 15 as the model that best represents this biological system, in spite of the fact that it cannot perfectly mimic phospho-ERK *in vitro* behaviour.

Additionally, the behaviour of DUSP gene expression was predicted and experimentally confirmed. I resume the procedure in the following steps:

- Implement 35 alternative models that account for different regulation mechanisms of IL-10 regulation;
- Systematically fit and test these models;

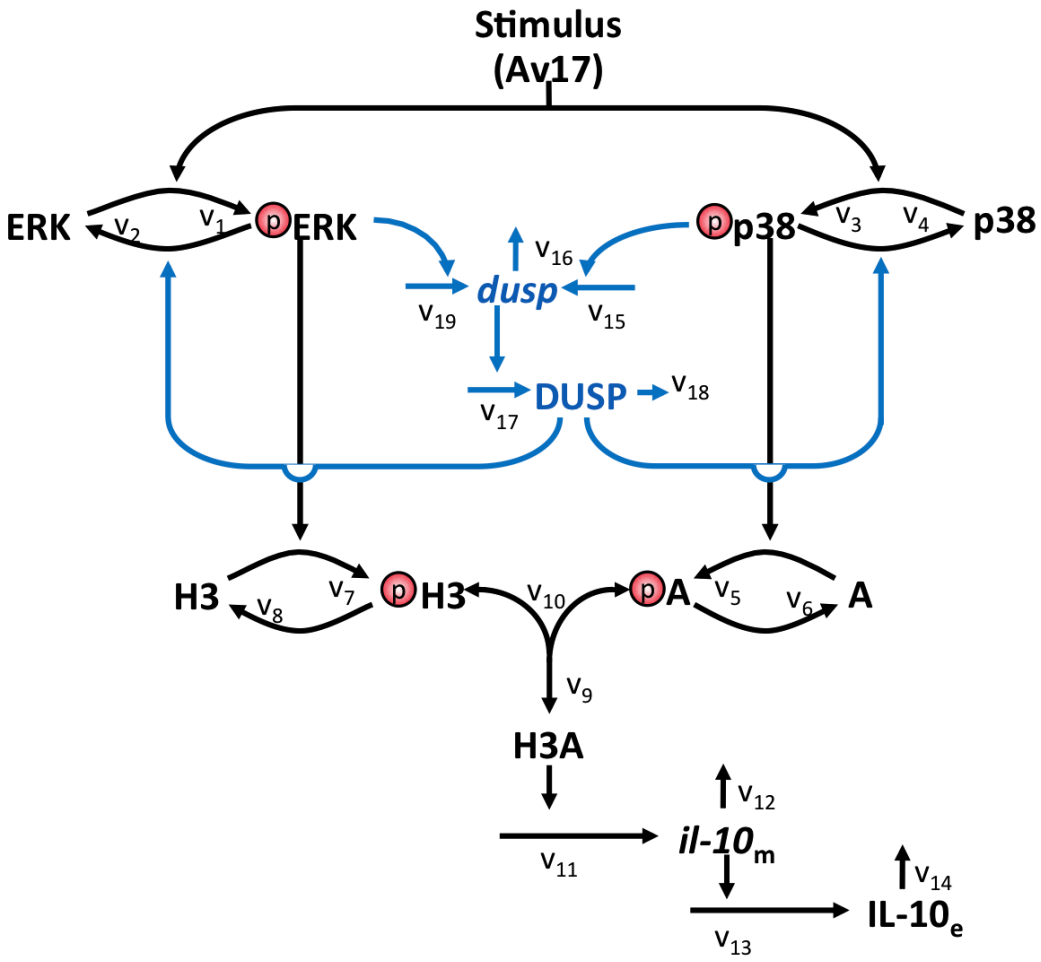

Figure 10.5.: Graphical representation of model 15 of Table 10.1.

- Model selection based on the AIC indicated a model with regulation through IL-10;
- Experimental testing of IL-10 kinetics when IL-10 blocking antibodies are added, suggests that IL-10 does not play a role in regulating the MAPKs;
- A model that includes DUSP as a regulator of ERK and P38 is selected;
- Experimental testing of DUSP suggests that DUSP1 and DUSP2 are present after Av17 stimulation and supports the selected mathematical model.

Taken together, the mathematical model hypothesises that DUSPs implement a negative feedback mechanism acting on p38 and ERK.

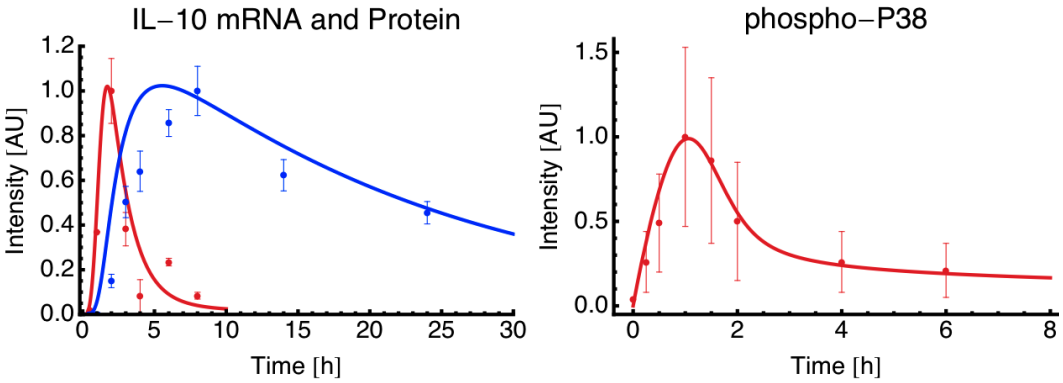

(a) (b)

Figure 10.6.: Fitted (lines) and experimental values (dots) for (a) IL-10 secreted protein and *il-10* mRNA (maximum value at 2 h). (b) phospho P38

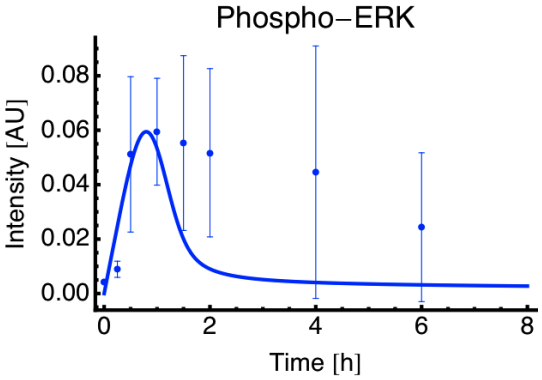

Figure 10.7.: Prediction of phospho-ERK dynamics. Line: simulated dynamics. Dots: experimental data points

11. Testing the model with further experimental data

11.1. Av17 induced differential expression of DUSPs

The selected model predicted a time dependent expression of *dusp* mRNA, having its maximum at time point t=1.7 h. To validate the predicted role of *dusps*, the kinetics of the mRNA expression of several *dusp* was experimentally tested after Av17 treatment. The tested phosphatases have all been associated with the regulation of activated MAP kinases (Liu et al., 2007). The expression of *dusp1* and *dusp2* mRNA was observed at 30 Min in Av17 stimulated macrophages. *dusp1* expression had the maximum peak at 60 Min and *dusp2* expression was constant between 30-240 Min after Av17 stimulation. There was a slight increase in the expression of *dusp5* mRNA between 30-120 Min. The mRNA levels of *dusp3*, *dusp6* and *dusp10* were not altered in Av17 treated macrophages, as Figure 11.1 pictures.

This data support the selected mathematical model and suggest that DUSP1 and DUSP2 are relevant for Av17 modulation of macrophages, since both have been described as targets and regulators of p38 and ERK (Jeffrey et al., 2006; Chi et al., 2006; Anderson and Mosser, 2002b). Moreover, a preliminary microarray data analysis suggests the presence of different *dusps* in Av17 stimulated macrophages. Please refer to Appendix C for details. I plotted the *in vitro* expression of *dusp1* and *dusp2* mRNA and *in silico* prediction of *dusp* mRNA in one graph and found that the model showed a similar trend of the expression curves and a slightly delayed expression pattern compared to experimental expression of *dusp1* and *dusp2* mRNA (Figure 11.2). The predicted *dusp* mRNA kinetics of the mathematical model reflects *dusp1* mRNA expression better than *dusp2*, indicating that *dusp1* might be more important in regulating this biological system. Moreover, a phosphorylation of DUSP1 has also been observed 11.1(B).

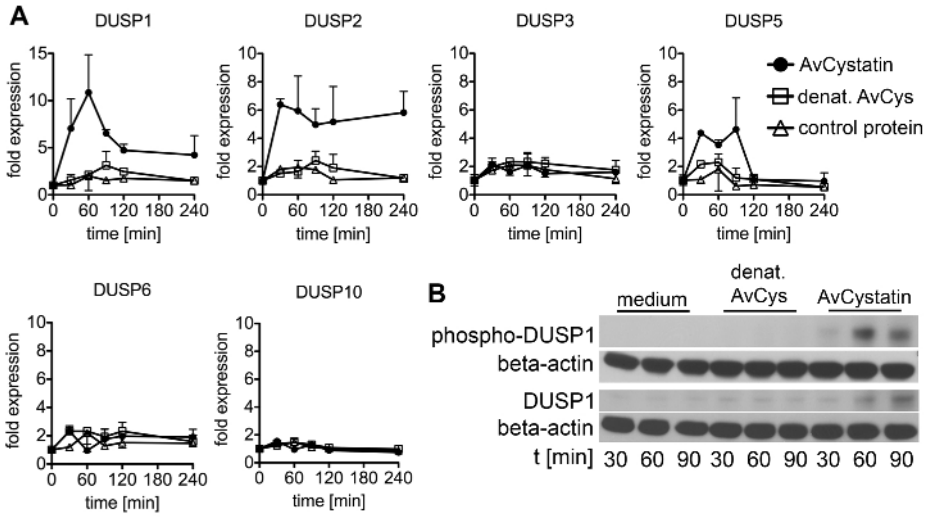

Figure 11.1.: Expression of *dusp1* and *dusp2* in macrophages by Av17. (A) Real time PCR analysis of the mRNA levels of *dusp1, dusp2, dusp3, dusp5, dusp6* and *dusp10*. (B) Western blot using antibodies against phospho-DUSP1 and DUSP1, respectively, and beta-actin. The experimental procedures of these experiments can be found in Klotz et al. (2011).

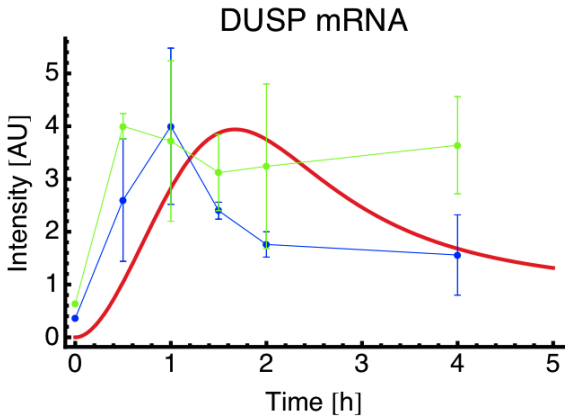

Figure 11.2.: Mapping the experimental data from *dusp1* and *dusp2* with predicted *dusp* mRNA. The values of *dusp1* and *dusp2* mRNA were converted to arbitrary units and overlay with predicted *dusp* mRNA from model 15. Line: simulated dynamics. Dots: experimental data points.

11.2. *dusp1* regulates IL-10 expression in macrophages

To further investigate the role of DUSPs, IL-10 expression and MAPK activation after Av17 treatment in macrophages from $dusp1^{-/-}$ mice were analysed (Klotz et al., 2011). Macrophages from wild type (wt) mice showed a transient *il-10* mRNA expression after Av17 treatment, whereas $dusp1^{-/-}$ macrophages showed a sustained

and increased IL-10 expression, confirming an important role of DUSP1 in IL-10 regulation in macrophages following Av17 treatment. Av17 stimulated macrophages from *dusp1*$^{-/-}$ mice showed high accumulation of phospho-p38 and slightly reduced phospho-ERK levels as compared to macrophages from wild type animals (Figure 11.3). In conclusion, this data are in accordance to the model predictions and emphasised the importance of DUSP1 for the regulation of MAPK activation and cytokine regulation in Av17 stimulated macrophages.

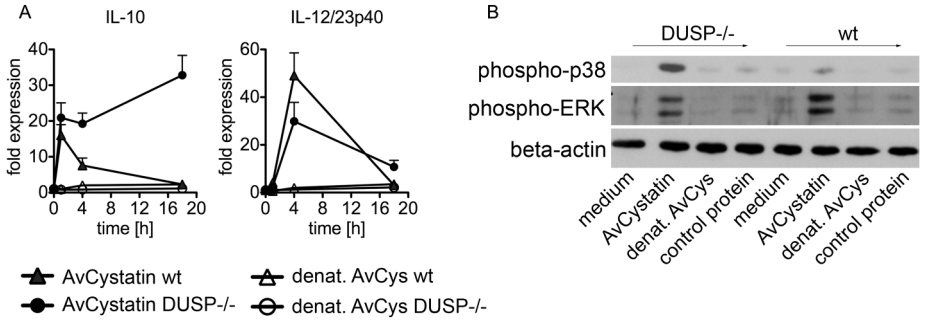

Figure 11.3.: (A,B) Macrophages from *dusp1*$^{-/-}$ mice and wt were treated with Av17 or the same amount of denaturated Av17 as a control. (A) Real time PCR analysis was performed for IL-10 and IL-12/23p40. (B) Western blot using antibodies against phospho-p38, phospho-ERK and beta-actin. Normalised data are expressed as fold induction compared to untreated controls. The experimental procedures of these experiments can be found in Klotz et al. (2011)

The dissimilarities between the model and the experimental data seen in Figure 11.2 are possibly because different DUSPs have distinct functions and for that reason their behaviour cannot be totally reflected by one representative DUSP in the model. Nevertheless, the model correctly predicts an overall effect of DUSPs on MAPK regulation.

11.3. *in-vivo dusp* measurements are closer to model predictions

In vivo measurements are important to clarify the relevance of these findings. The data revealed the induction of *dusp1* and *dusp2* mRNA expression, as well as IL-10 transient expression. I compared the DUSP *in silico* predictions with *dusp1* and *dusp2 in vivo* kinetics. Figure 11.4 shows the measurements of *dusp1*, *dusp2* and *dusp5 in vivo*.

Surprisingly, the model can more accurately predict the *in vivo* kinetics of *dusp1* and *dusp2* as of the *in vitro* kinetics, as Figure 11.5 shows.

Taken together, this data indicate that ERK and p38 activation in Av17 stimulated macrophages activate DUSP1 and DUSP2 (mRNA and protein). DUSP1 and DUSP2

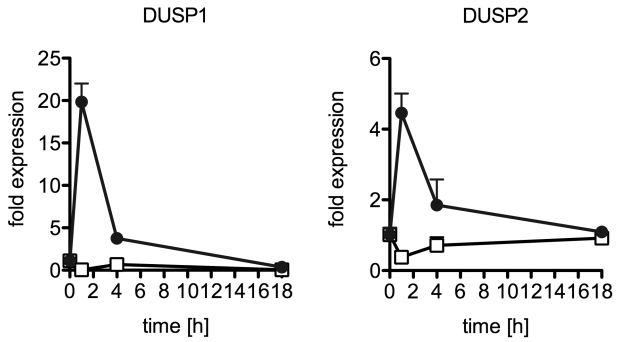

Figure 11.4.: *In vivo* effect of Av17 in macrophages shows DUSP expression. Mice were treated with Av17 or denaturated Av17 as a control for 1 h, 4 h or 18 h. This figure shows the real time PCR analysis for (A) *dusp1* and *dusp2*. Detailed experimental procedures of these experiments can be found in Klotz et al. (2011)

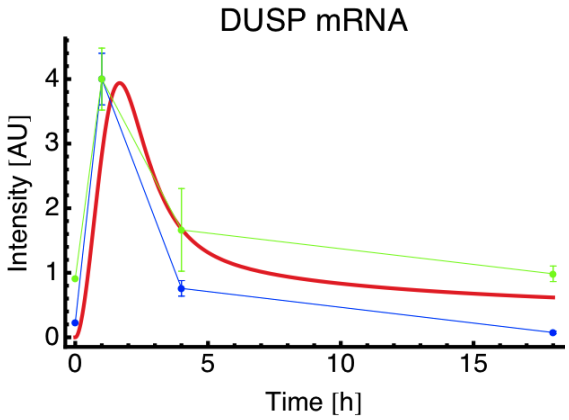

Figure 11.5.: Mapping the in vivo data from *dusp1* and *dusp2* with *in silico* DUSP. The values of *dusp1* and *dusp2* mRNA were converted to arbitrary units and overlay with predicted DUSP from model 15. Line: simulated dynamics. Dots: experimental data points.

are the feedback elements that regulate ERK and p38 activation and, consequently, IL-10 (mRNA and protein) production. These findings were supported not only by *in vitro* testing, but also by *in vivo* experiments.

11.4. A sensitivity analysis revealed that DUSP mediates crosstalk between individual MAPKs

The selected model proposes a wiring scheme that interconnects ERK and P38 through DUSP, and these components interact together in the regulation of IL-10 expression. Cross regulation is often observed between different elements of signal transduction networks. To determine possible crosstalk between ERK and p38 in Av17 stimulated macrophages and to understand the hierarchical steps of the signalling cascades, I computed a sensitivity analysis. This analysis consisted on studying how the perturbation of one species interferes with the activity of another, while keeping the remaining species untouched. More specifically, I hypothesised that DUSP mediates crosstalk between the individual MAPK components. To test this hypothesis, I perturbed the phosphorylation rate of ERK and p38 individually and I analysed the sensitivity (Equation 2.18) of p38, ERK, IL-10 protein and *dusp* mRNA in terms of signal amplitude (concentration or phosphorylation rate of the component) and the time it takes to reach signal maximum.

I used perturbation factors of 10 (reflecting increase) and 0.1 (reflecting decrease) to evaluate the effect of a higher and lower phosphorylation rate of one of the MAPK p38 and ERK, respectively, and compared them to the unperturbed values.

I compared the results of these sensitivity analysis with experimental data on the phosphorylation levels of ERK and p38 in the presence of specific inhibitors. These experimental results are in total agreement with the *in silico* sensitivity analysis.

Perturbations in the phosphorylation rate of ERK produced no effect on p38 11.6(d). In contrast, a higher or a lower phosphorylation rate of p38 produced a decreasing or an increasing effect on ERK phosphorylation rate (Figure 11.6(a)).

Experimental testing of phospho-ERK in the presence of p38 inhibitor and Av17, yielded approximately 50% stronger ERK phosphorylation levels compared to the ERK stimulation by Av17 only, indicating a negative regulatory effect of p38 on ERK phosphorylation. Interestingly, the inhibition of ERK phosphorylation did not affect the phosphorylation levels of p38 in Av17 stimulated macrophages (Figure 11.7).

Hence, the experimental data together with the mathematical model, suggested an autocrine crosstalk of p38 acting on ERK.

Next, I checked the influence of ERK or p38 on *il-10* gene expression. The sensitivity analysis showed that a perturbation of the ERK phosphorylation rate had a strong and linear effect on *il-10* expression level (Figure 11.8(a)). Inhibition of p38 phosphorylation levels resulted in the inhibition of IL-10 amplitude and a total inhibition of phospho-p38 completely blocked *il-10* expression. The experimental data, published in Klotz et al. (2011), further confirmed the model. Amplification of p38 phosphorylation levels did not affect IL-10 expression (Figure 11.8(b)). This can be explained by a possible saturation effect. Perturbations of both MAPK elements showed no significant variations on IL-10 signal build up time (Figures 11.8(a) and 11.8(b)) These results suggest that, although p38 also affects IL-10 expression levels, ERK phosphorylation is dominant in determining the level of the IL-10 expression.

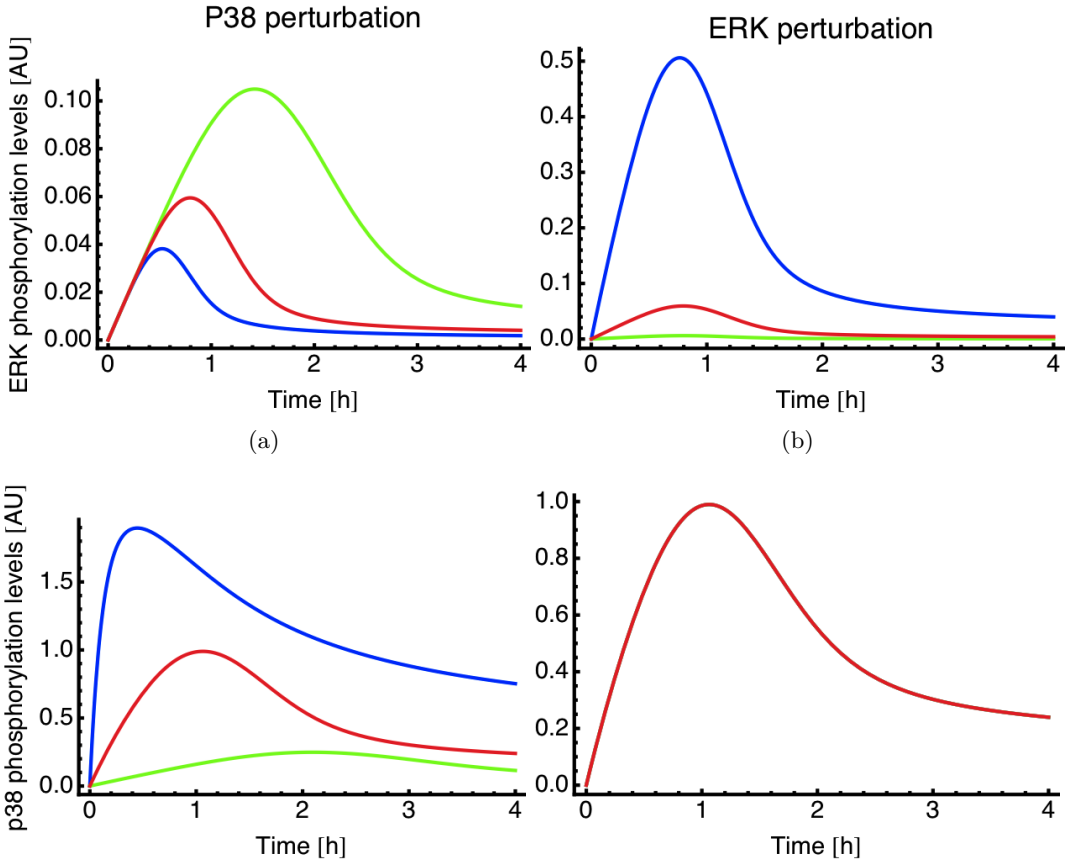

Figure 11.6.: The effect of ERK perturbations on p38 activation (a) and the effect of p38 perturbations on ERK activation (b). Range of perturbation: factor 10 and factor 0.1. Red line: no perturbation. Green line: factor of perturbation is 0.1. Blue line: factor of perturbation is 10. (a) perturbations in the phosphorylation rate of ERK produced no effect on p38 (b) higher/lower phosphorylation rate of p38 produced a decrease/increase on ERK phosphorylation rate (signal amplitude) and an increase/decrease in signal build up time

Interestingly, ERK perturbations did not affect DUSP (Figure 11.9(a)). In contrast, perturbations of p38 phosphorylation rate produced a linear effect on DUSP expression (Figure 11.9(b)).

Overall, the mathematical and experimental evidences showed that ERK affects mainly IL-10 production and regulation, whereas p38 affects mainly IL-10 and DUSP activation. Moreover, phospho-p38 inhibits the strength of ERK phosphorylation through an autocrine crosstalk.

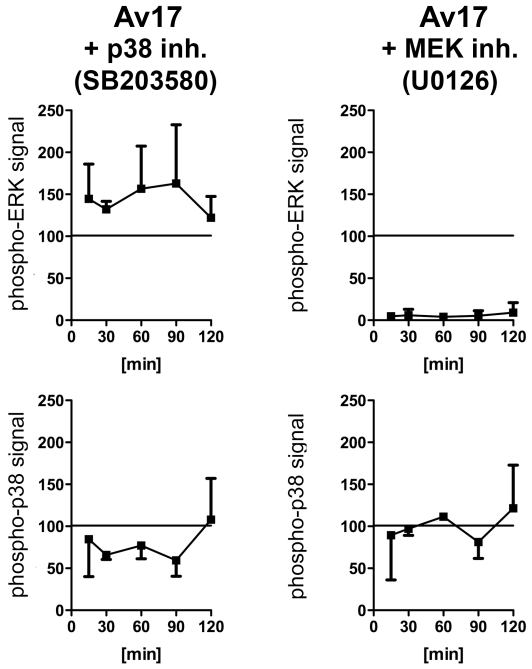

Figure 11.7.: Av17 stimulated macrophages were treated with p38 (first column) or MEK1/2 inhibitor (second column). After indicated times total cell extracts were isolated and analysed by western blot. Densitometric analysis of (a) phospho-ERK and (b) phospho-p38. Phospho-ERK and phospho-p38 signals (y-axis) are represented in percentual terms. A level of 100% means that there is no difference between the experiment with the inhibitor and its respective control. Levels between 0% and 100%, reflect inhibition of phosphorylation; levels above 100% reflect increase of phosphorylation. Experimental details in Klotz et al. (2011).

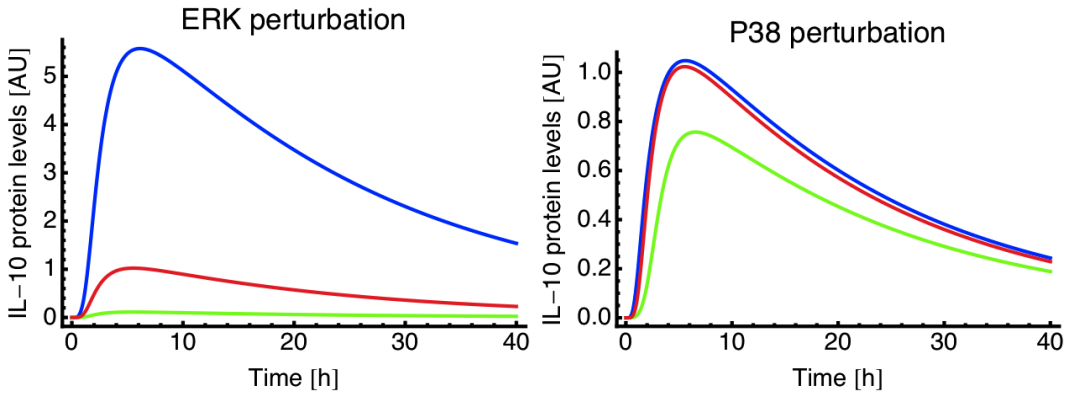

(a) (b)

Figure 11.8.: Perturbations of ERK and P38 activation on IL-10. Range of perturbation: factor 10 and factor 0.1. Red line: no perturbation. Green line: factor of perturbation is 0.1. Blue line: factor of perturbation is 10. (a) ERK phosphorylation rate had a strong and linear effect on IL-10 protein levels (b) perturbation of p38 phosphorylation rate had only a minor effect on the IL-10 amplitude.

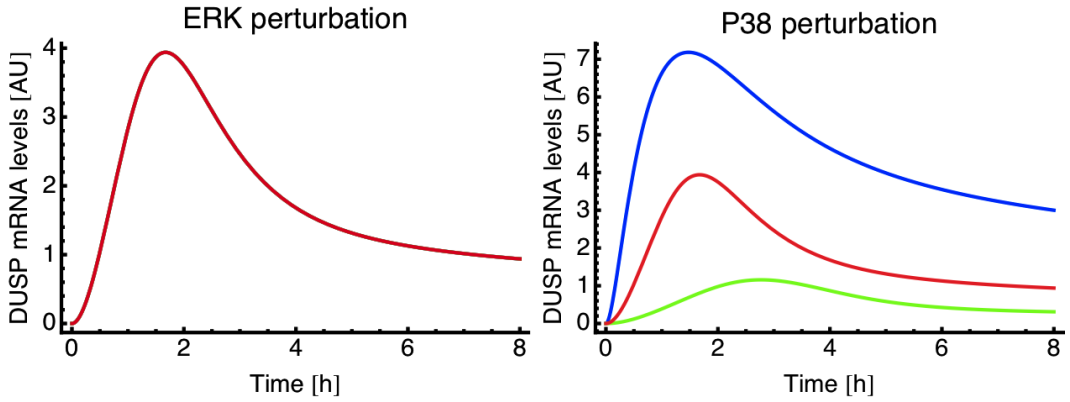

(a) (b)

Figure 11.9.: Perturbations of ERK and P38 activation on DUSP. Range of perturbation: factor 10 and factor 0.1. Red line: no perturbation. Green line: factor of perturbation is 0.1. Blue line: factor of perturbation is 10. (a) perturbations of ERK phosphorylation rate did not affect DUSP (b) a higher/lower phosphorylation rate of p38 decreases/increases the signal build up time and increases/decreases the amplitude of DUSP mRNA expression.

12. Discussion of Part II

In this part of my thesis, I used a systems biology approach to clarify which pathways lead to IL-10 regulation in macrophages after Av17 stimulation. This work was done in cooperation with the Department of Parasitology, Humboldt-Universität zu Berlin. The mathematical models developed in Figueiredo et al. (2009) and presented in chapter 4.1, hypothesised that Av17 activates the signalling cascades ERK and p38 in parallel, and that both signalling cascades are essential for IL-10 production. Experimental testing of these pathways validated the model hypothesis. However, the transient behaviour of these MAPKs suggested a regulation mechanisms acting on both ERK and p38. Therefore, I adapted the original mathematical model to include regulation mechanisms acting both on ERK and p38. I suggested that IL-10 regulation happens at the signalling level and that there are 3 different ways to achieve it:

1. IL-10 itself deactivates the MAPKs expression;
2. Phosphatases such as *dusps* deactivate the MAPKs;
3. An independent molecule (i.e., a molecule not activated by Av17) deactivates the MAPKs.

Modelling and experiments suggested that this activation is regulated by a feedback mechanism involving *dusps*.

Regulation by negative feedback mechanisms control intracellular events stimulated extracellularly. When there is activation of MAPKs, phosphatases such as DUSPs are the main characters of these control mechanisms (Jeffrey et al., 2007; Liu et al., 2007; Blüthgen et al., 2009). The selected mathematical model predicted that DUSPs regulate IL-10 production and this was validated by dedicated experiments. Av17 induced the expression of *dusp1*, *dusp2 in vitro* and *in vivo*. Moreover, in *dusp1*$^{-/-}$ mice, IL-10 expression is sustained and p38 phosphorylation is stronger than in wt mice, revealing the essential role of *dusp1* on IL-10 regulation (Klotz et al., 2011). The selected model was able to correctly predict the biological data. Consequently, I used this model to further analyse the biological network, doing *in silico* experiments more difficult to undergo *in vivo* or *in vitro*.

For this, a systems biology approach enabled the study of interconnections between the elements that compose the molecular network. I perturbed single components of the system (while keeping the remaining constant) and observed the behaviour of other components. Specifically, I disturbed ERK or p38 and checked the influence of each on p38, ERK, IL-10 and *dusp*. This model revealed that perturbations of ERK

do not affect p38 phosphorylation levels, but perturbations of p38 negatively affect ERK phosphorylation levels. This is in total accordance with the experimental data. Chemical inhibition of ERK did not influence p38 phosphorylation levels, whereas the chemical inhibition of p38 translated into a higher phosphorylation level of ERK (Klotz et al., 2011).

Moreover, ERK but not p38 positively affects IL-10 production after Av17 treatment. This is in accordance with a recent publication suggesting a linear correlation between the strength of ERK phosphorylation and IL-10 production in different cell types (Kaiser et al., 2009).

Taken together, this part of my thesis characterises the signalling mechanisms addressed by the immunomodulatory molecule Av17 in macrophages. Using a successfull approach that interlaces experiments and modelling, I present a mathematical model that can explain the biological processes addressed by the parasite *A. viteae* to induce IL-10 production in macrophages and therefore blunt an effector immune response that could kill the parasite. The ability of the parasite to explore regulatory mechanisms of its host immune system allows the survival of the parasite for more than one decade in the host.

Part III.

Robustness of IL-10 production and regulation

13. Synopsis

Robustness is a property observed in biological systems that assures their function, in spite of perturbations. I hypothesised that the interaction between parasitic nematodes and their mammalian host has been shaped to be robust, because the parasite can persist for more than 10 years within its host, by blunting the proper immune response that can eliminate the nematode. This suggests that the specific host-parasite interaction has developed mechanisms of achieving robustness against biological variations. Moreover, I assumed that the IL-10 levels' long term presence will strongly influence the interaction between this parasite and its host. Here, I compared two mathematical models with different feedback topologies and studied their properties in terms of robustness to intrinsic and extrinsic noise. In this particular case, I used the term robustness as a way of testing the variations of IL-10 steady state when the system was intrinsically and extrinsically perturbed. I say that one perturbed system is more robust than the other if the variations in IL-10 steady state of the former are lower than the variations in IL-10 steady state of the latter. I defined extrinsic noise as random perturbations imposed to the input of the system (Av17) and I defined intrinsic perturbations as random perturbations on the whole parameter set. I suggest that the model selected in the previous part is robust to intrinsic and extrinsic noise and that the negative feedback mechanism provides robustness to this particular system. Moreover, I propose a method of model discrimination based on a time dependent sensitivity analysis.

14. A Monte Carlo analysis suggests that integral feedback is more robust then transient feedback

14.1. The models

I compared the selected model of Part II, Model DUSP (model 15 of table 10.1, Figure 14.1) with model IL10 (model 17 of table 10.1, Figure 14.2). Both models picture the signalling events that lead to IL-10 production and regulation. In the first model, I assume that MAPK-induced DUSP promotes the negative feedback. In the second model, I assume that IL-10 acts as the feedback promoter. Both models comprise a transcriptional feedback and IL-10 production after a complex formation. The models are distinguished by the type of feedback: the first model acts as an integral feedback and the second one acts as a transient feedback. Transcriptional feedbacks can be integral, depending on the parameter sets and degradation rate of the elements. An integral feedback, integrates the error between the effective and the desired output. It guarantees that the desired output level is reached, because otherwise, the error would always be increasing. The parameter set defines the type of feedback. I say that model DUSP has an integral feedback, because it achieves almost perfect adaptation and that model IL10 has a transient feedback because the element that implements the feedback, IL-10 protein, is transient.

14.2. Random perturbation of the input

The concentration of parasite and of its byproducts may not always be constant in time. I assumed a biological variation of 20% around a basal value of Av17 concentration. To study the effect of these variations on IL-10 steady state, I performed a Monte Carlo analysis over the variable responsible for the input ($s(t)$).

I simulated the extrinsic noise by assuming that the variable $\xi(t)$ of equation 2.15 is a Normal distribution with mean 0 and standard deviation 0.1, which samples 100 random values in the time interval between 0 and 100 [h], around 20% of the original input value ($s_0 = 1$). I interpolated the random function and summed it to the unperturbed input value.

Figure 14.3 illustrates an example of the randomly perturbed input, $s(t)$ of equation 2.15.

I generated 50 different perturbed inputs with the same characteristics described

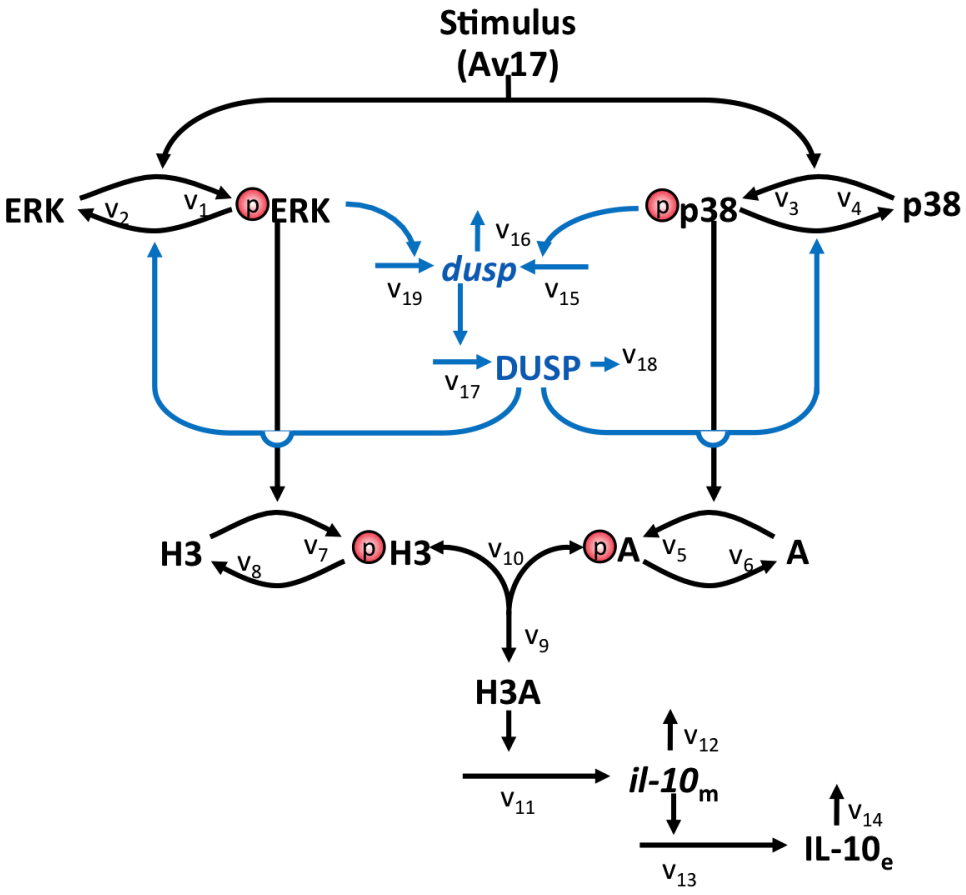

Figure 14.1.: Model DUSP: transcriptional feedback through DUSP - acts as an integral feedback with almost perfect adaptation.

above. I fed these 50 different input functions to the model and, for each, I calculated the steady state of IL-10.

Figures 14.4(a) and 14.4(b) plot the effect of extrinsic noise on IL-10 dynamics for model DUSP and model IL10, respectively. The highest level of perturbation happens when IL-10 reaches the maximal amplitude in both models, but model DUSP presents the highest perturbation for IL-10 maximal amplitude and the lowest for IL-10 steady state. Model IL10, in contrast, has a constant perturbation span over time. Both models are robust to input perturbations, but at the level of IL-10 steady state, model DUSP is more robust, as the histogram of Figure 14.6(a) indicates.

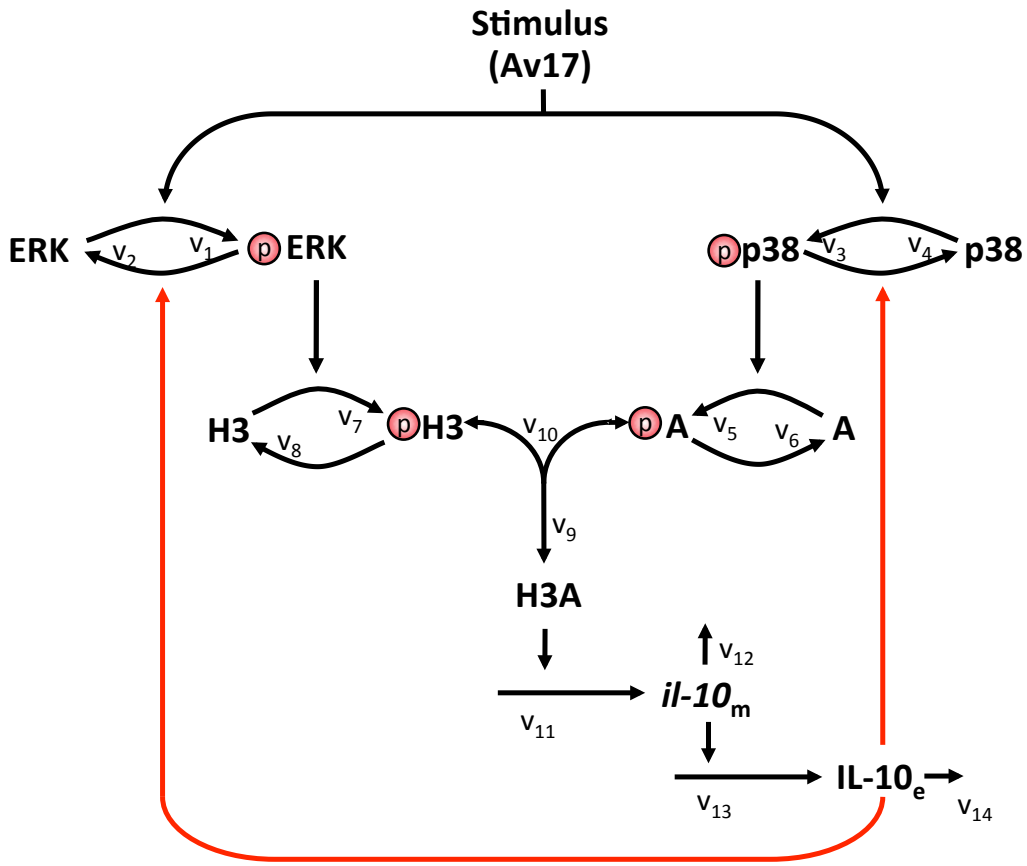

Figure 14.2.: Model IL10: transcriptional feedback through IL10 - acts as a transient feedback where the steady state of IL-10 stays at half of the maximal amplitude of the signal.

14.3. Random perturbation of the whole parameter set

I simulated intrinsic noise by perturbing the whole parameter set of each model at once. These were random perturbations of 20% around each element of the parameter set. Assuming that the parameter set is $P = \{p_1, p_2, ..., p_n\}$, for each p_i, I generated a random value r_i, which was limited to 20% around p_i, ie, $p_i * 0.8 < r_i < p_i * 1.2$. I did this for each parameter, constructing then a perturbed parameter set $\tilde{P} = \{\tilde{p}_1, \tilde{p}_2, ..., \tilde{p}_n\}$. I created 50 different parameter sets $\tilde{P}$ and computed the IL-10 steady state for each.

I observed that intrinsic noise has a more profound impact when measuring IL-10 steady state than extrinsic noise. Model DUSP presents less variations in IL-10 steady state than Model IL-10 when faced with changes in the whole parameter set.

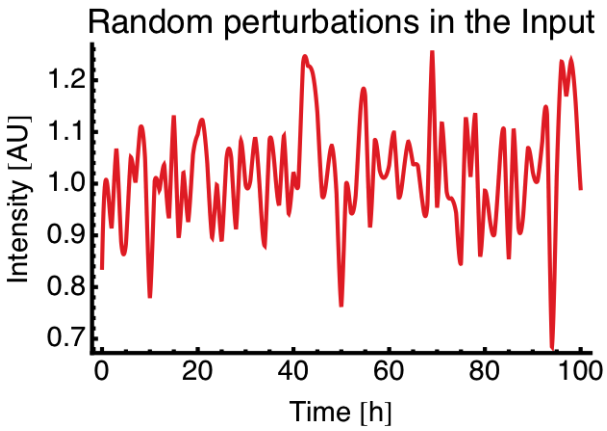

Figure 14.3.: Example of a perturbed input signal. 100 random values were sampled from a Normal Distribution with mean 0 and standard deviation 0.1 around the original input value and then interpolated.

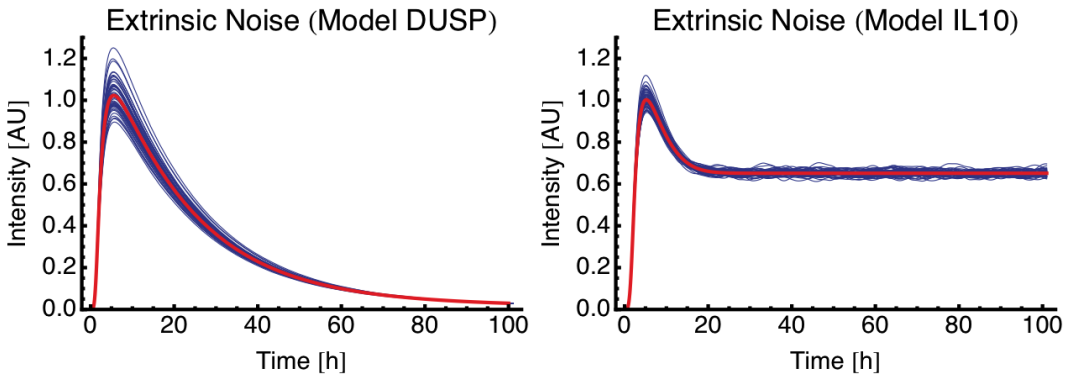

(a) (b)

Figure 14.4.: Random perturbations on Av17 concentration affect IL10 production. IL-10 dynamics for (a) Model DUSP (b) Model IL-10.

Figures 14.5(a) and 14.5(b)show the time courses of IL-10 dynamics and Figure 14.6(b) shows the histogram of IL-10 steady state when both models are faced with intrinsic perturbations. The large spread of values observed for model IL10, indicates that IL-10 steady state varies much more than the IL-10 steady state of Model DUSP, when exposed to variations. (Intrinsic noise provokes a standard deviation of 0.01 in model DUSP and of 0.07 in model IL10). As in the case of extrinsic perturbation, model DUSP adapts better to perturbations than model IL10. This result is expected, because model DUSP implements an integral feedback, which has the characteristic of achieving adaptation. Hence, despite the fact that model DUSP has broader variations at the maximal amplitude than model IL10, the former can adapt, achieving residual values and a variation close to zero, whereas the latter, for

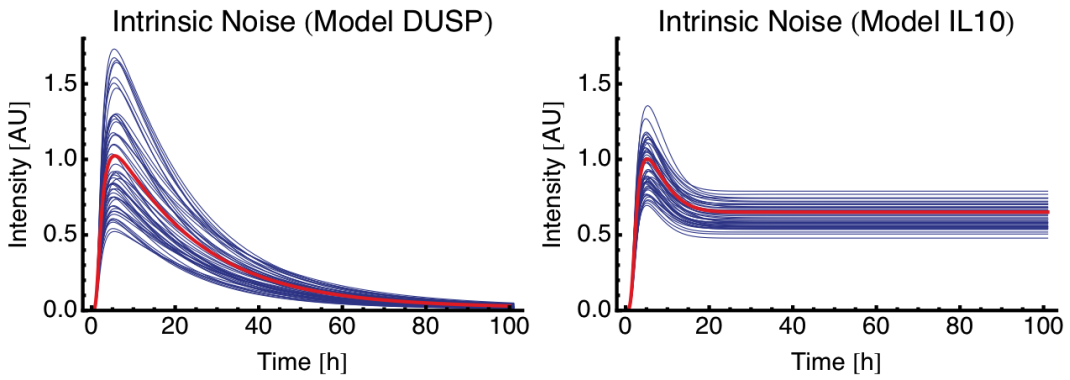

(a) (b)

Figure 14.5.: Random perturbations on the parameter set affect IL10 production. IL-10 dynamics for (a) Model DUSP (b) Model IL10.

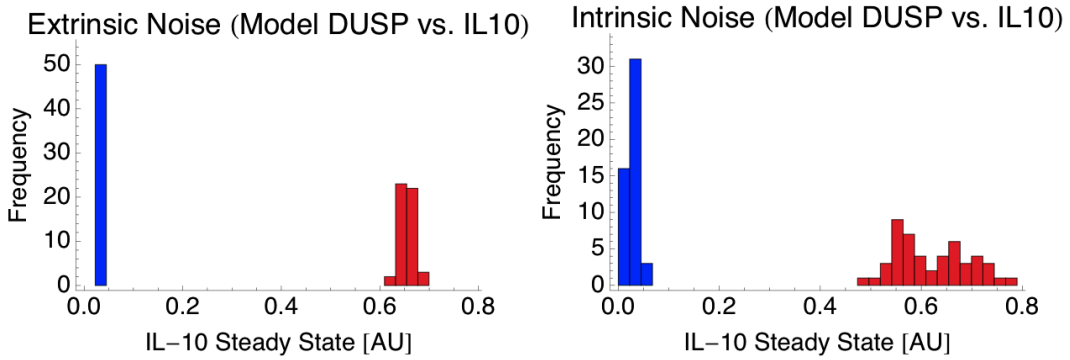

(a) (b)

Figure 14.6.: Histogram of IL-10 steady states when the model is subject to: (a) extrinsic perturbations. (b) intrinsic perturbations. Blue: Model DUSP. Red: Model IL10.

the studied parameter sets, cannot attain perfect adaptation.

15. Feedback provides robustness in model DUSP

I pruned the arm responsible for the feedback mechanism on each model and I did the Monte Carlo analysis described in chapter 14 on these models without feedback. I compared the model with feedback and without feedback. The Monte Carlo analysis here described, consists of simulating extrinsic and intrinsic noise (as explained in chapter 14)

15.1. Extrinsic noise

The feedback mechanism clearly provides robustness to model DUSP. Model IL10 is slightly more robust with feedback than without in terms of IL-10 steady state. Interestingly, in terms of maximal concentration of IL-10, the models have opposite behaviours when the feedback is cut out. In model DUSP, the feedback attenuates the maximal concentration of IL-10, whereas in model IL10, it amplifies it. Figure 15.1 shows the perturbations of model DUSP, with and without feedback.

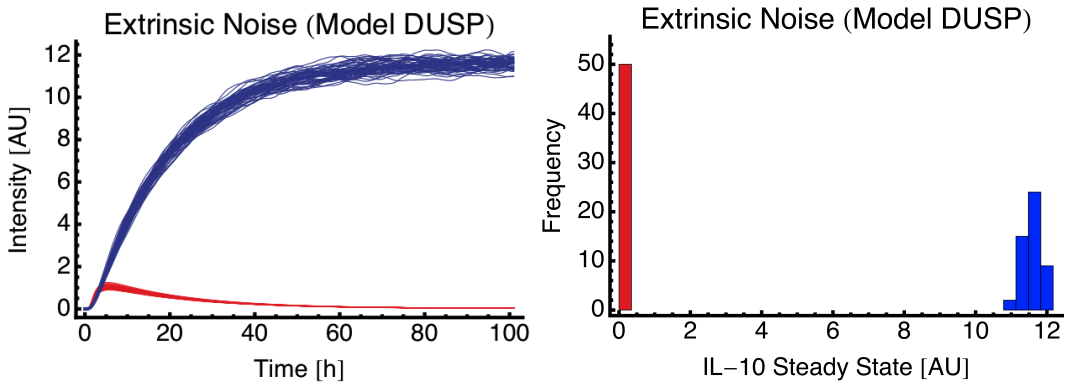

(a) (b)

Figure 15.1.: Comparison of model DUSP with feedback (Red) and without (Blue). Feedback provides robustness against extrinsic noise in terms of IL-10 steady state. (a) IL-10 dynamics. (b) Histogram of IL-10 steady state.

Interestingly, a feedback mechanism does not bring much of robustness to model IL10. In the absence of feedback, the dynamics of IL-10 are sustained and the

maximal amplitude is lower than in the model IL10 with feedback. Figure 15.2 compares model IL10 in both versions.

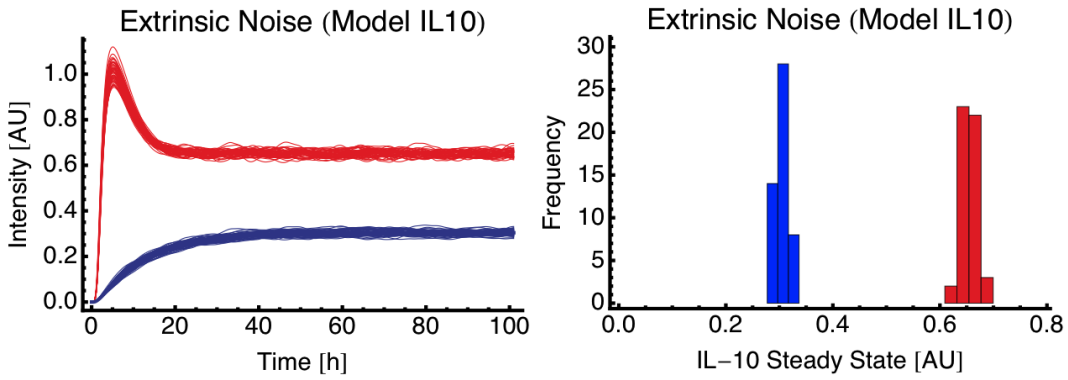

(a) (b)

Figure 15.2.: Comparison of model IL10 with feedback (Red) and without (Blue). Feedback provides robustness against extrinsic noise in terms of IL-10 steady state. (a) IL-10 dynamics. (b) Histogram of IL-10 steady state.

15.2. Intrinsic noise

Intrinsic noise has a very similar effect on model DUSP as extrinsic noise, when comparing this model with and without feedback. Figure 15.3 is very similar to Figure 15.1.

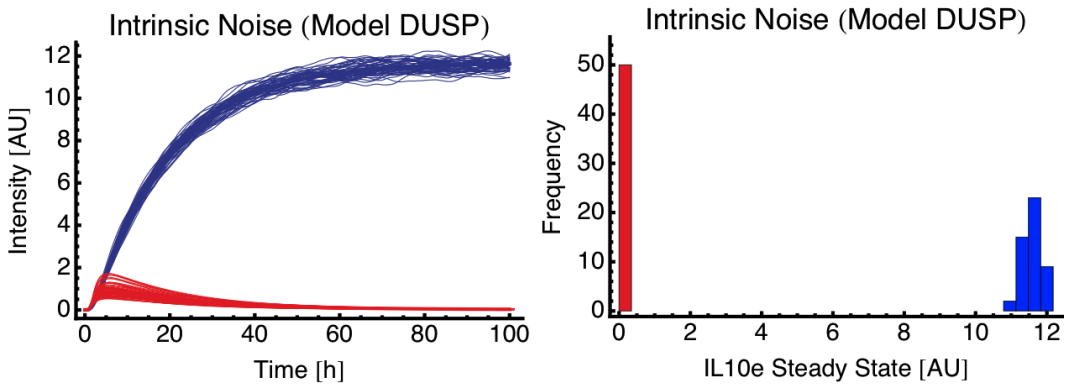

(a) (b)

Figure 15.3.: Comparison of Model DUSP with feedback (red) and without (blue), when subject to intrinsic noise. (a) IL-10 dynamics. (b) Histogram of IL-10 steady state.

The difference in robustness between model IL10 with and without feedback, is more striking when both models are subject to intrinsic noise. In this case, model

IL10 without feedback is clearly more robust than its counterpart with feedback, as Figure 15.4 shows.

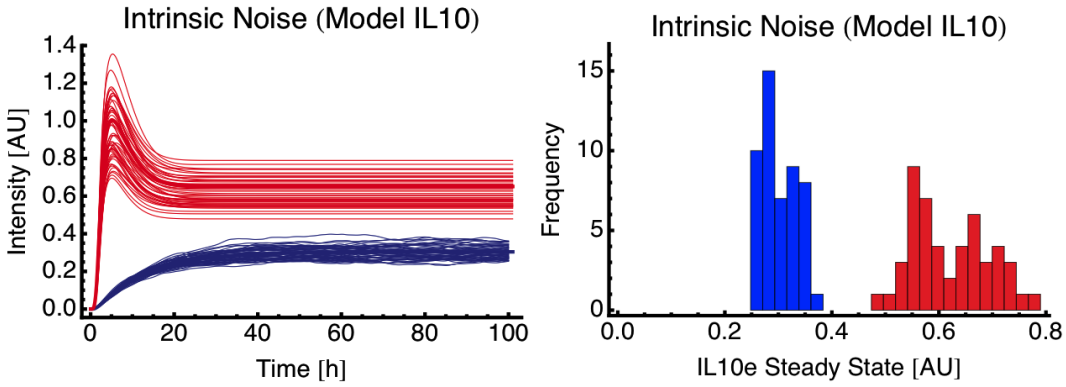

(a) (b)

Figure 15.4.: Comparison of Model IL10 with feedback (red) and without (blue), when subject to intrinsic noise. (a) IL-10 dynamics. (b) Histogram of IL-10 steady state.

Negative feedback mechanisms bring about robustness at the cost of maximal amplitude, that is, a system with a negative feedback mechanism is, by definition, more robust than the same system without feedback, where the former does not reach the same maximal amplitude as the latter. Model IL10 goes against this hallmark of feedback regulation. In this particular case, the absence of a feedback mechanism lowers the maximal concentration of IL10. This happens because the maximal value of the variable $IL10e(t)$ was normalised to 1. By pruning the arm that provides feedback to model IL10, I set the reaction $v_2 = k_2 \cdot ERK_p\,(t) \cdot IL10e\,(t)^h$, to $v_2 = k_2 \cdot ERK_p\,(t)$. This corresponds to setting the variable $IL10e(t)$ to its maximal value, 1. To override this problem, the normalisation of $IL10e(t)$ could be done by setting its maximal value to 100, for instance.

Model DUSP and model IL10 have opposite behaviours when the feedback is cancelled. Model DUSP has a higher amplification and higher variation of IL-10 steady state, when the feedback mechanism is cut. Model IL10 has a lower amplification and a lower variation without regulation.

The difference between these two models without feedback lies on the production of DUSP and on the specific parameter sets. The fact that model IL10 is more robust to noise when there is no feedback, is due to its particular parameter set and to $IL10e(t)$ normalisation factor.

16. Single parameter perturbations do not affect the overall robustness of the models

I perturbed each single parameter on 10%, 20% and 50% around its original value and analysed its effect on IL-10 steady state. I calculated the sensitivity of each perturbation, using the formula 2.18.

Model DUSP Table 16.1 shows the sensitivity of each parameter of model DUSP to the perturbations mentioned above.

	-10%	-20%	-50%	10%	20%	50%
k_1	-0.89	-0.79	-0.49	-1.09	-1.19	-1.49
k_2	0.99	0.99	0.99	0.99	0.99	0.99
k_3	-0.009	-0.008	-0.006	-0.01	-0.01	-0.01
k_4	0.010	0.01	0.008	0.01	0.01	0.01
k_5	-0.89	-0.79	-0.49	-1.09	-1.19	-1.49
k_6	0.99	0.99	0.99	0.99	0.99	0.99
k_7	-0.89	-0.79	-0.49	-1.09	-1.19	-1.49
k_8	0.99	0.99	0.99	0.99	0.99	0.99
k_9	1	1	1	1	1	1
k_{10}	-0.89	-0.79	-0.49	-1.09	-1.19	-1.49
k_{11}	-0.89	-0.79	-0.5	-1.1	-1.2	-1.5
k_{12}	1	1	1	1	1	1
k_{13}	-0.89	-0.79	-0.5	-1.1	-1.2	-1.5
k_{14}	1.19	1.25	1.92	1.13	1.11	1.08
k_{15}	1	1.01	1.01	1	1	1
k_{16}	-0.91	-0.81	-0.5	-1.1	-1.22	-1.53
k_{17}	1	1.01	1.01	1	1	1
k_{18}	-0.01	-0.01	-0.008	-0.01	-0.02	-0.02
k_{19}	$\sim$0	$\sim$0	$\sim$0	$\sim$0	$\sim$0	$\sim$0

Table 16.1.: Table of sensitivities for model DUSP.

A detailed analysis of the table indicates that most of the parameters are insensitive to changes (section 2.2.4). Two main groups can be defined: parameters with positive sensitivities and parameters with negative sensitivities.

Parameters $k_2, k_4, k_6, k_8, k_9, k_{12}, k_{14}, k_{15}$ and k_{17} have positive sensitivities. This means that an inhibition of the parameter will reflect an inhibition of the output. Attempting to Figure 14.1, the reader can observe that the positive parameters correspond to the reactions of dephosphorylation (k_2, k_4, k_6, k_8), complex disagreggation (k_9) and IL-10 degradation (k_{12}, k_{14}), except for reactions k_{15} and k_{17}, which correspond to DUSP transcription and translation. ERK and p38 induce the parallel expression of two concurrent genes: *il-10* and *dusp*. DUSP represses ERK and p38 and, consequently, represses IL-10 production. More DUSP increases the dephosphorylation rate of ERK and p38, hence decreasing IL-10 concentration. So, if k_2 goes up, IL-10 maximal value should go down. It might be that, at steady state, IL-10 changes at the same rate as ERK dephosphorylation rate changes. It should also be noted that the parameters responsible for DUSP transcription and translation are the only ones that have positive sensitivities and refer to production. All the others refer either to degradation or disaggregation. Also interesting is that all positive sensitivities, except the one referent to IL-10 degradation, have the same value for different perturbations.

The second group, the negative sensitivities, is mainly constituted by reactions of phosphorylation, complex formation and production, except for the case of DUSP. The sensitivity of the parameter for *dusp* mRNA degradation is positive and for DUSP protein degradation is close to zero. All negative sensitivities vary with the specific perturbation value (except for k_4 and k_{18}, which yield a sensitivity value close to zero) and the perturbation of 50% yields the highest sensitivity. Interestingly, in the group of positive sensitivities, all parameters present the same sensitivity for different perturbations, except k_{14}, which yields the highest sensitivity when the perturbation is -50%. Nevertheless, a system is said to be sensitive when $S >> 2$ (2.18). This last observation is in line with the last chapter, where I show that model DUSP is robust to variations. This sensitivity analysis shows that the system is also robust to single parameter perturbations.

Model IL10 Table 16.2 shows the sensitivities of model IL10. They were calculated as previously described for model DUSP.

Interestingly, model IL10 has a very defined pattern of sensitivities. All phosphorylation reactions have negative sensitivities, whereas the respective dephosphorylation reactions have a positive S. But, contrary to the previous case, the complex formation X2, *il-10* mRNA expression and IL-10 protein production have negative sensitivities and their counterpart reactions (complex disagreggation, IL-10 (mRNA and protein) degradation) have positive sensitivities.

All sensitivities were below two for both models. Therefore, I can conclude that both models are robust to single parameter perturbations.

	-10%	-20%	-50%	10%	20%	50%
k_1	-0.29	-0.27	-0.2	-0.33	-0.35	-0.4
k_2	0.3	0.28	0.23	0.32	0.33	0.36
k_3	-0.2	-0.27	-0.2	-0.33	-0.35	-0.4
k_4	0.3	0.29	0.24	0.33	0.34	0.36
k_5	-0.33	-0.3	-0.22	-0.37	-0.4	-0.46
k_6	0.34	0.32	0.27	0.36	0.37	0.4
k_7	-0.33	-0.31	-0.22	-0.38	-0.4	-0.46
k_8	0.34	0.33	0.28	0.37	0.38	0.41
k_9	0.35	0.33	0.28	0.37	0.38	0.41
k_{10}	-0.34	-0.31	-0.22	-0.38	-0.41	-0.47
k_{11}	-0.34	-0.31	-0.22	-0.39	-0.41	-0.47
k_{12}	0.35	0.33	0.28	0.37	0.38	0.41
k_{13}	-0.34	-0.31	-0.22	-0.39	-0.41	-0.47
k_{14}	0.35	0.33	0.28	0.37	0.38	0.41

Table 16.2.: Table of sensitivities for model IL10.

17. Time dependent sensitivity analysis

I conducted a time dependent sensitivity analysis by applying infinitesimal changes in each parameter and checking its effect on IL-10. This method, presented in section 2.2.5 shows how the sensitivity of a specific element to a single parameter changes over time, in terms of its response coefficients. The aim of this chapter is to propose a method of model selection based on a dedicated experiment, which tests the element that presents a higher difference between the concurrent models.

Response coefficients indicate the change in a species concentration after infinitesimal perturbations. I calculated the response coefficients for IL-10. The infinitesimal perturbations were imposed to each parameter and to the initial condition of each species.

17.1. Model DUSP

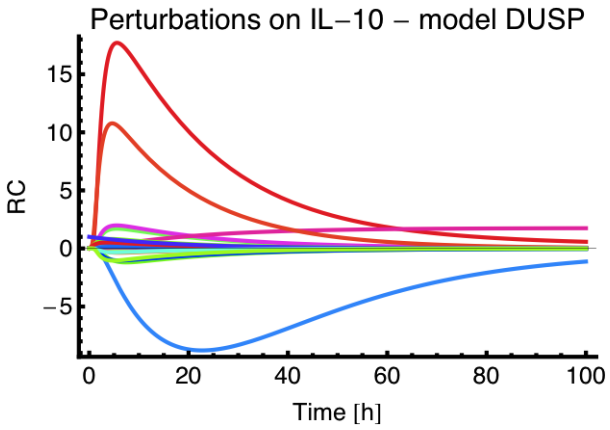

Figure 17.1.: Positive and negative sensitivities of model DUSP with the highest absolute maximal values. Red: positive sensitivity (k_1 with maximal amplitude of 17.7 at t=5.6. Green: Negative sensitivity k_{14} with minimal amplitude of -8.78 at t= 22.7

Figure 17.1 shows the response coefficients for IL-10 over time. k_1, the parameter responsible for ERK phosphorylation, influences IL-10 the most, at t=5.6h. Interestingly, IL10 reaches maximal amplitude at t=5.5h. The parameters responsible for species phosphorylation (k_1, k_3, k_5 and k_7) are all positive and have a time course similar to IL-10 species. k_{10} (X2 complex disaggregation), k_{11} and k_{13} (*il-10* mRNA and IL-10 protein production), k_{k16} and k_{k18} (DUSP (mRNA and protein degradation), also have positive sensitivities. Reversely, the parameters that dephosphorylate

the model species (k_2, k_4, k_6 and k_8), have negative sensitivities, although the absolute time course is similar to the previous case. Other parameters with negative sensitivity and transient time course are k_9 (complex formation X2), k_{12} and k_{14} (*il-10* mRNA and IL-10 protein degradation, respectively), k_{15} and k_{19} (*DUSP* mRNA production), and k_{17} (DUSP protein production). Interestingly, IL-10 and DUSP have reverse characteristics. If the parameters for IL-10 production have a positive time course sensitivity, those for DUSP have a negative time course sensitivity and vice versa. The fact that DUSP plays an indirect role on IL-10 decrease explains this observation. The positive sensitivity with the highest maximal amplitude is k_1 and the negative sensitivity with the highest minimal amplitude is k_8, which is the parameter responsible for histone 3 dephosphorylation. Figure 17.2 shows both sensitivities.

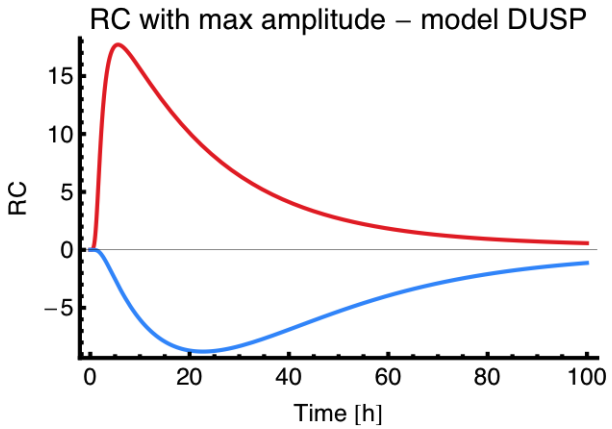

Figure 17.2.: Sensitivity with highest positive and negative maximal amplitudes, model DUSP.

Atypical time dependent sensitivities I selected the sensitivities with an atypical time course and analysed why they are different from the typical pattern of sensitivities, that has a transient time course.

Figure 17.3 shows the parameters and initial conditions with higher sensitivity and higher dynamic changes.

If a parameter switches its influence on a certain species over time, *e.g.*, if the time dependent sensitivity analysis change from positive to negative, then the parameter changes its influence over the species along the specific temporal trajectory. This happens with the sensitivity of IL-10 to p38p[0], the initial condition of phosphorylated p38 (Orange curve of Figure 17.3).

To understand better how this sensitivity correlates with IL-10 dynamics, I calculated the parametric plot, represented in Figure 17.4.

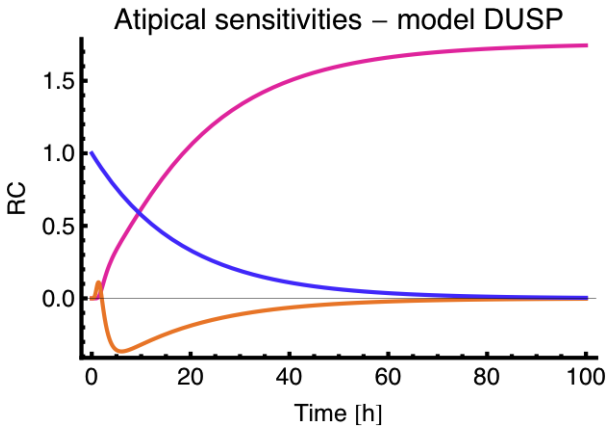

Figure 17.3.: Most relevant time dependent sensitivities of Model DUSP. Pink: parameter k_{18} - DUSPp degradation; Orange: P38p initial condition;Violet: IL10e initial condition.

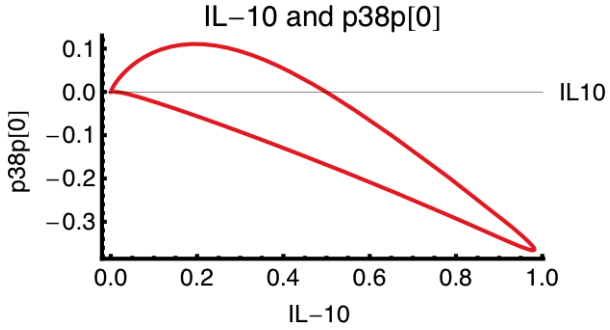

Figure 17.4.: Parametric plot of IL-10 dynamics and the time dependent sensitivity of IL-10 to p38p initial condition.

IL-10 dynamics and the sensitivity of p38p[0] grow until the sensitivity of p38p[0] reaches its maximum (0.11 AU). IL-10 keeps growing and the sensitivity of IL-10 to p38p[0] starts decreasing. When IL-10 reaches 0.5 AU (the half of its maximal amplitude) the sensitivity of IL-10 to p38p[0] switches from positive to negative. This means that at IL-10 half amplitude, p38p[0] starts having a negative influence on this cytokine.

A sensitivity of value 1 means that a perturbation of value x on a specific parameter will reflect a perturbation of the same value x on the output of the system. The sensitivity of IL-10 to IL-10 initial condition is 1. This trivial observation leads to the analysis of the sensitivity time course. The violet curve of Figure 17.3 shows that this sensitivity decreases with time, approaching zero. A sensitivity that tends to zero means that a very high perturbation has a very small effect in the output. To better understand why is it that the dynamic sensitivity of IL-10 to its own initial condition is not constant in time, I analysed the parametric plot shown in Figure 17.5(a).

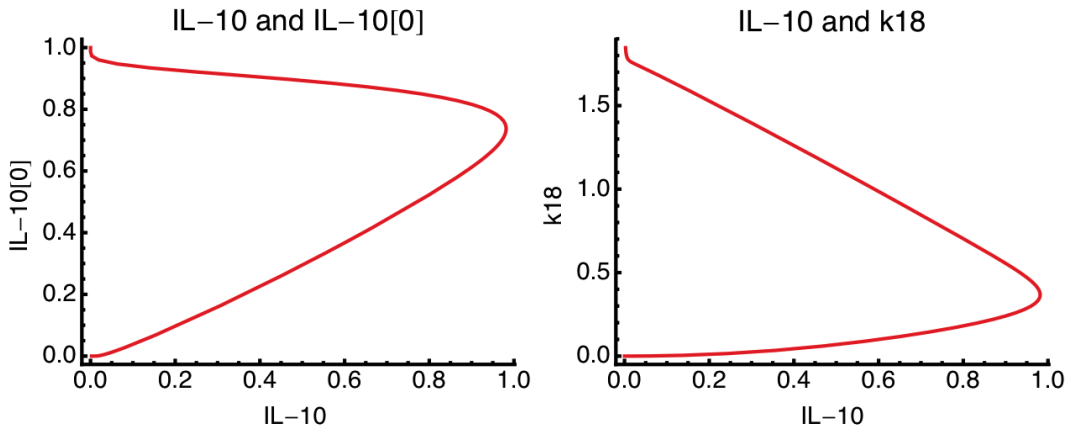

(a) (b)

Figure 17.5.: (a) Parametric plot of IL-10 dynamics and the time dependent sensitivity of IL-10 to IL-10 protein initial condition (b) parametric plot between k_{18} and IL-10.

IL-10 amplitude grows from 0 to 1 as the sensitivity of IL-10 to its initial condition decreases from its initial value 1. When S=0.75, IL-10 reaches its maximal value and starts decreasing until approaching zero. This sensitivity has a time course that resembles a negative exponential curve.

The sensitivity of IL-10 to perturbations on k_{18}, which is the degradation rate of DUSP protein has a contrasting behaviour with the sensitivity of IL-10 to perturbations on its own initial condition. The former has an exponential trend and the latter, a logarithmic trend. DUSP has a slow growth and a sustained time course at t=40 000 h. It therefore indicates a very low degradation, confirmed by the value of $k_{18} = 0.0001$, the parameter responsible for its degradation. DUSP is a phosphatase that dephosphorylates p38p and ERKp, consequently decreasing the levels of IL-10 production. Figure 17.5(b) depicts the dynamics of DUSP and the parametric plot between k_{18} and IL-10.

The time course of this sensitivity resembles a logarithmic curve (as opposed to the previously analysed sensitivity) and follows the sustained dynamics of DUSP. Although with opposite dynamics, the relation between k_{18} perturbations and IL-10 is similar to the relation between IL-10 and the perturbation of its initial condition, as Figures 17.5(a) and 17.5(b) show.

17.2. Model IL10

Figure 17.6 shows the time dependent sensitivities of IL-10 to each parameter and initial condition.

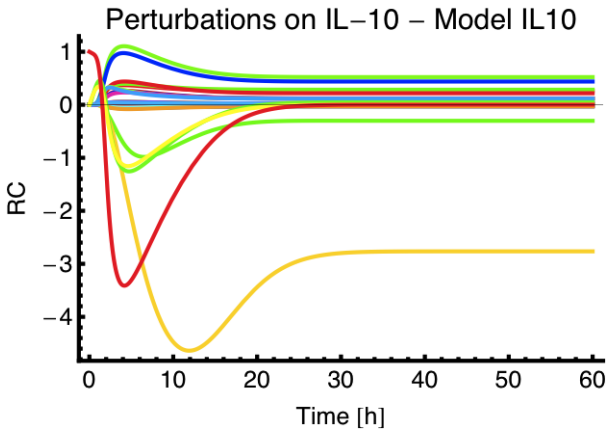

Figure 17.6.: Response coefficients for IL-10, model IL10. Represents the sensitivity of IL-10 to infinitesimal changes in all the parameters and initial conditions along time.

The sensitivities of model IL10 are all transient and mostly follow the dynamics pattern of IL-10. Positive sensitivities correspond to the processes of phosphorylation, production and constitution, whereas negative sensitivities correspond to processes of dephosphorylation, degradation and disaggregation. The exception to this observation lies on the sensitivities to the initial conditions of X2, *il-10* mRNA and IL-10 protein, which has a positive and negative sensitivity.

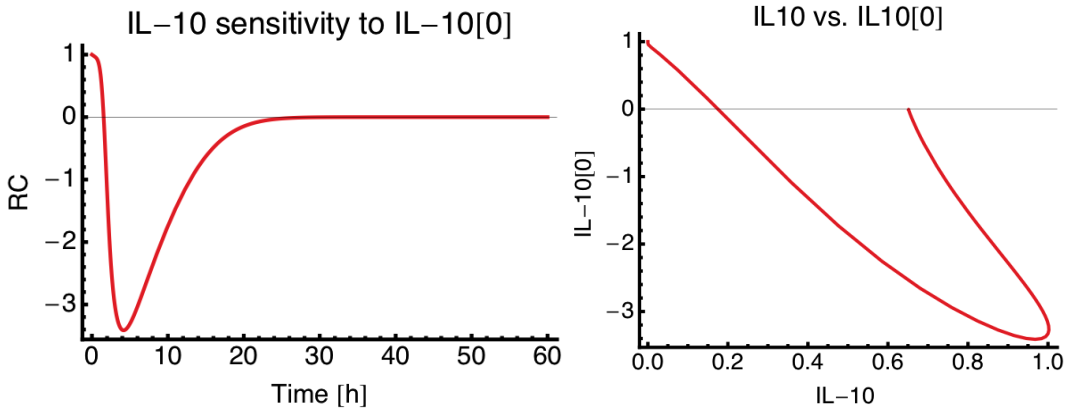

(a) (b)

Figure 17.7.: (a) Time dependent sensitivity of IL-10 to its initial condition, (b) parametric plot between IL10 and its sensitivity to its initial condition

Atypical time dependent sensitivities IL-10 sensitivity to its own initial condition (IL10[0]) starts in 1 and changes to the negative side of the axis when IL-10 has an amplitude of 0.35. It keeps on decreasing, reaching its minimal amplitude (highest negative sensitivity) of -3.6 when IL-10 reaches its maximum. At this point, both

elements decrease: IL-10 decreases until its steady state of 0.6 AU and the sensitivity approaches zero at time t=80h.

17.3. A method for model discrimination

When having two concurrent models, it is not always clear which model can best represent the biological system. To help select the best model, I propose a method for optimal experimental design that suggests an experiment on the specific parameter that best distinguishes the models and the specific time point. This method consists of the following steps:

- Have two concurrent models;
- Calculate the time dependent sensitivity analysis (RC) for each parameter of each model;
- Find the maximal difference between the RCs of each model, *i.e.*, the Max(RC_{k_iM1}-RC_{k_iM2});
- This suggests a specific experiment that should address the parameter with Max(RC_{k_iM1}-RC_{k_iM2}), at the specific time point when this difference is maximal.

Figure 17.8 shows the time dependent sensitivity analysis for all the parameters and initial conditions of both models.

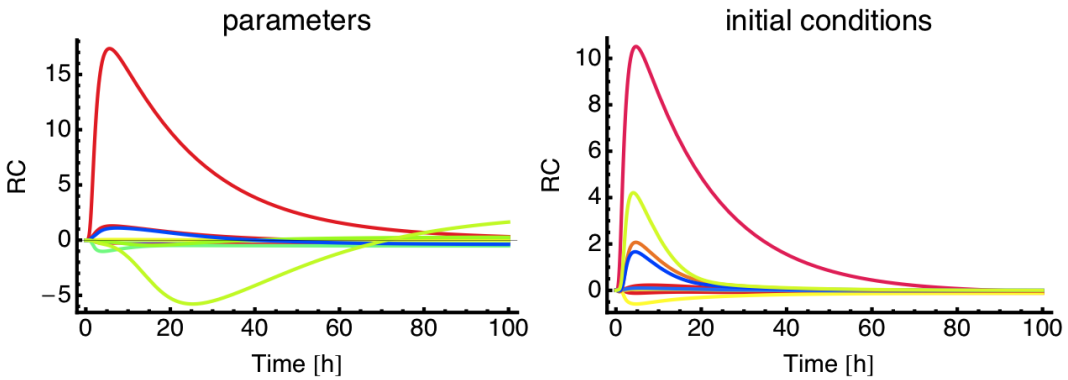

(a) (b)

Figure 17.8.: Differences between the time dependent sensitivity analysis of model DUSP and model IL10. (a) Parameter (b) initial conditions

In the case of model DUSP and model IL10, the Max(RC_{k_iM1}-RC_{k_iM2}) happens for parameter k_1 at time point t=7.5 h. This parameter is responsible for ERK phosphorylation and is represented in Figure 17.9.

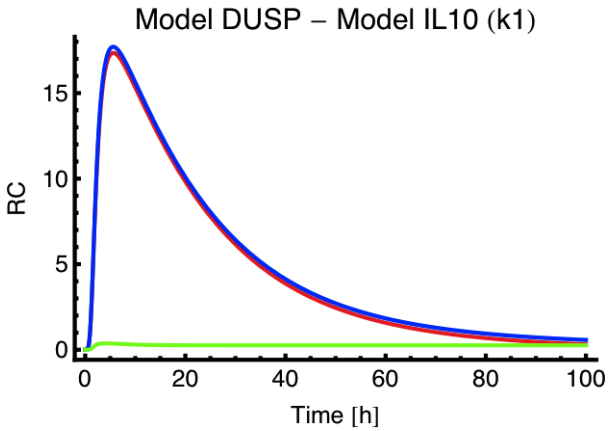

Figure 17.9.: Comparing the *RC* of k_1 between Model DUSP and Model IL10. Red: k_1 of Model DUSP; Green:k_1 of Model IL10; Blue: Difference between both

Hence, this method suggests that the perturbation of ERK phosphorylation should be experimentally tested at time point t=7.5 h and observe which model best follows the experimental data.

18. Discussion of Part III

Robustness, sensitivity and homeostasis are properties of biological systems that interconnect with each other. These three properties provide a dynamic self-regulation of the system, by setting the functional limits of each element of the network. A robust gene network system might have alternative mechanisms of gene expression that assure the transcription of the gene in question when one of the arms of the network is deleted (robustness by redundancy). The same system should also be sensitive enough to sense changes in the environment and change its behaviour accordingly. The orchestration of these two figures together, brings about the definition of homeostasis, which is the dynamic self-regulation of open or closed systems, ensuring the constancy of its performance (Cannon, 1932). Self regulation, or feedback, is one strategy of living systems to achieve robustness.

One hypothesis of my PhD thesis, mentioned in chapter 4.1, is that a negative feedback mechanism regulates the production of IL-10 in macrophages after exposure to an immunomodulatory molecule of the parasitic nematode *A.viteae*. The available experimental data strongly suggest that this feedback occurs at the MAPK level, as I indicated in Part II of this work. I analysed the robustness of two models by studying the effect of extrinsic and intrinsic noise on the level of IL-10 steady state. Extrinsic noise reflects the possible variations on the total concentration of secreted Av17. These perturbations may happen because the total parasite population may vary along time. Intrinsic noise refers to perturbations on the parameter set and reflects the possible biological variation within a cell. I used a Monte Carlo analysis to simulate the extrinsic and intrinsic noise assuming a variation of 20% around the unperturbed value in both cases. I compared two concurrent models of IL-10 production and regulation: model DUSP, where the regulation of IL-10 happens through the activation of a phosphatase that dephosphorylates the signalling pathways responsible for IL-10 production (integral feedback); model IL10, where IL-10 itself regulates its own production by deactivating the signalling pathways responsible for its production (transient feedback). Both models implement a transcriptional feedback and its negative form is known to filter out noise (Blüthgen, 2010)

The results of this work indicate that model DUSP, the model selected after biological evidences, is more robust then model IL10.

When analysing the effect of extrinsic noise on IL-10 steady state, model DUSP is slightly more robust than mode IL10 (although both models are relatively robust). Nevertheless, the analysis of IL-10 time course suggests that model DUSP can better adapt to changes in the environment. This is explained by the fact that model DUSP implements an integral feedback. Integral feedback is a common topology in control engineering to achieve perfect adaptation and override the effect of perturbations

(Ang et al., 2010; Cloutier and Wellstead, 2010). In accordance, model DUSP can adapt to variations and filter out intrinsic and extrinsic noise. Consequently, IL-10 reaches residual values at steady state, independently of the perturbation.

A characteristic of negative feedback regulation is that systems are normally more robust to perturbations, but they cannot achieve such high maximal amplitude as systems without feedback can. This is observed in model DUSP but, interestingly, not in model IL10. The models have opposite behaviours when the feedback is cut out. In model DUSP, the feedback attenuates the maximal concentration of IL-10, whereas in model IL10, it amplifies it. This unexpected result can be understood by the fact that IL-10 varies from 0 to 1 and, when the variable $IL10e(t)$ is cut out from the reaction that provides feedback, it increases the strength of the dephosphorylation reactions, v_2 and v_4.

To further analyse the robustness of these systems, I did a sensitivity analysis by varying each parameter at the time. I varied each single parameter 10%, 20% and 50% around its original value and calculated the sensitivity of IL-10 steady state to each parameter. Results indicate that both systems are not sensitive to single parameter changes at the level of IL-10 steady state, which goes in line with the results from the previously described Monte Carlo analysis.

To understand if the models are always insensitive to changes, I computed a time dependent sensitivity analysis, which tells how the sensitivity of one parameter changes over time. This is specially of interest when studying signalling and adaption mechanisms. This method has been suggest by Ingalls and Sauro (2003) and has been applied on studying the systemic properties of yeast, when faced with perturbations along a temporal trajectory (Klipp et al., 2005; Kühn et al., 2008). The method assumes that each parameter and the initial condition of each species is subject to infinitesimal changes over time. In the context of this thesis, this method revealed that, for IL-10 steady state, most parameters and initial conditions are insensitive to changes. Nevertheless, when IL-10 reaches its maximal amplitude, the models also achieve their maximal sensitivity. The most sensitive parameter of model DUSP is the parameter responsible for ERK phosphorylation.

A sensitivity can be positive or negative, and its sign indicates if the effect of the specific parameter/initial condition on the output is positive or negative. In model DUSP, the parameter responsible for IL-10 degradation has a negative effect on IL-10, which is an expected result.

The parameters referring to phosphorylation, activation and production reactions are positive, in contrast with the parameters referring to dephosphorylation, degradation and complex disagreggation, which are negative in both models. Species DUSP (protein and mRNA) are the exception to this pattern: the sensitivities of IL-10 to these parameters are positive when referring to mRNA and protein degradation and negative when referring to DUSP transcription and translation. This result was expected, because DUSP is responsible for IL-10 degradation.

Finally, I suggest a method of model selection by optimal experimental design. This method consists of computing the differences between the corresponding sensitivities

of both models and experimentally testing the parameter that yields the maximal RC difference between models, at the specific time point when this difference is maximal. In terms of amplitude, the most striking difference is between parameter k_1 of both models and, in terms of dynamics, are the parameters k_{10} and k_{14}. These parameters can be experimentally investigated, as future work. Nevertheless, it is important to mention that, experimentally, it is practically impossible to test infinitesimal variations of one element and its influence in the others. This method is of value to know which element can best distinguish between two concurrent models, and at which time point this element should be experimentally tested.

This part of my thesis suggests that different feedback topologies influence the robustness of the biological network and proposes a method of model selection by optimal experimental design.

Part IV.

General discussion, summary and outlook

19. General discussion and summary

One of the most fascinating results of observing host-parasite interactions is the elegance with which parasitic nematodes divert an effector immune response of their host to a blunted immune response. This diverting process may protect the host against allergies and auto-immune diseases. Understanding how parasitic nematodes modulate their host immune response could be a breakthrough to research and further develop medicines against immune disorders like allergies or auto-immune diseases. As a first investigation step in this direction, I aimed at understanding which molecules and pathways are involved in the modulation of the immune response. To achieve this, I used a systems biology approach, which uses mathematical methods to help understanding biological interactions. This is a desireable procedure when studying specific questions of host-parasite interactions. Combining experimental data with mathematical models holds various benefits. It offers the investigator not only a panorama of the problem at hand, but also allows to undergo *in silico* experiments that may not be realistic to do *in vitro* or *in vivo* for a question of time, money and resources.

The main objective of this thesis was to understand the host-parasite interaction that leads to the downregulation of the host's immune response directed against the parasite. To examine the questions that arose from here, I interlaced mathematical modelling with experimental data[1].

The parasitic nematode *A.viteae* secretes an immunomodulatory molecule, Av17, that binds to the macrophages of its host and induces the expression of the anti-inflammatory cytokine IL-10, which modulates the host immune response. I constructed mathematical models based on literature and on experimental data to understand which pathways this nematode exploits to induce IL-10 production. These models hypothesised that Av17 activates the MAP kinases ERK and p38 and that both are essential for IL-10 production (Yang et al., 2007; Zhang et al., 2006). According to Lucas et al. (2005); Staples et al. (2007); Gee et al. (2007), CREB, SP1 and STAT3 are transcription factors involved in *il-10* transcription. I constructed mathematical models to describe these facts and the experimental data, showing that Av17 stimulated macrophages express IL-10 with transient dynamics (Figueiredo et al., 2009). The first hypothesis of this mathematical model, that Av17 activates the signalling pathways ERK and p38, was experimentally validated. Western blots testing the phosphorylation of ERK and p38 have shown that Av17 indeed activates the signalling pathways ERK and p38, but not JNK in macrophages exposed to this

[1] All the experimental data presented in this thesis was provided by the Department of Parasitology of the Humboldt-Universität, Berlin.

immunomodulatory molecule. The second hypothesis, that ERK and p38 are both necessary for IL-10 transcription was also experimentally tested, again validating this model hypothesis. The blockage of ERK or p38 showed that IL-10 production depends on both kinases (Klotz et al., 2011). Moreover, the involvement of CREB and STAT3 in *il-10* transcription, has been stated by the same authors.

To understand the origin of the transient IL-10 dynamics, I hypothesised that a negative feedback, acting on the signalling pathways, regulated IL-10 expression. Macrophages express the IL-10 receptor complex on their surface and the literature suggests a negative autoregulatory role for IL-10 for LPS or lipoprotein stimulated IL-10 production in monocytes and monocyte-derived macrophages (de Waal Malefyt et al., 1991; Giambartolomei et al., 2002; Staples et al., 2007; Ward et al., 2005). The deactivation of signalling pathways can happen either by the action of phosphatases or kinases (Kholodenko, 2006). Accordingly, I assumed that the feedback mechanism acting on ERK could happen by phosphatase activation or kinase inhibition. I tested the kinetics of IL-10 when both models were faced to increases in the input and I observed that kinase inhibition is a more efficient signal amplifier than phosphatase activation, but the latter is more robust to input perturbations than the former. Moreover, the feedback mechanism of kinase inhibition is non-linear, so it quickly activates and deactivates the ERK signal, meanwhile keeping a constant plateau for ERK duration. In contrast, regulation by phosphatase activation phosphorylates and dephosphorylates ERK in a linear fashion (Figueiredo et al., 2009). To further characterise the different feedback mechanisms, I used the concepts of integral, maximal amplitude, steady state, overshoot and signal duration. In terms of signal concentration (total and maximal), kinase inhibition produces more IL-10 than phosphatase activation. That model can also adapt better, showing a higher overshoot than phosphatase activation. But phosphatase activation yields a longer IL-10 duration than kinase inhibition. This is in accordance with Hornberg et al. (2005b), who states that "...kinases control amplitudes more than duration, whereas phosphatases tend to control both." I further investigated the effect of perturbations on the specific elements of the network. I did a sensitivity analysis, by imposing perturbations on the phosphorylation level of ERK or p38, and checked the effect of these perturbations on p38, ERK and IL-10. I observed that there is an autocrine crosstalk that connects ERK, p38 and IL-10. This sensitivity analysis revealed a wiring scheme connecting p38 to ERK through IL-10, but not ERK to p38. That is, perturbations on p38 affect ERK activity through the IL-10 feedback mechanism, but ERK perturbations do not affect p38.

In Part II of this thesis, I compared the ERK and p38 dynamics measured experimentally with the predictions of the same components, for kinase inhibition and phosphatase activation. Both models show a transient phosphorylation of ERK and a sustained phosphorylation of p38, but the experimental data show a transient activation of both kinases. Faced with these facts, I included a feedback mechanism acting on p38. I did a systematic analysis to test the alternative regulation motifs with biological significance that combine different regulation approaches. The sys-

tems biology approach helped identifying a model that can explain the data and make correct predictions. In this approach, experiments were done after theoretical predictions were made, or the model was refined after experimental evidence (Figure 10.2). The selected mathematical model identified DUSPs as the molecules responsible for the regulation mechanisms of IL-10 production. This model hypothesised that ERK and p38 independently activate DUSPs and these, in turn, deactivate the original MAPKs.

DUSP activity was experimentally measured, as a dedicated experiment to validate the model hypothesis about the regulation mechanism. *In vitro* experiments identified DUSP1 and DUSP2 as regulators of IL-10 production. To confirm, tests in Av17 stimulated macrophages of *dusp1*$^{-/-}$ mice revealed that IL-10 kinetics are sustained, in contrast with the transient IL-10 kinetics of wild type animals. Moreover, experiments *in vivo* revealing the presence of DUSP1 and DUSP2, have very similar dynamics to the DUSP *in silico* prediction.

A sensitivity analysis showed that DUSP mediates crosstalk between individual MAPKs. The wiring scheme of ERK, DUSP and p38 reveals that all these elements are interconnected, but one cannot scrutinise the specific influence of one element on another. This was done *in silico* by perturbing one element of the network and testing the effect of this perturbation in the other elements. The model revealed that ERK perturbations affect only IL-10 expression and that p38 perturbations affect IL-10 and DUSP in a linear manner. Interestingly, the perturbation of p38 has a negative impact in ERK phosphorylation, *i.e.*, inhibition/increase of p38 produces a increase/inhibition in the phosphorylation levels of ERK. Moreover, the reverse mechanism was not verified, *i.e.*, ERK perturbations have no effect on phospho-p38 levels. This was experimentally tested and the *in vitro* results agree with the model. The combination of modelling and experiments shown in this part of my thesis, allowed to select a model that can correctly predict experimental data and make right and reliable predictions.

My hypothesis, in Part III, is that the host-parasite interaction studied in this work has been shaped to be robust. I tested wether the selected model in part II is robust to noise, by comparing it with a model that implements regulation through IL-10. This part of my thesis discussed the robustness of IL-10 steady state of two concurrent models when exposed to intrinsic or extrinsic noise. Based on a Monte Carlo analysis, I suggest that the model selected after the experimental evidences is more robust than its concurrent. This model implements an integral feedback and has a better signal adaptation than the model with transient feedback.

Mathematical modelling is an elegant and efficient way of making *in silico* predictions that otherwise would be too expensive in terms of time and money. Thereby, it effectively - and at low costs - identifies new experiments that may give further information about the biological system. Indeed, the combination of experimental approaches and mathematical modelling allowed to understand how the nematode *A.viteae* explores the regulation mechanisms of the immune system by activating specific signalling events that manipulate macrophage functions and allow its evasion

to the expectable immune attack.

Figure 19.1 shows the main results of this work.

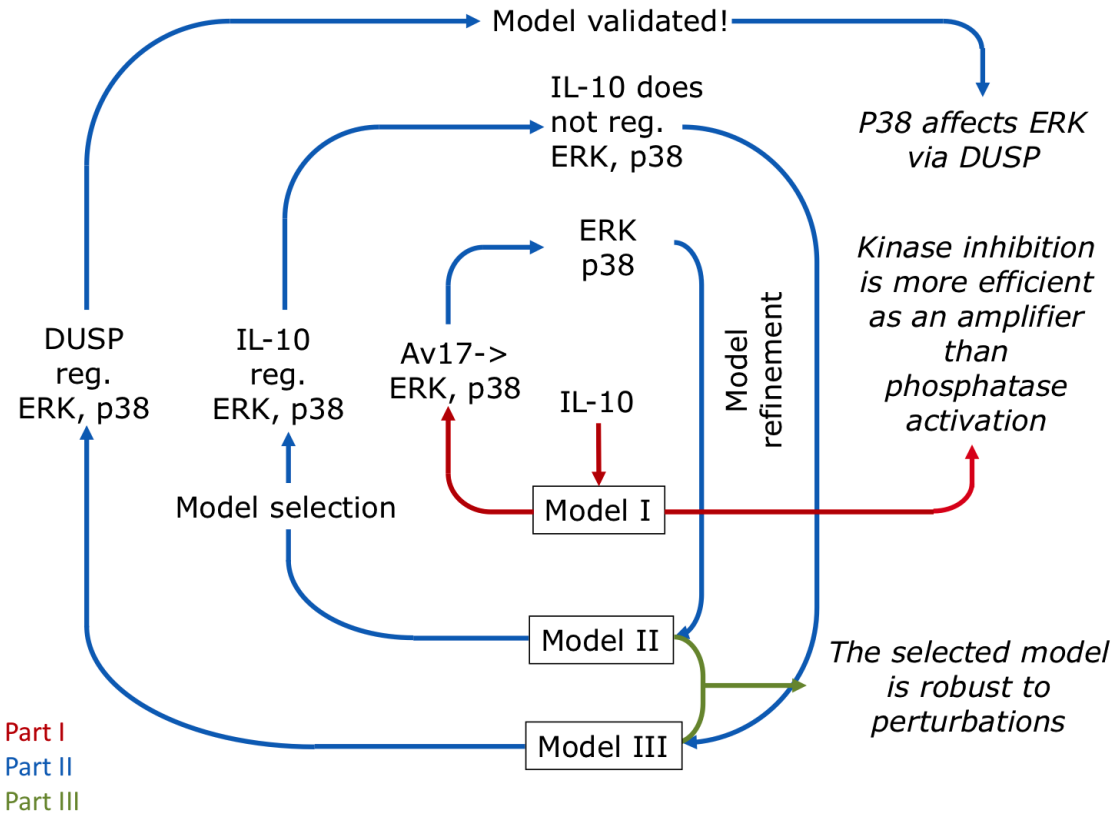

Figure 19.1.: Flow diagram describing the main results of this thesis.

20. Outlook

In this particular work, the elucidation of the signalling mechanisms that induce the regulation of immune cells after exposure to immunomodulatory molecules of nematodes, brought up the questions explored in the next sections. The contribution of this work will allow approaching these further questions with a greater understanding.

20.1. Discrimination of crosstalk between ERK, p38 and JNK in IL-10 production and regulation - zooming in

It is not yet clear the role of the MAPK JNK in this biological system. The inhibition of this MAPK did not affect cytokine production in Av17 stimulation. The crosstalk established between ERK, JNK, p38 and DUSPs is not yet fully understood. Moreover, the presence of IL-12/23p40 was also reported for this system. The connections between IL-10, IL-12/23p40, the MAPKs and the DUSPs could be first approached by a mathematical model focusing on the particular signalling events that regulate this biological system.

20.2. A systemic view of the effect of Av17 manipulated macrophages at the organismic levels - zooming out

In this thesis, I suggest a mathematical model that explains how Av17 triggers macrophages to produce IL-10. However, how this immunomodulatory molecule binds to the macrophages is still an open question. The malarial parasite *Plasmodium falciparum* activates the ERK signalling cascade through the induction of proteins that bind to the scavenger receptor CD36 (Yipp et al., 2003), diverting the monocytes to IL-10 production. The ERK signalling cascade is also activated by *Leishmania mexicana*, but through FccR (Yang et al., 2007). In addition, Buxbaum and Scott (Buxbaum and Scott, 2005) have shown that removal of IL-10 or FccR leads to resolution of *L. mexicana* disease. This suggests that engagement of FccR through parasite products or immune complexes leads to IL-10 production. The eggs of the blood fluke *Schistosoma mansoni* release phosphatidylserines that bind to and activate Toll-like receptor 2 (TLR2), an event leading to the production of IL-10. All of these receptors (CD36, FccR, and TLR2) signal through the ERK signalling cascade, which makes them attractive for studying the production and regulation of this cytokine via Av17. It is, however, likely that the recognition of products of

parasitic nematodes is highly specific and that no common receptor recognising the products of different parasites exists (Perrigoue et al., 2008).

After exposure to Av17, macrophages alter their functions. The effect of these altered macrophages in the host, is a question that remains unanswered. The type of stimuli that these cells receive, defines the macrophage phenotype. Av17 altered macrophages show notable resemblance to M2b macrophages. M2b macrophages can be generated after p38 and ERK activation, through Fc-γ receptors and inflammatory signals such as TNF (Anderson and Mosser, 2002b,a; Sutterwala et al., 1998). M2b macrophages and Av17 stimulated macrophages induce both IL-10 production and a Th2 response.

With which cells do these altered macrophages interact and how do they signal to other cells? The effects of IL-10 on the macrophage population in particular and on the immune system in general is still an open question.

To explore these questions, I suggest the performance of a high troughput experiment (*e.g.*, microarray experiment) to analyse the genotypic differences between the stimuli that lead to different macrophage phenotypes. Av17 stimulated macrophages, macrophages without any stimuli and M2b macrophages could be tested at several time points. A preliminary microarray data analysis was performed and described in Appendix C.

The answer to these questions can open the doors to develop a model that depicts these interactions and better understand this particular host-parasite interaction in a more systemic view. Furthermore, the knowledge acquired from the analysis of the host-parasite interactions might pave the way for developing pharmaceutical approaches to fight allergies and autoimmune diseases with immunomodulatory proteins of parasitic nematodes.

Part V.

Appendix

A. Notations, estimated parameters and materials and methods

A.1. Notations

The models are available in the Systems Biology Markup Language (SBML) format, which is a widely accepted standard of ODE models in systems biology (Hucka et al., 2003).

A.2. *il-10* mRNA half-life

Half-life values of *il-10* mRNA were extracted from the literature.

Values of *il-10* mRNA are shown in Table A.1 and the respective parameter (k_{12}) was set to the average of the available values. Fitting was performed with COPASI (Hoops et al., 2006), using the algorithms for evolutionary programming and simulated annealing, available in the software package of COPASI.

Cell type	Stimulus	*il-10* mRNA $t_{1/2}[h]$	Reference
MNT1	Nonstimulated	1.25	Brewer et al. (2003)
Leucocytes	LPS	1.25	Gibson et al. (2001)
EL-4 cell	Nonstimulated	1	
	PMA	3	Powell et al. (2000)

Table A.1.: Values of *il-10* mRNA half-life extracted from literature.

A.3. Estimated parameters of the studied models

	Model 1	Model 2	Model MKP	Model IL10
k_1	2.17	0.09	0.05	0.78
k_2	83.39	478.04	3.44	8.05
k_3	8.87	0.87	0.84	0.73
k_4	29.39	0.01	0.88	10
k_5	0.08	3.83	0.54	1.06
k_6	3.53	0.005	9.99	7.57
k_7	0.19	0.58	9.95	0.45
k_8	2.68	6.87	6.32	10
k_9	9.43	6.42	9.65	7.53
k_{10}	38.67	3.41	4.67	1.98
k_{11}	85.17	10.52	10	9.67
k_{12}	0.78	0.78	0.78	0.78
k_{13}	0.49	0.39	0.49	0.54
k_{14}	0.05	0.06	0.05	0.08
k_{15}	-	-	6.99	-
k_{16}	-	-	1.3	-
k_{17}	-	-	0.72	-
k_{18}	-	-	0.0001	-
k_{19}	-	-	0.0001	-
k_f	85.09	-	-	-
h	2.54	1.09	-	-

Table A.2.: Table with the parameter values of model 1, model 2, model MKP and model IL10.

A.4. Materials and methods

IL-10 regulation in macrophages stimulated with Av17 and anti IL-10 receptor anti body Peritoneal exudate cells from BALB/c mice that were flushed with PBS/2mM EDTA from the peritoneum were used. These cells were seeded (2 million cells) into wells of a 24 well plate in cDMEM (10% FCS, 1 mM L-Glutamin, 100 U/ml Penicillin G and 100 μg/ml Streptomycin). After 2 hours, cells were washed twice with cDMEM to get rid of non adherent cells. Remaining macrophages were treated with 0.5 μM Av17 or the same amount of SNAP, denaturated Av17, and Av17 in combination with 10 μg/ml anti-IL-10R ab or ab control for different timepoints (2h, 18h, 24h). Cells were afterwards washed with PBS, RNA was extracted (innuPREP RNA Mini Kit, JenaAnalitk) and rewritten into cDNA (High Capacity RNA-to-cDNA Kit, Applied Biosystems). To analyse the expression of IL-10, real time PCR by using the FastStart Universal SYBR Green Master(Rox) Kit from Roche was performed. For

normalization PPIA was used as housekeeping gene and the DeltaDeltact method described for qRT-PCR was applied. The anti-IL-10R ab was kindly provided by Dr. Hyun-Dong Chang, Deutsches Rheuma-Forschungszentrum Berlin. This experiment was performed by Thomas Ziegler, Department of Parasitology, Humboldt-Universität zu Berlin.

B. Model discrimination lists

Table B.1.: Frequencies of each model on the top 10 list, AIC average and median.

Frequencies		**Average AIC**		**Median AIC**	
model 17	10	model 17	-55.82	model 16	-12.93
model 19	10	model 18	-49.22	model 13	2.8
model 18	9	model 16	-48.91	model 19	18.41
model 29	9	model 1	-33.6	model 17	32.45
model 25	8	model 13	-28.91	model 21	36.82
model 2	7	model 11	-20.62	model 29	42.53
model 21	7	model 6	-16.78	model 2	44.11
model 4	6	model 15	-15.64	model 18	44.65
model 13	6	model 19	-10.71	model 4	45
model 16	6	model 9	-10.45	model 9	46.45
model 35	6	model 3	-6.19	model 11	53.32
model 6	5	model 8	5.13	model 15	54.26
model 9	5	model 25	10.27	model 14	54.93
model 15	5	model 14	15.63	model 27	57.02
model 1	4	model 4	21.09	model 25	58.77
model 3	4	model 21	21.31	model 12	59.54
model 7	4	model 12	22.67	model 7	62.62
model 11	4	model 27	22.88	model 20	62.71
model 14	4	model 2	23.99	model 33	67.25
model 27	4	model 24	25.37	model 5	69.04
model 5	3	model 29	42.97	model 6	70.32
model 20	3	model 7	48.29	model 28	70.67
model 8	2	model 20	51.6	model 10	71.22
model 12	2	model 33	60	model 1	72.53
model 24	2	model 10	65.44	model 8	75.26
model 28	2	model 28	66.83	model 23	75.26
model 10	1	model 5	67.6	model 3	75.87
model 23	1	model 26	67.71	model 24	81.34
model 26	1	model 23	79.81	model 26	91.03
model 30	1	model 32	87.93	model 31	92.53
model 32	1	model 31	113.46	model 32	102.04
model 33	1	model 30	113.52	model 22	103.86
model 22	0	model 35	113.7	model 35	106.39
model 31	0	model 22	114.01	model 30	109.48
model 34	0	model 34	139.77	model 34	131.81

Table B.2.: AIC values for each model and each fit of data set 1. k corresponds to the number of parameters of each model.

Model	k	**Fit 1**	**Fit 2**	**Fit 3**	**Fit 4**	**Fit 5**	**Fit 6**	**Fit 7**	**Fit 8**
model 1	17	75.76	72.31	102.15	72.75	-168.51	151.97	75.18	74.96
model 2	15	66.49	42.27	43.49	70.59	141.54	34.08	44.04	44.18
model 3	17	85.76	87.83	102.78	101.3	-188.39	-201.82	99.19	73.9
model 4	15	65.51	61.65	52.34	70.85	141.71	-84.34	39.53	40.37
model 5	15	66.49	70.17	49.62	70.67	141.79	-236.58	39.66	67.91
model 6	17	88.55	87.81	107.55	90.33	-111.42	137.04	70.08	129.06
model 7	15	73.8	61.52	55.57	63.72	141.73	-34.18	64.34	40.04
model 8	17	101.9	89	83.9	102	-102.57	103.07	75.21	75.3
model 9	15	61.93	59.28	59.19	69.98	-111.68	-177.67	44.32	69.47
model 10	15	65.7	64.63	59.19	69.95	141.76	76.48	69.45	72.48
model 11	18	118.91	94.31	119.03	95.44	-257.13	-12.14	97.74	89.28
model 12	16	75.2	83.98	83.94	75.34	145.57	-11.37	58.89	50.49
model 13	18	116.33	109.95	102.04	112.27	-198.55	-94.29	95.14	93.14
model 14	16	63.65	63.86	81.38	84.95	-188.06	141.98	53.69	53.06
model 15	16	79.36	59.69	79.41	80.45	-146.97	-95.81	53.89	54.63
model 16	17	93.47	100.81	99.31	90.4	-112.79	-111.21	64.72	103
model 17	13	34.76	24.93	51.33	48.9	17.46	148.03	8.13	11.63
model 18	17	84.86	106.53	87.06	84.32	-200.3	71.4	75.41	76.02
model 19	15	52.29	51.91	74.59	53.12	-209.36	-123.96	43.93	69.8
model 20	15	60.51	54.31	74.52	74.73	-125.31	104.94	44.46	64.91
model 21	13	39.3	33.43	34.64	39.01	-145.21	89.47	45.43	24.28
model 22	17	106.77	100.95	110.48	106.99	152.19	145.61	96.18	96.06
model 23	15	75.43	74.55	70.2	75.09	146.31	-222.13	69.45	64.09
model 24	17	106.77	86.29	87.6	106.97	-116.3	-54.72	71.6	84.89

Continued on next page

Table B.2 – Continued from previous page

Model	k	**Fit 1**	**Fit 2**	**Fit 3**	**Fit 4**	**Fit 5**	**Fit 6**	**Fit 7**	**Fit 8**
model 25	15	59.04	74.55	58.5	74.83	-156.15	104.19	39.98	70.14
model 26	17	99.47	100.79	96.86	90.3	147.62	89.87	90.56	90.59
model 27	15	59.68	55.75	73.23	58.3	-116.13	-20.66	77.3	60.08
model 28	15	63.66	61.52	61.71	64.06	141.87	-148.46	77.3	77.29
model 29	13	42.45	39.61	39.83	48.82	-13.91	-190.38	38.15	42.6
model 30	17	99.04	97.88	97.88	98.94	150.55	-156.83	109.3	109.41
model 31	15	69.98	65.89	70.87	70.66	141.76	147.62	77.31	78.3
model 32	17	102.61	101.47	127.64	96.47	-100.97	79.8	94.89	109.28
model 33	15	66.74	59.45	66.35	85.66	-108.06	-199.63	61.81	67.76
model 34	17	106.77	106.54	106.54	106.82	152.14	154.63	109.29	109.32
model 35	13	53.58	52.54	56.58	52.86	142.3	207.94	55.31	70.48

Table B.3.: AIC values for each model and each fit of data set 2. k corresponds to the number of parameters of each model.

Model	k	**Fit 9**	**Fit 10**	**Fit 11**	**Fit 12**	**Fit 13**	**Fit 14**	**Fit 15**	**Fit 16**
model 1	17	89.42	77.38	-189.98	-176.76	-184.72	-180.29	-177.43	-251.85
model 2	15	38.01	47.1	-195.85	100.04	51.45	-87.21	45.02	-101.44
model 3	17	79.2	77.84	-60.66	-228.31	-114.27	135.51	41.88	-190.72
model 4	15	44.56	45.44	123.59	-221.26	-8.64	-180.57	-0.92	147.55
model 5	15	78.13	67.51	123.44	27.34	179.79	131.54	58.29	145.79
model 6	17	70.9	70.56	-235.1	-198.09	-205.23	-234.37	-48.45	-87.72
model 7	15	64.63	46.6	-185.87	87.43	1	148.87	147.29	-3.89
model 8	17	102.54	77.48	-196.49	-178.64	22.93	-179.49	53.48	-147.54
model 9	15	71.05	47.11	-347.03	-104.49	-14.89	-87.24	45.79	147.59
model 10	15	77.4	77.19	-182.33	67.63	56.73	82.69	100.88	147.21
model 11	18	97.55	99.25	-99.04	17.37	-317.49	-181.27	-58.57	-233.11
model 12	16	59.66	61.13	-189.68	-189.38	59.43	-85.46	150.99	-66.01
model 13	18	97.59	121.8	-216.04	-226.7	-160.44	-218.72	-108.59	-87.55
model 14	16	58.9	81.72	-214.1	55.05	29.83	-183.39	54.82	12.68
model 15	16	57.86	81.75	-227.13	65.23	-173.7	-182.09	26.54	-63.34
model 16	17	77	77.53	-196.47	-200.54	-178.91	-345.64	-90.59	-252.67
model 17	13	14.04	45.57	-105.39	-217.08	-4.78	-298.74	30.56	19.37
model 18	17	95.84	77.42	-194.96	-194.24	-185.41	-183.91	-197.15	-194.74
model 19	15	51.53	70.42	-200.06	118.07	-187.29	-183.81	-199.39	151.22
model 20	15	50.78	67.55	125.14	124.82	-16.72	-87.43	56.55	151.85
model 21	13	25.05	45.52	-101.19	-98.92	126.29	-91.58	124.83	150.6
model 22	17	96.54	96.67	82.47	81.74	85.78	151.77	156.98	157.04
model 23	15	66.32	69.92	140.46	108.69	88.44	148.07	150.98	151.12

Continued on next page

Table B.3 – Continued from previous page

Model	k	**Fit 9**	**Fit 10**	**Fit 11**	**Fit 12**	**Fit 13**	**Fit 14**	**Fit 15**	**Fit 16**
model 24	17	76.07	77.8	-223.55	153.27	-183.06	-181.62	156.98	157.02
model 25	15	69.73	45.38	-224.73	-216.22	44.73	-182.26	151.33	151.33
model 26	17	106.9	91.47	-34.12	184.6	122.63	-40.72	-66.04	-87.51
model 27	15	77.55	58.8	-38.29	-38.5	31.58	-40.35	-78.83	146.63
model 28	15	77.59	77.64	-23.76	176.45	184.43	185.28	-4.03	-3.23
model 29	13	43.08	55.6	-16.76	-18.49	108.43	181.36	143.28	143.91
model 30	17	109.55	109.61	184.21	169.31	187.84	188.88	106.69	154.12
model 31	15	77.59	77.6	180.09	132.96	184.49	185.35	106.77	148.2
model 32	17	97.59	109.59	184.16	-2.78	125.26	188.91	-56.3	149.24
model 33	15	77.56	77.6	180.13	182.22	186.05	185.33	3.14	-32.05
model 34	17	111.49	109.61	184.63	185.49	189.39	189.12	157.28	157.22
model 35	13	55.63	55.68	176.97	179.2	184.66	181.28	147.15	147.07

C. Microarray data analysis

Mice macrophages were stimulated Av17, E1 (Active peptide of Av17, responsible for IL-10 production) and Cysele (cystatin of *C. elegans*). Total RNA was extracted from the macrophages at 24 hours after stimulation with Av17, E1 or Cysele. Samples were hybridised in the Affymetrix microarray chip MG4302.0. Data normalisation, as well as differential gene expression, were done using Bioconductor (`http://www.bioconductor.org/about/`) and R (`http://www.r-project.org`).

C.1. Differential gene expression

C.1.1. Cysele *vs.* Av17

Method:

- Select the present genes from the complete list of genes;
- Compute $FC = \log\left(\frac{\text{Cysele}}{\text{Av17}}\right)$;
- Select genes, such that $|FC| > 1.5$;
- Genes that have a positive FC value, are upregulated in Cysele; genes that have a negative FC value, are upregulated in Av17.

Table C.1.: Differential gene expression. FC positive values represent the upregulated genes in Cysele and FC negative values represent the upregulated genes in Av17.

FC	**Gene**	**Gene description**	**GenBank ID**
3.54	*Mrps14*	*M. musculus* mitochondrial ribosomal protein S14	NM_025474.1
3.28	*Il1b*	*M. musculus*, similar to interleukin 1 beta	NM_008361.1
2.70	-	Moderately similar to CDA11 protein (*H.sapiens*)	BB761179
2.29	*Lfng*	*M. musculus* adult male lung cDNA (lunatic fringe gene homolog)	AK004642.1
2.24	*Scyb2*	small inducible cytokine subfamily, member 2	NM_009140.1

Continued on next page

Table C.1 – Continued from previous page

FC	**Gene**	**Gene description**	**GenBank ID**
2.18	*Cish3*	cytokine inducible SH2-containing protein 3	BB241535
2.14	*Serpinb2*	*M. musculus* serine (or cysteine) proteinase inhibitor	NM_011111.1
2.11	*Rassf1*	ras association (RalGDSAF-6) domain family 1	NM_019713.1
2.10	*Fn1*	fibronectin 1	BM234360
2.09	*Mlp*	MARCKS-like protein	AV215438
2.08	*Dab2*	unknown (protein for MGC:18401)	BC006588.1
2.06	*Cmkbr2*	*M. musculus* chemokine (C-C) receptor 2	U51717.1 NM_009915.1 U56819.1 U47035.1
2.03	*Cmkbr5*	*M. musculus* chemokine (C-C) receptor 5	NM_009915.1
2.02	*Swap2-pending*	suppressor of white apricot homolog 2-pending	-
2.01	*Cmkbr2*	*M. musculus* JE receptor (chemokine (C-C motif) receptor 2)	U51717.1 NM_009915.1 U56819.1 U47035.1
2.00	*Cpne3*	copine III	-
1.95	*Fbxl5*	f-box and leucine-rich repeat protein 5	-
1.91	*Calm1*	*M. musculus* calmodulin 1	-
1.90	*Nfil3*	*M. musculus* embryo implantation related NFIL3E4BP4-like transcription factor	AY061760.1 NM_017373.1
1.88	*Olfm1*	*M. musculus* mRNA for pancortin-3	AF028740.1 D78264.1
1.87	*Timp*	*M. musculus*, Similar to tissue inhibitor of metalloproteinase	BC008107.1 M17243.1 NM_011593.1
1.81	*Ywhaz*	tyrosine 3-monooxygenasetryptophan 5-monooxygenase activation protein, zeta polypeptide	-
1.80		*M. musculus* mRNA for C-C chemokine receptor 5	U47036.1 D83648.1
1.78	*Cish3*	cytokine inducible SH2-containing protein 3	BB831725
1.71	*Gro1*	*M. musculus* GRO1 oncogene	NM_008176.1 J04596.1

Continued on next page

Table C.1 – Continued from previous page

FC	**Gene**	**Gene description**	**GenBank ID**
1.70	*Ikbkg*	inhibitor of κB kinase gamma	AF069542.1 BC021431.1 NM_010547.1
1.68		*M. musculus*, Similar to peroxisomal biogenesis factor 6	
1.68	*Scya24*	*M. musculus* eotaxin-2	NM_019577.1 AF281075.1 AF244367.1
1.68	*Ldlr*	*M. musculus* low density lipoprotein receptor	AF425607.1 BC019207.1 NM_010700.1
1.68	*Gpaa1*	GPI anchor attachment protein 1	-
1.67	-	*M. musculus*, Similar to cortactin isoform B	-
1.67	*Col3a1*	procollagen, type III, alpha 1	-
1.67		*M. musculus*, Similar to pM5 protein	BC024503.1
1.66	*Smpdl3b*	sphingomyelin phosphodiesterase, acid-like 3B	AU045240
1.66	*Oxsm*	3-oxoacyl-ACP synthase, mitochondrial	C80494
1.66	*Dcn*	*M. musculus* decorin mRNA	NM_007833.1
1.65	*angie2*	*M. musculus* CXC chemokine	AF030636.1 BC012965.1 AF044196.1 NM_018866.1
1.64	*Cish3*	*M. musculus* cytokine inducible SH2-containing protein 3	NM_007707.1
1.64	*Scya2*	*M. musculus* strain NODLtJ small inducible cytokine A2 precursor	NM_011333.1
1.63		Weakly similar to TYROSINE-PROTEIN KINASE JAK3	BB460570
1.63	*Smurf1*	SMAD specific E3 ubiquitin protein ligase 1	-
1.62	*Serpinh1*	serine (or cysteine) proteinase inhibitor, clade H (heat shock protein 47)	NM_009825.1
1.61	*Clecsf10*	*M. musculus* strain BALBc dectin-2 beta isoform	AF240358.1
1.61	*Ubc*	ubiquitin C	-
1.61	*Mmp19*	matrix metalloproteinase 19	NM_021412.1
1.61	*Tmem87b*	transmembrane protein 87B	AU014804
1.60	*Cmkbr1*	chemokine (C-C) receptor 1	U29678.1 NM_009912.1 BC011092.1

Continued on next page

Table C.1 – Continued from previous page

FC	**Gene**	**Gene description**	**GenBank ID**
1.59	*Mmp19*	*M. musculus* matrix metalloproteinase 19	NM_021412.1 AF162446.1 AF153199.1 AF155221.1
1.59	*Ltbp3*	latent transforming growth factor beta binding protein 3	-
1.58	*Arg1*	*M. musculus* arginase 1, liver	NM_007482.1 U51805.1 BC013341.1
1.58	*Actb*	*M. musculus* actin, beta, cytoplasmic	J04181.1 NM_007393.1
1.58	*Serpinb1*	*M. musculus* EIA Serpin mRNA	NM_025429.1 BC011140.1 AF426024.1
1.57	*Nedd4a*	neural precursor cell expressed, developmentally down-regulated gene 4a	U96635.1
1.57	*Map2k2*	mitogen activated protein kinase kinase 2	BC014830.1 NM_023138.1
1.57	*Myo1h*	*M. musculus* myosin IH	NM_026145.1
1.56	*Neo1*	neogenin	NM_008684.1
1.56	*Col3a1*	procollagen, type III, alpha 1	-
1.56	*Actn1*	*M. musculus*, clone IMAGE:3483627	-
1.55	*Selel*	selectin, endothelial cell, ligand	NM_009149.1 BC021306.1
1.55	*Abcc5a*	*M. musculus* ATP-binding cassette protein	-
1.55	*Tex189*	testis expressed gene 189	-
1.55	*Sh3bp1*	*M. musculus* SH3-domain binding protein 1	NM_009164.1 BC004598.1
1.55	*Gas5*	*M. musculus*, similar to growth arrest specific 5	BC004622.1
1.54	*Scyb5*	*M. musculus* small inducible cytokine B subfamily, member 5	BC024392.1 U27267.1 NM_009141.1
1.54	*Cp*	*M. musculus* ceruloplasmin	U49430.1 NM_007752.1

Continued on next page

Table C.1 – Continued from previous page

FC	**Gene**	**Gene description**	**GenBank ID**
1.54	*Cd86*	*M. musculus*, CD86 antigen	AF065897.1 AF065900.1 AF065899.1 AF065898.1 BC013807.1 NM_019388.1 L25606.1
1.54	*Hif1a*	hypoxia inducible factor 1, alpha subunit	BC026139.1 NM_010431.1 AF003695.1
1.54	*Tcfec*	*M. musculus* transcription factor EC	AF077742.1 NM_031198.1
1.54	*Ppic*	*M. musculus* peptidylprolyl isomerase C	BC025861.1 M74227.1 NM_008908.1
1.52	*Enpp2*	*M. musculus*, ectonucleotide pyrophosphatasephosphodiesterase 2	BC003264.1 AF123542.1 NM_015744.1
1.52	*Rbp*	*M. musculus* retinol binding protein 1, cellular	BC018254.1 NM_011254.1
1.51	*Nisch*	nischarin	-
1.51	*Dab2*	*M. musculus* disabled homolog 2 (Drosophila)	NM_023118.1
-1.51	*Fabp3*	*M. musculus* fatty acid binding protein 3, muscle and heart	U02883.1 BC002082.1 NM_010174.1
-1.51	*Mmp9*	*M. musculus* matrix metalloproteinase 9	D12712.1 NM_013599.1
-1.51	*Abin*	*M. musculus* A20 binding inhibitor of NF-kappaB activation-2	NM_139064.1
-1.51	*Ifit2*	*M. musculus* interferon-induced protein with tetratricopeptide repeats 2	NM_008332.1 U43085.1
-1.51	*Pxf*	*M. musculus*, peroxisomal farnesylated protein	NM_023041.1 BC019767.1
-1.51	*Tst*	*M. musculus*, thiosulfate sulfurtransferase, mitochondrial	NM_009437.1 BC005644.1 U35741.1
-1.51	*Isg12*	*M. musculus* interferon stimulated gene 12	AY090098.1

Continued on next page

Table C.1 – Continued from previous page

FC	**Gene**	**Gene description**	**GenBank ID**
-1.52	*Dusp19*	*M. musculus* dual-specificity phosphatase 19	AB038769.1 BC021591.1 AF237618.1 NM_024438.1
-1.52	*Acas1*	*M. musculus* acetyl-Coenzyme A synthetase 1 (AMP forming)	AF216873.1 NM_019811.1
-1.52	-	*M. musculus* adult male testis, homolog to SERINE PHOSPHATASE	-
-1.54	*Rps27*	ribosomal protein S27	-
-1.55	*Slc41a3*	solute carrier family 41, member 3	AI480742 SLC41A1-L2
-1.55	-	solute carrier family 35 (UDP-galactose transporter), member 2	-
-1.56	*Slamf7*	*M. musculus* adult male testis cDNA, Novel LY9 (Lymphocyte antigen 9) NK Cell receptor, SLAM family member 7	-
-1.56	*Zbtb44*	zinc finger and BTB domain containing 44	-
-1.56	*Faim3*	*M. musculus* 10 day old male pancreas, homolog to anti Fas induced apoptosis, Fas apoptotic inhibitory molecule 3	MGC144825 MGC144826
-1.56	*Ercc4*	*M. musculus* excision repair cross-complementing rodent repair deficiency, complementation group 4	AF189285.1 NM_015769.1 BC026792.1
-1.56	*Tns*	*M. musculus* tensin	NM_027884.1
-1.57	*Paics*	phosphoribosylaminoimidazole carboxylase, phosphoribosylaminoribosylaminoimidazole, succinocarboxamide synthetase	-
-1.57	*Scya22*	*M. musculus*, Similar to small inducible cytokine subfamily A, member 22	FL=AF052505.1 BC012658.1 NM_009137.1 AF163476.1 AF076596.1
-1.58	*S100a1*	*M. musculus*, S100 calcium binding protein A1	AF087687.1 NM_011309.1 BC005590.1
-1.61	*Pja1*	praja1, RING-H2 motif	AF335250.1

Continued on next page

Table C.1 – Continued from previous page

FC	**Gene**	**Gene description**	**GenBank ID**
-1.62	*Rbx1*	*M. musculus*, ring-box 1	BC027396.1 AF140599.1 NM_019712.1
-1.62	*Tmem41b*	transmembrane protein 41B	AU018901 MGC38847 D7Ertd70e D7Ertd743e
-1.63	*Hai2*	*M. musculus* hepatocyte growth factor activator inhibitor type 2 splice variant 2	AF099020.1
-1.64	*Gtf2ird2*	*M. musculus* GTF2I repeat domain containing 2	-
-1.65	*Cbfa2t3h*	core-binding factor, runt domain, alpha subunit 2; translocated to, 3 homolog (human)	-
-1.66	*Ywhaq*	tyrosine 3-monooxygenasetryptophan 5-monooxygenase activation protein, theta polypeptide	
-1.68	*Usp18*	*M. musculus* ubiquitin specific protease 18	NM_011909.1 AF069502.1
-1.70	*IgG3*	*M. musculus* germline imunoglobulin gamma constant region	-
-1.70	*Pafah1b3*	*M. musculus* platelet-activating factor acetylhydrolase, isoform 1b, alpha1 subunit	U57746.1 NM_008776.1
-1.71	*Brd4*	*M. musculus*, similar to bone marrow stromal cell antigen 2	BC027328.1
-1.72	*H28*	*M. musculus* histocompatibility 28 (H28)	AF336221.1 NM_031367.1
-1.72	*Dhcr24*	*M. musculus*, similar to dual specificity phosphatase 9	BC004738.1 KIAA0018
-1.73	*Zadh1*	zinc binding alcohol dehydrogenase, domain containing 1	AI838763
-1.76	*Manbal*	*M. musculus* Manbal mannosidase, beta A, lysosomal-like	AI836500
-1.84	*Ppicap*	*M. musculus* peptidylprolyl isomerase C-associated protein	L16894.1 NM_011150.1
-1.87	*IgL*	*M. musculus* Igl-V1 immunoglobulin lambda chain, variable 1	-
-1.88	*Fkbp4*	*M. musculus*, FK506 binding protein 4	NM_010219.1 BC003447.1
-2.11	*Siah1a*	seven in absentia 1A	NM_009172.1

Continued on next page

Table C.1 – Continued from previous page

FC	**Gene**	**Gene description**	**GenBank ID**
-2.11	*Sts*	*M. musculus* steroid sulfatase	NM_009293.1 U37545.1
-2.12	*Ptdss2*	phosphatidylserine synthase 2	
-2.52	*Scya5*	*M. musculus* small inducible cytokine A5	AF128187.1 AF065944.1 NM_013653.1 M77747.1 AF065947.1 AF065946.1 AF065945.1
-2.54	*Polr3k*	polymerase (RNA) III (DNA directed) polypeptide K	AI196849 AU014893

C.1.2. Cysele *vs.* (Av17 AND E1)

Method:

- Select the present genes from the complete list of genes;
- Compute $FC_1 = \log\left(\frac{\text{E1}}{\text{Av17}}\right)$;
- Select the genes with $FC_1 \sim 0$ (E1Av17 - genes with similar expression in E1 and Av17);
- Compute $FC_2 = \log\left(\frac{\text{Cysele}}{\text{Av17}}\right)$;
- Select genes, such that $|FC_2| > 1.5$;
- Genes that have a positive FC_2 value, are upregulated in Cysele; genes that have a negative FC value, are upregulated in the group E1Av17.

Table C.2 shows the resulting genes of this analysis.

C.2. Gene ontology

Gene ontology is an international standard to annotate genes and gene products (Ashburner et al., 2000). I used the software GOSSIP (Blüethgen, 2005) to test which gene ontology groups are significantly enriched in the group of genes previously presented. The significantly enriched groups are present in Table C.3.

Genes upregulated in E1Av17
M. musculus, platelet-activating factor acetylhydrolase,isoform 1b, alpha1 subunit *(Pafah1b3)*
M. musculus, S100 calcium binding protein A1 *(S100a1)*
dual-specificity phosphatase *(5930436K22Rik)*
M. musculus steroid sulfatase (*Sts)*
M. musculus germline immunoglobulin gamma constant region *(IgG3)*
M. musculus tensin *(Tns)*
Genes upregulated in Cysele
M. musculus EIA *(Serpinb1)*
M. musculus GRO1 oncogene *(Gro1)*
M. musculus transcription factor EC *(Tcfec)*
M. musculus arginase 1, liver *(Arg1)*
chemokine (C-C) receptor 1 *(Cmkbr1)*
M. musculus small inducible cytokine B subfamily, member 5 *(Scyb5)*
M. musculus mitochondrial ribosomal protein S14 *(Mrps14)*
M. musculus chemokine (C-C) receptor 5 *(Cmkbr5)*
M. musculus mRNA for pancortin-3 *(Olfm1)*
M. musculus mRNA for C-C chemokine receptor 5 *(CCR5)*
M. musculus, Similar to nucleolar GTPase (gb:BM199850)
suppressor of white apricot homolog 2-pending *(Swap2-pending)*
f-box and leucine-rich repeat protein 5 *(Fbxl5)*
M. musculus ras association (RalGDSAF-6) domain family 1 *(Rassf1)*
M. musculus, Similar to interleukin 1 beta *(Il1b)*
M. musculus small inducible cytokine subfamily, member 2 *(Scyb2)*
M. musculus low density lipoprotein receptor mRNA *(Ldlr)*
M. musculus, Similar to pM5 protein (gb:BC024503.1)
M. musculus, Similar to tissue inhibitor of metalloproteinase *(Timp)*

Table C.2.: Differential gene expression of Cysele and E1Av17 (genes with similar expression in E1 and Av17) .

C.3. Outlook

Further microarray data can complement this analysis in two ways. First, to better understand which genes are involve in IL-10 production and regulation: expose mice macrophages to Av17 and extract the RNA at the time points 1h, 2h, 4h, 8h. As control, extract RNA of macrophages and medium, at the same time point. These time points picture the dynamics of the RNA expression of *Il10* and Dusp1, present in Figures 4.3(a) and 11.1, respectively. Second, to better understand the genotype of Av17 stimulated macrophages: extract RNA from Av17 stimulated macrophages, macrophages without stimuli and M2 macrophages. This approach could help char-

GO Term	Name	FDR
5578	extracellular matrix (sensu Metazoa)	3.62E-06
31012	extracellular matrix	3.62E-06
5576	extracellular region	3.81E-05
45202	synapse	4.02E-05
5509	calcium ion binding	4.02E-05
5887	integral to plasma membrane	0.000333
45211	postsynaptic membrane	0.000333
19226	transmission of nerve impulse	0.000333
31226	intrinsic to plasma membrane	0.000333
7268	synaptic transmission	0.000384
16503	pheromone receptor activity	0.001338
7606	sensory perception of chemical stimulus	0.001629
50877	neurophysiological process	0.001629
16021	integral to membrane	0.001927
31224	intrinsic to membrane	0.002631
5615	extracellular space	0.003511
5230	extracellular ligand-gated ion channel activity	0.005233
7156	homophilic cell adhesion	0.005233
7267	cell-cell signaling	0.010298

Table C.3.: GO terms extracted by the software package GOSSIP, for the list of genes of table C.1. FDR stands for false discovery rate and gives an estimate of the proportion of the expected number of false discoveries, for a given p-value (Blüethgen, 2005). Groups with a FDR>0.01 were rejected.

acterising the type of macrophage induced by Av17 and, furthermore, the effect of these cells on other cells and on the immune system in general.

D. Abbreviations

Abbreviation	Description
A. viteae	*Acanthocheilonema viteae*
AIC	Aikaike information criterion
AU	arbitrary units
Av17	cystatin from *A. viteae* (GenBank: L43053.1)
CREB	cAMP responsive element binding protein 1
dusp	dual specificity phosphatase mRNA
DUSP	dual specificity phosphatase protein
dusp1$^{-/-}$	*dusp1* knockout mice
ERK	extracellular signal-regulated kinase
H3	histone 3
il-10	interleukin-10 mRNA
il-10$^{-/-}$	interleukin-10 knockout mice
IL-10	interleukin-10 protein (GenBank: CAG46825.1)
JNK	c-Jun N-terminal kinase
LPS	lipopolysaccharide
MAPK	mitogen-activated protein kinase
MKP	mitogen-activated protein kinase phosphatase
O.volvulus	*Onchocerca volvulus*
ODE	ordinary differential equation
rAV17	recombinant cystatin from *A. viteae*
RSS	residual sum of squares
SP1	Sp1 transcription factor
STAT3	signal transducer and activator of transcription
wt	wild type

Bibliography

Abbas, A., Lichtman, A., and Pober, J. (2000). *Cellular and Molecular Immunology*. Elsevier Science.

Alon, U. (2007). *An introduction to systems biology. Design principles of biological circuits*. Chapman & Hall/CRC.

Ananieva, O., Darragh, J., Johansen, C., Carr, J. M., McIlrath, J., Park, J. M., Wingate, A., Monk, C. E., Toth, R., Santos, S. G., Iversen, L., and Arthur, J. S. C. (2008). The kinases msk1 and msk2 act as negative regulators of toll-like receptor signaling. *Nat Immunol*, 9(9):1028–1036.

Anderson, C. F. and Mosser, D. M. (2002a). Cutting edge: biasing immune responses by directing antigen to macrophage fc gamma receptors. *J Immunol*, 168(8):3697–3701.

Anderson, C. F. and Mosser, D. M. (2002b). A novel phenotype for an activated macrophage: the type 2 activated macrophage. *J Leukoc Biol*, 72(1):101–106.

Ang, J., Bagh, S., Ingalls, B. P., and McMillen, D. R. (2010). Considerations for using integral feedback control to construct a perfectly adapting synthetic gene network. *J Theor Biol*, 266(4):723–738.

Araujo, M. I. and de Carvalho, E. M. (2006). Human schistosomiasis decreases immune responses to allergens and clinical manifestations of asthma. *Chem Immunol Allergy*, 90:29–44.

Asadullah, K., Sterry, W., and Volk, H. D. (2003). Interleukin-10 therapy–review of a new approach. *Pharmacol Rev*, 55(2):241–269.

Ashburner, M., Ball, C. A., Blake, J. A., Botstein, D., Butler, H., Cherry, J. M., Davis, A. P., Dolinski, K., Dwight, S. S., Eppig, J. T., Harris, M. A., Hill, D. P., Issel-Tarver, L., Kasarskis, A., Lewis, S., Matese, J. C., Richardson, J. E., Ringwald, M., Rubin, G. M., and Sherlock, G. (2000). Gene ontology: tool for the unification of biology. the gene ontology consortium. *Nat Genet*, 25(1):25–29.

Baldi, P. and Brunak, S. (2001). *Bioinformatics - The machine learning approach*. The MIT Press.

Blüethgen, N. (2005). *Systems Biological approach to Ras-mediated signal transduction*. PhD thesis, Institute of Theoretical Biology, Humboldt University, Berlin.

Blüthgen, N. (2010). Transcriptional feedbacks in mammalian signal transduction pathways facilitate rapid and reliable protein induction. *Mol Biosyst*, 6(7):1277–1284.

Blüthgen, N., Legewie, S., Kielbasa, S. M., Schramme, A., Tchernitsa, O., Keil, J., Solf, A., Vingron, M., Schäfer, R., Herzel, H., and Sers, C. (2009). A systems biological approach suggests that transcriptional feedback regulation by dual-specificity phosphatase 6 shapes extracellular signal-related kinase activity in ras-transformed fibroblasts. *FEBS J*, 276(4):1024–1035.

Box, G. and Draper, N. (1987). *Empirical model-building and response surfaces*. Wiley New York.

Brewer, G., Saccani, S., Sarkar, S., Lewis, A., and Pestka, S. (2003). Increased interleukin-10 mrna stability in melanoma cells is associated with decreased levels of a + u-rich element binding factor auf1. *J Interferon Cytokine Res*, 23(10):553–564.

Burnham, K. and Anderson, D. (2002). *Model selection and multimodel inference*. New York: Spinger-Verlag.

Buxbaum, L. U. and Scott, P. (2005). Interleukin 10- and fcgamma receptor-deficient mice resolve leishmania mexicana lesions. *Infect Immun*, 73(4):2101–2108.

Cannon, W. B. (1932). *The Wisdom of the Body*.

Cao, S., Zhang, X., Edwards, J., and Mosser, D. (2006). Nf-kappab1 (p50) homodimers differentially regulate pro- and anti-inflammatory cytokines in macrophages. *Biol Chem*.

Carvalho, E. M., Bastos, L. S., and Araújo, M. I. (2006). Worms and allergy. *Parasite Immunol*, 28(10):525–534.

Chi, H., Barry, S. P., Roth, R. J., Wu, J. J., Jones, E. A., Bennett, A. M., and Flavell, R. A. (2006). Dynamic regulation of pro- and anti-inflammatory cytokines by mapk phosphatase 1 (mkp-1) in innate immune responses. *Proc Natl Acad Sci U S A*, 103(7):2274–2279.

Cloutier, M. and Wellstead, P. (2010). The control systems structures of energy metabolism. *J R Soc Interface*, 7(45):651–665.

Couper, K. N., Blount, D. G., and Riley, E. M. (2008). Il-10: the master regulator of immunity to infection. *J Immunol*, 180(9):5771–5777.

de Waal Malefyt, R., Abrams, J., Bennett, B., Figdor, C. G., and de Vries, J. E. (1991). Interleukin 10(il-10) inhibits cytokine synthesis by human monocytes: an autoregulatory role of il-10 produced by monocytes. *J Exp Med*, 174(5):1209–1220.

Figueiredo, A. S. (2005). Integration of open source software tools for the in silico design of metabolic pathways using flux balance analysis - an application to the production of recombinant human proteins. Master's thesis, Faculdade de Ciências da Universidade de Lisboa.

Figueiredo, A. S., Höfer, T., Klotz, C., Sers, C., Hartmann, S., Lucius, R., and Hammerstein, P. (2009). Modelling and simulating interleukin-10 production and regulation by macrophages after stimulation with an immunomodulator of parasitic nematodes. *FEBS J*, 276(13):3454–3469.

Fiorentino, D. F., Bond, M. W., and Mosmann, T. R. (1989). Two types of mouse t helper cell. iv. th2 clones secrete a factor that inhibits cytokine production by th1 clones. *J Exp Med*, 170(6):2081–2095.

Flöttmann, M., Schaber, J., Hoops, S., Klipp, E., and Mendes, P. (2008). Modelmage: a tool for automatic model generation, selection and management. *Genome Inform*, 20:52–63.

Gee, K., Angel, J. B., Mishra, S., Blahoianu, M. A., and Kumar, A. (2007). Il-10 regulation by hiv-tat in primary human monocytic cells: involvement of calmodulin/calmodulin-dependent protein kinase-activated p38 mapk and sp-1 and creb-1 transcription factors. *J Immunol*, 178(2):798–807.

Giambartolomei, G. H., Dennis, V. A., Lasater, B. L., Murthy, P. K., and Philipp, M. T. (2002). Autocrine and exocrine regulation of interleukin-10 production in thp-1 cells stimulated with borrelia burgdorferi lipoproteins. *Infect Immun*, 70(4):1881–1888.

Gibson, A. W., Edberg, J. C., Wu, J., Westendorp, R. G., Huizinga, T. W., and Kimberly, R. P. (2001). Novel single nucleotide polymorphisms in the distal il-10 promoter affect il-10 production and enhance the risk of systemic lupus erythematosus. *J Immunol*, 166(6):3915–3922.

Goldbeter, A. and Koshland, D. E. (1981). An amplified sensitivity arising from covalent modification in biological systems. *Proc Natl Acad Sci U S A*, 78(11):6840–6844.

Gregory, W. F. and Maizels, R. M. (2008). Cystatins from filarial parasites: evolution, adaptation and function in the host-parasite relationship. *Int J Biochem Cell Biol*, 40(6-7):1389–1398.

Hammerstein, P. (1981). The role of assymetries in animal contests. *Animal Behaviour*.

Hartmann, S., Kyewski, B., Sonnenburg, B., and Lucius, R. (1997). A filarial cysteine protease inhibitor down-regulates t cell proliferation and enhances interleukin-10 production. *Eur J Immunol*, 27(9):2253–2260.

Hartmann, S. and Lucius, R. (2003). Modulation of host immune responses by nematode cystatins. *International Journal for Parasitology*, 33:1291–1302.

Heinrich, R., Neel, B. G., and Rapoport, T. A. (2002). Mathematical models of protein kinase signal transduction. *Mol Cell*, 9(5):957–970.

Heinrich, R. and Rapoport, T. A. (1974). A linear steady-state treatment of enzymatic chains. general properties, control and effector strength. *Eur J Biochem*, 42(1):89–95.

Hilgenboecker, K., Hammerstein, P., Schlattmann, P., Telschow, A., and Werren, J. H. (2008). How many species are infected with wolbachia?–a statistical analysis of current data. *FEMS Microbiol Lett*, 281(2):215–220.

Hoops, S., Sahle, S., Gauges, R., Lee, C., Pahle, J., Simus, N., Singhal, M., Xu, L., Mendes, P., and Kummer, U. (2006). Copasi: a complex pathway simulator. *Bioinformatics*.

Hornberg, J. J., Binder, B., Bruggeman, F. J., Schoeberl, B., Heinrich, R., and Westerhoff, H. V. (2005a). Control of mapk signalling: from complexity to what really matters. *Oncogene*, 24(36):5533–5542.

Hornberg, J. J., Bruggeman, F. J., Binder, B., Geest, C. R., de Vaate, A. J. M. B., Lankelma, J., Heinrich, R., and Westerhoff, H. V. (2005b). Principles behind the multifarious control of signal transduction. erk phosphorylation and kinase/phosphatase control. *FEBS J*, 272(1):244–258.

Hu, J.-H., Chen, T., Zhuang, Z.-H., Kong, L., Yu, M.-C., Liu, Y., Zang, J.-W., and Ge, B.-X. (2007). Feedback control of mkp-1 expression by p38. *Cell Signal*, 19(2):393–400.

Hucka, M., Finney, A., Sauro, H. M., Bolouri, H., Doyle, J. C., Kitano, H., Arkin, A. P., Bornstein, B. J., Bray, D., Cornish-Bowden, A., Cuellar, A. A., Dronov, S., Gilles, E. D., Ginkel, M., Gor, V., Goryanin, I. I., Hedley, W. J., Hodgman, T. C., Hofmeyr, J.-H., Hunter, P. J., Juty, N. S., Kasberger, J. L., Kremling, A., Kummer, U., Novère, N. L., Loew, L. M., Lucio, D., Mendes, P., Minch, E., Mjolsness, E. D., Nakayama, Y., Nelson, M. R., Nielsen, P. F., Sakurada, T., Schaff, J. C., Shapiro, B. E., Shimizu, T. S., Spence, H. D., Stelling, J., Takahashi, K., Tomita, M., Wagner, J., Wang, J., and Forum, S. B. M. L. (2003). The systems biology markup language (sbml): a medium for representation and exchange of biochemical network models. *Bioinformatics*, 19(4):524–531.

Ingalls, B. P. and Sauro, H. M. (2003). Sensitivity analysis of stoichiometric networks: an extension of metabolic control analysis to non-steady state trajectories. *J Theor Biol*, 222(1):23–36.

Jeffrey, K. L., Brummer, T., Rolph, M. S., Liu, S. M., Callejas, N. A., Grumont, R. J., Gillieron, C., Mackay, F., Grey, S., Camps, M., Rommel, C., Gerondakis, S. D., and Mackay, C. R. (2006). Positive regulation of immune cell function and inflammatory responses by phosphatase pac-1. *Nat Immunol*, 7(3):274–283.

Jeffrey, K. L., Camps, M., Rommel, C., and Mackay, C. R. (2007). Targeting dual-specificity phosphatases: manipulating map kinase signalling and immune responses. *Nat Rev Drug Discov*, 6(5):391–403.

Kaiser, F., Cook, D., Papoutsopoulou, S., Rajsbaum, R., Wu, X., Yang, H.-T., Grant, S., Ricciardi-Castagnoli, P., Tsichlis, P. N., Ley, S. C., and O'Garra, A. (2009). Tpl-2 negatively regulates interferon-beta production in macrophages and myeloid dendritic cells. *J Exp Med*, 206(9):1863–1871.

Kholodenko, B. N. (2006). Cell-signalling dynamics in time and space. *Nat Rev Mol Cell Biol*, 7(3):165–176.

Klipp, E., Liebermeister, W., Wierling, C., Kowald, A., Lehrach, H., and Herwig, R. (2009). *Systems Biology - A Textbook*. Wiley-Blackwell.

Klipp, E., Nordlander, B., Krüger, R., Gennemark, P., and Hohmann, S. (2005). Integrative model of the response of yeast to osmotic shock. *Nat Biotechnol*, 23(8):975–982.

Klotz, C., Ziegler, T., Figueiredo, A. S., Rausch, S., Hepworth, M., Obsivac, N., Sers, C., Lang, R., Hammerstein, P., Lucius, R., and Hartmann, S. (2011). A helminth immunomodulator exploits host signaling events to regulate cytokine production in macrophages.

Koehncke, A., Telschow, A., Werren, J. H., and Hammerstein, P. (2009). Life and death of an influential passenger: Wolbachia and the evolution of ci-modifiers by their hosts. *PLoS One*, 4(2):e4425.

Kühn, C. (2010). *Modeling and Analysis of Yeast Osmoadaptation in Cellular Context*. PhD thesis, Mathematisch-Naturwissenschaftlichen Fakultät I.

Kühn, C., Petelenz, E., Nordlander, B., Schaber, J., Hohmann, S., and Klipp, E. (2008). Exploring the impact of osmoadaptation on glycolysis using time-varying response-coefficients. *Genome Inform*, 20:77–90.

Kühn, R., Löhler, J., Rennick, D., Rajewsky, K., and Müller, W. (1993). Interleukin-10-deficient mice develop chronic enterocolitis. *Cell*, 75(2):263–274.

Li, L., Chen, S.-F., and Liu, Y. (2009). Map kinase phosphatase-1, a critical negative regulator of the innate immune response. *Int J Clin Exp Med*, 2(1):48–67.

Liu, Y., Shepherd, E. G., and Nelin, L. D. (2007). Mapk phosphatases–regulating the immune response. *Nat Rev Immunol*, 7(3):202–212.

Ljung, L. (1999). *System identification. Theory for the user*. Prentice Hall.

Ljung, L. and Glad, T. (1994). *Modelling of dynamic systems*. Prentice Hall.

Lucas, M., Zhang, X., Prasanna, V., and Mosser, D. M. (2005). Erk activation following macrophage fcgammar ligation leads to chromatin modifications at the il-10 locus. *J Immunol*, 175(1):469–477.

Lucius, R. and Loos-Frank, B. (2008). *Biologie von parasiten*. Springer.

Marshall, C. (1995). Specificity of receptor tyrosine kinase signalling: transient versus sustained extracellular signal-regulated kinase activation. *Cell*, 80:179–185.

Medzhitov, R. and Janeway, C. (2000). Innate immunity. *N Engl J Med*, 343:338–344.

Moore, K. W., de Waal Malefyt, R., Coffman, R. L., and O'Garra, A. (2001). Interleukin-10 and the interleukin-10 receptor. *Annu Rev Immunol*, 19:683–765.

Mueller, T. (2002). *Modeling complex systems with differential equations*. PhD thesis, Albert-Ludwigs-Universität Freiburg in Breisgau.

Murphy, K., Travers, P., and Walport, M. (2008). *Janeway's Immunobiology*. Garland Science.

Noble, D. (2008). *The music of life: biology beyond genes*. Oxford University Press, USA.

O'Garra, A., Barrat, F. J., Castro, A. G., Vicari, A., and Hawrylowicz, C. (2008). Strategies for use of il-10 or its antagonists in human disease. *Immunol Rev*, 223:114–131.

O'Garra, A. and Vieira, P. (2007). T(h)1 cells control themselves by producing interleukin-10. *Nat Rev Immunol*, 7(6):425–428.

Patterson, K. I., Brummer, T., O'Brien, P. M., and Daly, R. J. (2009). Dual-specificity phosphatases: critical regulators with diverse cellular targets. *Biochem J*, 418(3):475–489.

Perrigoue, J. G., Marshall, F. A., and Artis, D. (2008). On the hunt for helminths: innate immune cells in the recognition and response to helminth parasites. *Cell Microbiol*, 10(9):1757–1764.

Plaisier, A. P., van Oortmarssen, G. J., Remme, J., and Habbema, J. D. (1991). The reproductive lifespan of onchocerca volvulus in west african savanna. *Acta Trop*, 48(4):271–284.

Powell, M. J., Thompson, S. A., Tone, Y., Waldmann, H., and Tone, M. (2000). Posttranscriptional regulation of il-10 gene expression through sequences in the 3'-untranslated region. *J Immunol*, 165(1):292–296.

Renaud, F. and de Meeüs, T. (1991). A simple model of host-parasite evolutionary relationships. parasitism: compromise or conflict? *J Theor Biol*, 152(3):319–327.

Sackmann, A., Formanowicz, D., Formanowicz, P., and Blazewicz, J. (2009). New insights into the human body iron metabolism analyzed by a petri net based approach. *Biosystems*, 96(1):104–113.

Santos, S., Verveer, P., and Bastiaens, P. (2007). Growth factor-induced mapk network topology shapes erk response determining pc-12 cell fate. *Nature Cell Biology*.

Sasagawa, S., ichi Ozaki, Y., Fujita, K., and Kuroda, S. (2005). Prediction and validation of the distinct dynamics of transient and sustained erk activation. *Nat Cell Biol*, 7(4):365–373.

Sauro, H. M. and Kholodenko, B. N. (2004). Quantitative analysis of signaling networks. *Prog Biophys Mol Biol*, 86(1):5–43.

Schnoeller, C., Rausch, S., Pillai, S., Avagyan, A., Wittig, B. M., Loddenkemper, C., Hamann, A., Hamelmann, E., Lucius, R., and Hartmann, S. (2008). A helminth immunomodulator reduces allergic and inflammatory responses by induction of il-10-producing macrophages. *J Immunol*, 180(6):4265–4272.

Seber, G. and Wild, C. (2003). *Nonlinear Regression*. Wiley. NewYork.

Spellberg, B. and Edwards, J. E. (2001). Type 1/type 2 immunity in infectious diseases. *Clin Infect Dis*, 32(1):76–102.

Staples, K. J., Smallie, T., Williams, L. M., Foey, A., Burke, B., Foxwell, B. M. J., and Ziegler-Heitbrock, L. (2007). Il-10 induces il-10 in primary human monocyte-derived macrophages via the transcription factor stat3. *J Immunol*, 178(8):4779–4785.

Sutterwala, F. S., Noel, G. J., Salgame, P., and Mosser, D. M. (1998). Reversal of proinflammatory responses by ligating the macrophage fcgamma receptor type i. *J Exp Med*, 188(1):217–222.

Suzu, S., Hiyoshi, M., Yoshidomi, Y., Harada, H., Takeya, M., Kimura, F., Motoyoshi, K., and Okada, S. (2007). M-csf-mediated macrophage differentiation but not proliferation is correlated with increased and prolonged erk activation. *J Cell Physiol*, 212(2):519–525.

Sánchez-Tilló, E., Comalada, M., Xaus, J., Farrera, C., Valledor, A. F., Caelles, C., Lloberas, J., and Celada, A. (2007). Jnk1 is required for the induction of mkp1 expression in macrophages during proliferation and lipopolysaccharide-dependent activation. *J Biol Chem*, 282(17):12566–12573.

Vieira, P. and O'Garra, A. (2007). Regula'ten' the gut. *Nature Immunology*.

Voit, E. and Torres, N. (2002). *Pathway analysis and optimization in metabolic engineering*. Cambridge University Press.

Wang, X. and Liu, Y. (2007). Regulation of innate immune response by map kinase phosphatase-1. *Cell Signal*, 19(7):1372–1382.

Ward, C., Murray, J., Clugston, A., Dransfield, I., Haslett, C., and Rossi, A. (2005). Interleukin-10 inhibits lipopolysaccharide-induced survival and extracellular signal-regulated kinase activation in human neutrophils. *Eur J Immunol*.

Wilkinson, D. (2006). *Stochastic modelling for systems biology*. Chapman & Hall/CRC.

Wittmann, D. M., Krumsiek, J., Saez-Rodriguez, J., Lauffenburger, D. A., Klamt, S., and Theis, F. J. (2009). Transforming boolean models to continuous models: methodology and application to t-cell receptor signaling. *BMC Syst Biol*, 3:98.

Yang, Z., Mosser, D. M., and Zhang, X. (2007). Activation of the mapk, erk, following leishmania amazonensis infection of macrophages. *J Immunol*, 178(2):1077–1085.

Yi, T. M., Huang, Y., Simon, M. I., and Doyle, J. (2000). Robust perfect adaptation in bacterial chemotaxis through integral feedback control. *Proc Natl Acad Sci U S A*, 97(9):4649–4653.

Yipp, B. G., Robbins, S. M., Resek, M. E., Baruch, D. I., Looareesuwan, S., and Ho, M. (2003). Src-family kinase signaling modulates the adhesion of plasmodium falciparum on human microvascular endothelium under flow. *Blood*, 101(7):2850–2857.

Zdanov, A., Schalk-Hihi, C., Gustchina, A., Tsang, M., Weatherbee, J., and Wlodawer, A. (1995). Crystal structure of interleukin-10 reveals the functional dimer with an unexpected topological similarity to interferon gamma. *Structure*, 3(6):591–601.

Zhang, X., Edwards, J. P., and Mosser, D. M. (2006). Dynamic and transient remodeling of the macrophage il-10 promoter during transcription. *J Immunol*, 177(2):1282–1288.

List of Figures

List of Tables

Acknowledgements

First of all, I want to express my gratitude to Peter Hammerstein for his guidance during this work. In our stimulating discussions, there were always two ingredients I find vital for a successfull scientific work: support and freedom. I also want to thank Thomas Höfer for giving me the opportunity to do my PhD studies in such an exciting field. His initial guidance during my work was of great importance to reach the goals of my thesis.

But this work had never been possible without the cooperation of the Department of Parasitology from the Humboldt-Universität zu Berlin. I am very grateful to Richard Lucius and Susanne Hartmann for sharing with me their deep understanding on the biological system I studied. I extend my gratitude to Christian Klotz, who provided the experimental data I used in this thesis. We had the most stimulating discussions and their willingness to help and discuss problems was of great value during these years. I am also gratefull to Thomas Ziegler, who provided me the experimental data on anti-IL-10r antibodies.

I express my gratitude to Jörg Schaber for discussions about mathematical modelling and regulation and for reading this manuscript. I thank Matthias Futschik for his help on microarray data analysis. I also thank Hanspeter Herzel, Stefan Legewie, Nils Blüthgen and Christine Sers for discussions about signalling and regulation.

The friendly atmosphere of the ITB was essential for the good completion of this work. I want to thank my office colleagues Vitor Anaya and Arnulf Köhncke not only for the great relaxing moments we had. I also want to thank them for their friendship and support. Vitor was always available to share his experimental knowledge with me and Arnulf was always so patient correcting my German when I asked him. I also thank them for reading some parts of this thesis. I want to thank the past members of our office, in particular Kirsten Hilgenböcker for her initial support when I first arrived in Berlin and for her very special humour. I extend my gratitude to all members of the big Mensa group, who always waited patiently for me to finish the salad. I also thank Karin, Andreas and Elvira for their support and kindness. This thesis was financially supported by the Deutsche Forschungsgemeinschaft, SFB 618.

I thank my friend Jemima for reading this manuscript in the Mensa Cafe, in a train to Amsterdam, in a plane to India and for correcting my English. And I thank my friend Dirk for reading this thesis with the eyes of an amateur.

I am deeply gratefull to Jordi for his great support. In the times of greatest stress, he was patient and in times of self-doubt, he was encouraging. I extend my deepest gratitude to all my family in Portugal and friends, for their support and for believing in me. I also thank Helga for all her help.

And I thank Elenah for being such an inspiring force.

Selbständigkeitserklärung

Hiermit erkläre ich, die vorliegende Arbeit selbständig ohne fremde Hilfe verfaßt und nur die angegebene Literatur und Hilfsmittel verwendet zu haben.

Berlin, den 07.04.2011 Ana Sofia Cabrita Figueiredo